

ornl

ORNL/CON-34

**OAK
RIDGE
NATIONAL
LABORATORY**



**Performance Evaluation of a
Selected Three-Ton Air-to-Air
Heat Pump in the Heating Mode**

A. A. Domingorena
S. J. Ball

**OPERATED BY
UNION CARBIDE CORPORATION
FOR THE UNITED STATES
DEPARTMENT OF ENERGY**

Printed in the United States of America. Available from
National Technical Information Service
U.S. Department of Commerce
5285 Port Royal Road, Springfield, Virginia 22161
NTIS price codes—Printed Copy. A05 Microfiche A01

This report was prepared as an account of work sponsored by an agency of the United States Government. Neither the United States nor any agency thereof, nor any of their employees, makes any warranty, expressed or implied, or assumes any legal liability or responsibility for any third party's use or the results of such use of any information, apparatus, product or process disclosed in this report, or represents that its use by such third party would not infringe privately owned rights.

Contract No. W-7405-eng-26

PERFORMANCE EVALUATION OF A SELECTED THREE-TON
AIR-TO-AIR HEAT PUMP IN THE HEATING MODE

by

A. A. Domingorena*
Energy Division

S. J. Ball
Instrumentation and Controls Division

DEPARTMENT OF ENERGY
Division of Buildings and Community Systems

Date Published: January 1980

OAK RIDGE NATIONAL LABORATORY
Oak Ridge, Tennessee 37830
operated by
UNION CARBIDE CORPORATION
for the
DEPARTMENT OF ENERGY

* Now with Carrier Corporation, Bldg. TR-4, Box 4808, Carrier Parkway,
Syracuse, NY 13221.

PREVIOUSLY PUBLISHED REPORTS IN THIS SERIES

A. A. Domingorena, *Performance Evaluation of a Low-First-Cost, Three-Ton, Air-to-Air Heat Pump in the Heating Mode*, ORNL/CON-18 (October 1978).

TABLE OF CONTENTS

	<u>Page</u>
LIST OF FIGURES	vii
LIST OF TABLES	xi
ABSTRACT	1
1. INTRODUCTION	1
2. SUMMARY AND CONCLUSIONS	3
2.1 Heating Capacity and Coefficient of Performance under Steady-State (Nonfrosting) Conditions	3
2.2 Fan and Fan-Motor Efficiencies	3
2.3 Heat Exchanger and Orifice-Type Refrigerant Metering Device Performance	4
2.4 Heat Losses	5
2.5 Compressor Operation	5
2.6 Performance Under Frosting Conditions	5
2.7 Effect of Component Inefficiencies	7
2.8 Effect of Refrigerant Charge	7
3. DESCRIPTION OF TEST UNIT	11
4. DESCRIPTION OF TEST APPARATUS	13
4.1 Test Loops	13
4.2 Instrumentation	14
4.2.1 Temperature	14
4.2.2 Pressure	18
4.2.3 Refrigerant flow rate	18
4.2.4 Airflow rate	18
4.2.5 Electrical power input	19
4.2.6 Humidity	19
4.3 DAS and Program	19
5. TEST PROCEDURE	21
5.1 Steady-State Tests	21
5.2 Frosting-Defrosting Tests	21
5.3 Fan Tests	22
5.4 Refrigerant Charge Tests	22
6. STEADY-STATE TEST RESULTS	23
6.1 Heating Capacity and COP	23
6.2 Fan Performance	26
6.2.1 Indoor-unit fan	26
6.2.2 Outdoor-unit fan	29

	<u>Page</u>
6.3 Heat Exchanger and Refrigerant Metering Device Performance	29
6.3.1 Condenser (indoor coil)	31
6.3.2 Evaporator (outdoor coil)	31
6.4 System Heat Losses	36
6.5 Compressor Operation	37
7. FROSTING-DEFROSTING TESTS	41
7.1 System Performance Under Frosting Conditions	41
7.1.1 Test at 0.6°C (33°F) and 100% relative humidity	41
7.1.2 Tests at 0.6°C (33°F) and 92 to 97% relative humidity	42
7.1.3 Tests at -2.2°C (28°F) and 80 to 85% relative humidity	42
7.1.4 Defrost water collection	55
7.2 Compressor Performance During the Defrosting Period	55
8. REFRIGERANT CHARGE VARIATION TESTS	61
ACKNOWLEDGMENTS	68
REFERENCES	69
Appendix A — Experimental Data	73
Appendix B — Fan-Motor Efficiency Evaluation	79
Appendix C — Algorithms for Calculating Thermodynamic Properties of Refrigerant 22	83
Appendix D — Computer Program for the Data Acquisition System	85

LIST OF FIGURES

<u>Figure</u>	<u>Page</u>
2.1 Effect of component inefficiencies on system efficiency under steady-state, nonfrosting conditions	8
4.1 Schematic diagram of test loop for the indoor unit	15
4.2 Schematic diagram of test loop for the outdoor unit	15
4.3 Experimental apparatus	16
4.4 Schematic diagram of refrigerant circuit for the heat pump in the heating mode	17
4.5 DAS temperature measurement scheme	17
6.1 System heating capacity as a function of outdoor air temperature	24
6.2 System coefficient of performance as a function of outdoor air temperature	25
6.3 Power input as a function of outdoor air temperature	27
6.4 Indoor fan characteristics	28
6.5 Outdoor fan characteristics	30
6.6 Schematic diagram of the refrigerant circuits in the indoor coil	33
6.7 Temperature profiles for one refrigerant circuit of the indoor coil. The outdoor air temperature was 1.0°C (33.8°F) for run 1, 13.3°C (56.0°F) for run 2, 18.6°C (65.4°F) for run 3, and 5.7°C (42.3°F) for run 4	34
7.1 Heating capacity and COP during a 50 min frosting period with outdoor air at 0.6°C and 100% relative humidity	43
7.2 Outdoor-coil air pressure drop and airflow rate during 50 min frosting period with outdoor air at 0.6°C and 100% relative humidity	44
7.3 Refrigerant pressures and flow rates during a 50 min frosting period with outdoor air at 0.6°C and 100% relative humidity	45

<u>Figure</u>	<u>Page</u>
7.4 Compressor and outdoor-fan power consumption during a 50 min frosting period with outdoor air at 0.6°C and 100% relative humidity	46
7.5 Heating capacity and COP during a 90 min frosting period with outdoor air at 0.6°C and 92-97% relative humidity	47
7.6 Outdoor-coil air pressure drop and airflow rate during a 90 min frosting period with outdoor air at 0.6°C and 92-97% relative humidity	48
7.7 Refrigerant pressures and flow rates during a 90 min frosting period with outdoor air at 0.6°C and 92-97% relative humidity	49
7.8 Compressor and outdoor fan power consumption during a 90 min frosting period with outdoor air at 0.6°C and 92-97% relative humidity	50
7.9 Heating capacity and COP during a 90 min frosting period with outdoor air at -2.2°C and 80-85% relative humidity	51
7.10 Outdoor-coil air pressure drop and airflow rate during a 90 min frosting period with outdoor air at -2.2°C and 80-85% relative humidity	52
7.11 Refrigerant pressures and flow rates during a 90 min frosting period with outdoor air at -2.2°C and 80-85% relative humidity	53
7.12 Compressor and outdoor fan power consumption during a 90 min frosting period with outdoor air at -2.2°C and 80-85% relative humidity	54
7.13 Power consumption and system pressures during a defrosting period following a 50 min frosting interval with the outdoor air at 0.6°C and 100% relative humidity	57
7.14 Power consumption and system pressures during a defrosting period following a 90 min frosting interval with the outdoor air at 0.6°C and 92-97% relative humidity	58
7.15 Power consumption and system pressures during a defrosting period following a 90 min frosting interval with the outdoor air at -2.2°C and 80-85% relative humidity	59

<u>Figure</u>		<u>Page</u>
8.1	Suction gas superheat as a function of refrigerant charge	62
8.2	System pressures as a function of refrigerant charge . . .	63
8.3	Mass flow rate of refrigerant as a function of refrigerant charge	64
8.4	Heating capacity as a function of refrigerant charge . . .	66
8.5	Coefficient of performance as a function of refrigerant charge. The COP of the low-first-cost unit, which lacks a suction line accumulator, is shown for comparison	67

LIST OF TABLES

<u>Table</u>	<u>Page</u>
2.1 Observed vs rated performance of the heat pump at 8°C outdoor air temperature and 21°C indoor air temperature	3
2.2 Measured values of combined efficiency of the indoor and outdoor fan and fan-motor units	4
2.3 Conditions for frosting tests	6
2.4 Heat pump conditions at conclusion of the frosting periods	6
3.1 Principal features of test unit	12
6.1 Steady-state indoor coil (condenser) performance	32
6.2 Steady-state outdoor coil (evaporator) performance	35
6.3 System heat loss rates	36
6.4 Compressor operating characteristics	38
7.1 Frost accumulation as evaluated by defrost water drain collection	55
A.1 Test data from steady-state runs	75
A.2 Test data for frosting/defrosting tests	76
A.3 Test data for charge variation tests	77
B.1 Indoor-fan test data	79
B.2 Overall efficiency of the indoor fan-motor unit as a function of airflow rate	80
B.3 Outdoor-fan test data	81
B.4 Overall efficiency of the outdoor fan-motor unit as a function of airflow rate	81

PERFORMANCE EVALUATION OF A SELECTED THREE-TON
AIR-TO-AIR HEAT PUMP IN THE HEATING MODE

A. A. Domingorena
Energy Division

S. J. Ball
Instrumentation and Controls Division

ABSTRACT

An air-to-air split system residential heat pump of nominal three-ton capacity was instrumented and tested in the heating mode under laboratory conditions. This was the second of a planned series of experiments to obtain a data base of system and component performance for heat pumps. The system was evaluated under both steady-state and frosting-defrosting conditions; sensitivity of the system performance to variations in the refrigerant charge was measured.

From the steady-state tests, the heating capacity and coefficient of performance were computed, and evaluations were made of the performance parameters of the fan and fan motor units, the heat exchangers and refrigerant metering device, and the compressor. System heat losses were analyzed. The frosting-defrosting tests allowed the observation of system and component performance under dynamic conditions, and measurement of performance degradation under frosting conditions.

1. INTRODUCTION

This report describes the procedures and results of the second of a planned series of experiments that will establish a data base of the performance characteristics of commercially available heat pumps. The experiments are being conducted as part of a heat pump research program by the Oak Ridge National Laboratory for the Department of Energy, Office of Conservation and Solar Applications, Division of Buildings and Community Systems. The overall objective of this program is to identify and promote cost-effective modifications in heat pump design that can substantially reduce energy consumption in residential and commercial buildings. This objective is being approached in a combined experimental

and theoretical study. A data base on heat pump system and component performance is being obtained experimentally and computer models are being formulated to evaluate various candidate improvements analytically.

In order to provide the level of detail required for these analyses, the experiments are much more extensive than those that would be required for comparing heat pump ratings. The emphasis is on gathering information for design studies rather than providing consumer information.

The specific objectives of the experiments described herein are:

1. to determine the base-case performance of the selected heat pump and the characteristics of some of its components under both steady-state and frosting/defrosting conditions;
2. to measure experimentally the degradation of heat pump performance due to frost formation on the outdoor coil; and
3. to measure the sensitivity of the performance parameters to variations in the refrigerant charge.

Previous tests¹ were of a low-first-cost heat pump typical of those that might be selected by a speculative home builder. For the experiments reported herein, the tests were conducted on a "middle-of-the-line" nominal three-ton, air-to-air split system heat pump consisting of an indoor and an outdoor unit separated by 7.6 m (25 ft) of liquid-line and vapor-line refrigerant tubing. The test facility consisted of two "bootstrap" air duct loops which are described in this report. As in the previous tests, efforts were concentrated on the performance of the heat pump in the heating mode of operation. Performance improvements in this mode present the greater opportunity for enhancing the energy conserving potential of heat pumps.

2. SUMMARY AND CONCLUSIONS

2.1 Heating Capacity and Coefficient of Performance under Steady-State (Nonfrosting) Conditions

The observed capacity of the system under steady-state nonfrosting conditions compared reasonably well with rated values published by the Air Conditioning and Refrigeration Institute (ARI). ARI rating conditions for this test are: 1150 cfm of air at 70°F(db) at the indoor unit, 47°F(db) air at 43°F(wb) supplied to the outdoor unit. The observed values (Table 2.1) are from tests with 1200 cfm of air at 69.8°F supplied to the indoor unit, 47°F(db) air to the outdoor unit. No condensation of air moisture was observed on the outdoor coil. The heating capacity and COP were measured by two methods, air-side heat balance and refrigerant-side heat balance, which yielded reasonably close results. As shown in Table 2.1, the COP observed by the air-side measurements was 7% lower than the rated value; that observed by the refrigerant-side measurements was 14% lower than rated.

Table 2.1. Observed vs rated performance of the heat pump at 8°C outdoor air temperature and 21°C indoor air temperature

	Rated value	Observed value	
		Air	Refrigerant
Heating capacity, kW	9.96	9.96	9.37
COP	2.5	2.32	2.15
Power input, kW	4.05	4.35	

2.2 Fan and Fan-Motor Efficiencies

The measured combined efficiency of the indoor fan and fan-motor (defined as the ratio of the power used in moving the air to the electrical power to the fan-motor), was quite low, varying between 0.17 and 0.25 (Table 2.2).

Table 2.2. Measured values of combined efficiency of the indoor and outdoor fan and fan-motor units

	Motor speed (RPM)	Airflow		Combined efficiency
		(m ³ /s)	(ft ³ /min)	
Indoor unit	850	0.54	1150	0.17
	850	0.35	750	0.25
	950	0.54	1150	0.22
	950	0.50	1050	0.22
Outdoor unit	N.A.	1.32	2800	0.11
	N.A.	1.04	2200	0.14

For the outdoor fan and fan-motor unit, the combined efficiency was even lower, from 0.11 to 0.14 (Table 2.2). As in the case of the low-first-cost unit, it is concluded that the fan and fan-motor units are not operating at their best efficiency. The opportunity for improvement in the combined fan and fan-motor efficiencies is apparent.

2.3 Heat Exchanger and Orifice-Type Refrigerant Metering Device Performance

Heat exchanger performance is closely related to the flow characteristics of the refrigerant metering device. The restriction of the metering device establishes a condensing pressure such that the difference between the condensing temperature in the indoor coil and that of the indoor air entering the condenser is 17 to 31°C (30.6 to 56°F) for outdoor air temperatures ranging from -5 to 13°C (23 to 55°F). For this coil, the difference between the refrigerant exit temperature and the entering air temperature varies from 14.2 to 15.4°C (25.5 to 27.7°F). Measurement of refrigerant temperatures in this coil shows a marked variation in the amount of liquid refrigerant in the coil for different values of the ambient air entering the outdoor coil.

For the range of test values of outdoor air temperatures of -4.4 to 13.9°C (24 to 57°F), the refrigerant pressures at the evaporator exit allow the presence of liquid refrigerant in the suction-line accumulator;

superheat of the refrigerant delivered to the compressor shell is thus held to the range of 0 to 2.2 C° (0 to 4 F°). For the outdoor coil (evaporator), the difference between refrigerant exit temperature and entering air temperature varies from 5.9 to 10.8°C (10.6 to 19.4°F), falling within the expected range of values.

2.4 Heat Losses

About 0.9 to 1.2 kW (3100 to 4100 Btu/hr) are rejected as heat from the hermetically sealed shell containing the compressor and motor when the outdoor air temperature is in the range -5 to 13°C (23 to 55°F). This loss, 28 to 30% of the compressor-motor power input, helps cool the compressor but reduces the efficiency of the heat pump system in the heating mode. Heat losses from the discharge line vary from 0.41 kW (1400 Btu/hr) to 0.54 kW (1800 Btu/hr) for the same outdoor temperature range.

2.5 Compressor Operation

The combined compressor and compressor-motor efficiency, defined as the ratio of ideal (isentropic) work (based on refrigerant conditions at shell inlet and outlet) to measured electrical energy input, varied from about 0.41 at 13.9°C (57°F) outdoor air to about 0.52 at -4.4°C (24°F).

2.6 Performance under Frosting Conditions

Tests of the heat pump under three different conditions favoring frost formation on the outdoor coil were conducted at the outdoor air temperatures and humidities shown in Table 2.3. The test under the most severe frosting conditions was terminated after 50 min, by which time the airflow through the outdoor coil had decreased substantially, with concurrent rapid decrease in system high- and low-side refrigerant pressures. Performance summaries for the system at the conclusion of the frosting tests are shown in Table 2.4. The amount of frost formed

Table 2.3. Conditions for frosting tests

Condition No.	Relative humidity (%)	Outdoor air dry bulb temperature [°C (°F)]	Approximate frosting interval (min)
1	100	0.6-4.4 (33-40)	50
2	92-97	0.6-4.4 (33-40)	90
3	80-85	-2.2 (28)	90

Table 2.4. Heat pump conditions at conclusion of the frosting periods

	Condition		
	1	2	3
Outdoor-coil airflow, m ³ /s (cfm)	0.24 (510)	0.26 (550)	1.47 (3115)
Outdoor-coil air pressure drop, kPa (in. H ₂ O)	0.13 (0.52)	0.14 (0.56)	0.04 (0.16)
Outdoor fan-motor power, kW	0.49	0.45	0.42
Heating capacity, kW (Btu/hr)	6.56 (22400)	6.42 (21900)	6.74 (23000)
COP	1.75	1.74	1.78

on the coil was estimated by collecting the water drained from the coil during the subsequent defrost periods. The defrost water thus collected ranged from 1.1 liters (0.29 gallons) during the first defrosting period to 1.3 liters (0.34 gallons) for the second period when the system was operated with the outdoor air at 0.6°C (33°F) and at 100% relative humidity (condition 1). The COP values shown are those measured at the end of the frosting periods, just before the defrost cycle is initiated.

Graphs of the transient refrigerant pressures during the defrost cycles show that for condition 1 the high-side refrigerant pressure decreased to its lowest value after about 0.5 min of defrosting while the low-side (suction) pressure reached its lowest point after 1 min

of defrosting operation. These pressure variations may be explained by the condensation and subsequent accumulation of refrigerant in the cold outside coil. After about 1 min of defrosting, the pressures start to rise as heat is transferred to the frosted outside coil at a substantial rate.

2.7 Effect of Component Inefficiencies

An ideal vapor-compression cycle using R-22 as the working fluid would have a COP of 21.45 when it is operating between the temperature limits of 21 and 8°C (70 and 47°F). Temperature differences across the heat exchangers, a necessary condition for operation of a real system, reduce the computed COP substantially. Heat exchanger temperatures observed during the steady-state tests at 8°C outdoor air temperature were:

50°C (122°F) condensing -1.2°C (29.8°F) evaporating
14.6 C° (26.2 F°) subcooling 0 C° (0 F°) superheat

The computed COP using these temperature differences in an otherwise ideal system is 5.6, a 74% reduction from the ideal, reversible cycle COP.

The observed component inefficiencies and heat losses reduce the calculated COP further, as shown in Fig. 2.1. A combined compressor and motor efficiency of 0.47 reduces the COP to 3.2, an additional 43% loss. The substantial heat losses observed at the compressor shell reduce the COP an additional 16% to 2.7. Ideal fan power consumption would reduce the COP to 2.6; the observed fan and fan-motor inefficiencies reduce the COP an additional 15% to the value of 2.2, which is about the observed value for the heat pump operating in steady state at these conditions.

2.8 Effect of Refrigerant Charge

The experimental results indicate that the performance of this heat pump in the heating mode is insensitive to increases of the refrigerant

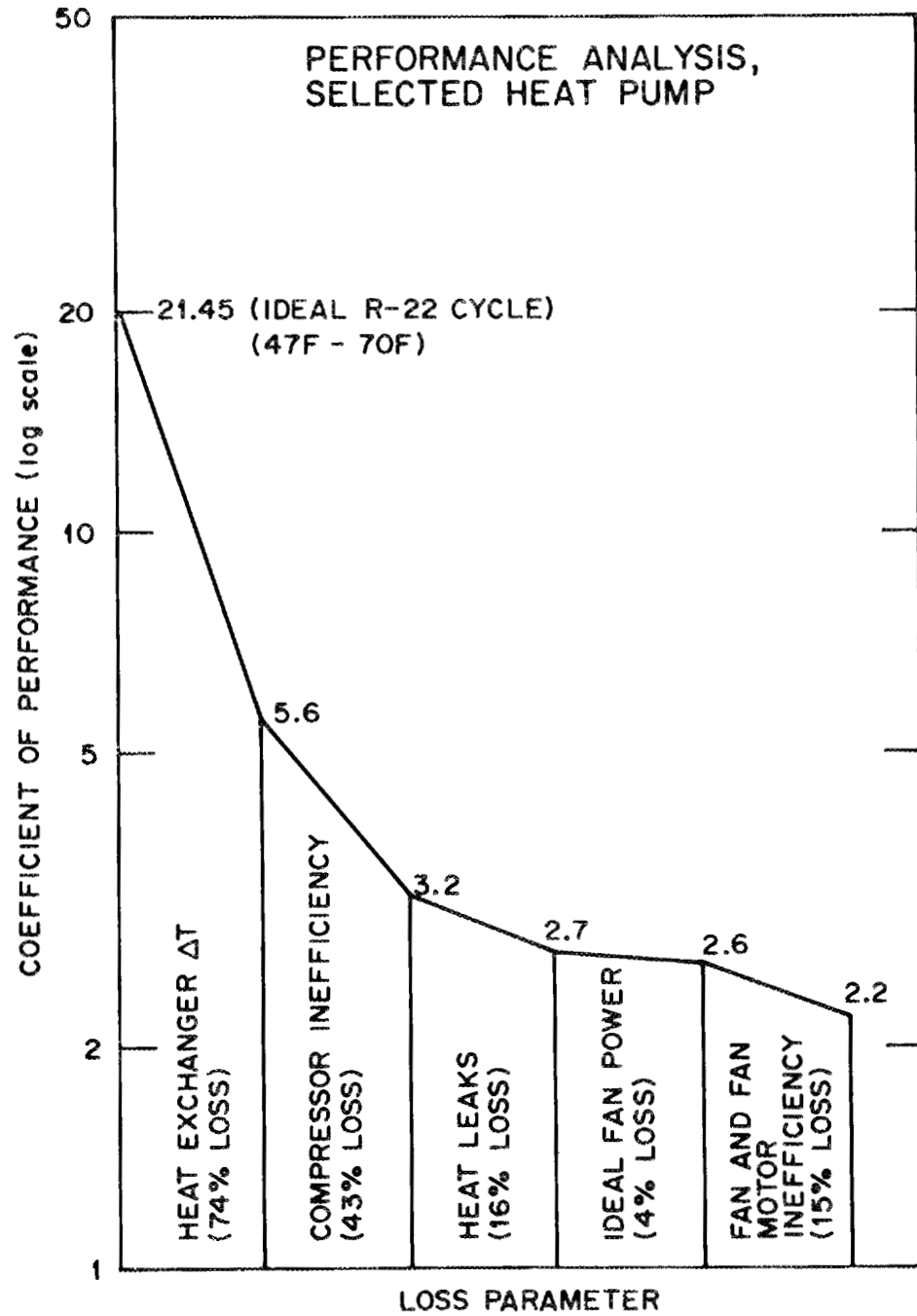


Fig. 2.1. Effect of component inefficiencies on system efficiency under steady-state, nonfrosting conditions.

charge by as much as 25% above the nominal value of 2.86 kg (6 lb, 5 oz), and is essentially insensitive to a charge reduction of 15% below the rated amount. This insensitivity is in contrast to the behavior of the low-first-cost unit previously tested,¹ which has no suction-line accumulator and showed an almost linear reduction of heating capacity and COP with reduction of refrigerant charge.

3. DESCRIPTION OF TEST UNIT

The heat pump evaluated in this study is a commercially available unit designated as an air-to-air split system, with a nominal capacity of three tons. The salient characteristics of this unit are presented in Table 3.1.

The defrosting control operates on a time-and-temperature principle. In order for the heat pump to enter the defrosting mode of operation, two sets of contacts must be closed: those on the defrost timer, and those on the defrost thermostat. The defrost thermostat is set to close its contacts at $-0.6 \pm 2.2^{\circ}\text{C}$ ($31 \pm 4^{\circ}\text{F}$). Every 90 minutes of heat pump running time, contacts on the defrost timer close for 10 seconds; if the defrost thermostat contacts are closed during those 10 seconds, the unit enters the defrosting mode.

The unit remains in the defrost period (cooling mode) until the temperature of the outdoor coil reaches $18.3 \pm 3.3^{\circ}\text{C}$ ($65 \pm 6^{\circ}\text{F}$), or 10 min have elapsed. Normally the frost is removed before the 10 min limit has been reached. At the end of the defrost interval, the unit is switched to the heating mode and the outdoor fan motor unit starts again.

Table 3.1. Principal features of test unit

Refrigerant	R-22
Compressor	Hermetically sealed compressor and motor Two-piston, reciprocating 65.3×10^{-6} -m ³ (3.986-in. ³) displacement 0.0413-m (1.625-in.) bore; 0.0244-m (0.961-in.) stroke Two-pole motor, 58.3 rps (3500 rpm) nominal speed
Outdoor coil	Aluminum plate fin and tube with return bends, 1.3 rows deep (avg.), 748 fins/m (19 fins/in.) 0.975-m ² (10.5-ft ²) face area 5-blade, 0.470-m (18.5-in.) propeller fan 1.32 m ³ /s (2800 cfm) nominal airflow
Indoor coil	Aluminum plate fin and tube with return bends, 3 rows deep, 512 fins/m (13 fins/in.) 0.294-m ² (3.16-ft ²) face area Forward-vane squirrel-cage fan rotor 0.543 m ³ /hr (1150 cfm) nominal airflow Rotor 0.267-m (10.5-in.) pitch diameter, 0.229-m (9-in.) long, double suction
Controls	Orifice-type refrigerant flow control and bypass valves for both heating and cooling Time-temperature defrost control Four-way refrigerant reversing valve
Accumulator	One, in refrigerant suction line
Rated Capacity	1. 9.08 kW (31,000 Btu/hr) cooling at 35°C (95°F) 2. 9.96 kW (34,000 Btu/hr) heating at 8.3°C (47°F) 3. 5.42 kW (18,500 Btu/hr) heating at -8.3°C (17°F)
Rated COP	2.5 at 8.3°C (47°F) db 1.7 at -8.3°C (17°F) db

4. DESCRIPTION OF TEST APPARATUS

4.1 Test Loops

The indoor and outdoor units of the heat pump were placed in separate "bootstrap" air loops that allowed for measurement and control of the temperature and humidity of air reaching the two units and provided the means for measurement of the airflow rates. The loops were constructed so that air could be recirculated after discharge from the fan-coil units and tempered, when necessary, with bleed air or supplemental heat. For the indoor unit, room air was introduced into the air loop to compensate for the heat rejected from the coil. Air pressure drops within that loop were small enough that desired airflow rates could be established by the fan in the indoor unit without recourse to booster fans.

For the steady-state (nonfrosting) tests, air from outside the building was induced into the outdoor-unit air loop. This air was tempered with air from the laboratory space both in order to compensate for heat absorbed by the coil and to reach temperatures higher than the ambient. Both sources provided air that was dry enough to preclude frosting. During the frosting tests, low temperatures and high humidity levels were desired at the outdoor coil. Accordingly, the air loop was sealed so that all of the air passing over the cold coil was recirculated; humidity was controlled by injecting steam into the air loop.

It was necessary to include a supplementary "booster" fan in the outdoor air loop to overcome the pressure drops due to the ducting. Thus, the airflow rates required for the outdoor unit could be established without penalizing the unit by requiring extra work from the outdoor fan motor. However, it was not possible in these tests to keep the airflow rates as close to the rated value of $1.32 \text{ m}^3/\text{s}$ (2800 cfm) as would be desired. Observed airflows were as much as 15% higher than the rated value during some of the tests because the speed of the booster fan could not be adjusted. In order to evaluate the effect of this deviation on other measured parameters, the ORNL heat pump model² was used to calculate the magnitudes of changes expected for 10 and 20% increases in outdoor airflow rates. The heating capacity, compressor motor power

consumption, and indoor fan motor power consumption were seen to change by less than 2%. Power consumption by the outdoor fan motor would increase if that fan were required to move more air. However, the booster fan is supplying the additional airflow, so errors caused by airflow rates in excess of the rated value are expected to be less than 5%. The change in the refrigerant evaporating temperature is expected to be less than 0.5°C (1°F).

Schematic diagrams of the two air loops are shown in Figs. 4.1 and 4.2; Fig. 4.3 is a photograph of the test loops. A schematic diagram of the refrigerant circuit is shown in Fig. 4.4.

4.2 Instrumentation

4.2.1 Temperature

Temperatures were monitored by chromel-alumel and copper-constantan thermocouples, with automatic readout and conversion by the data acquisition system (DAS) described in Sect. 4.3. Refrigerant temperatures were measured by thermocouples taped and clamped to the refrigerant lines and covered with foamed elastomer insulation. Air temperatures were measured by thermocouple grids at appropriate locations.

The typical readout scheme uses a floating reference junction and automatic correction for instrument drift, noted schematically in Fig. 4.5. The floating reference junction temperature is monitored by a highly accurate platinum-nickel resistance temperature detector (RTD); its reading is corrected for drift by referencing it to a precision resistor which has a very small temperature coefficient of resistivity. The thermocouple output signal as seen by the DAS is a function of the reference junction temperature as well as the thermocouple junction temperature. It was found that the NBS temperature vs millivolt relationships³ could easily be approximated to within 0.11°C (0.2°F) with reference junction temperatures between 21.1 and 32.2°C (70 and 90°F) and thermocouple junction temperatures between -12.2 and 65.6°C (10 and 150°F). The expressions used were:

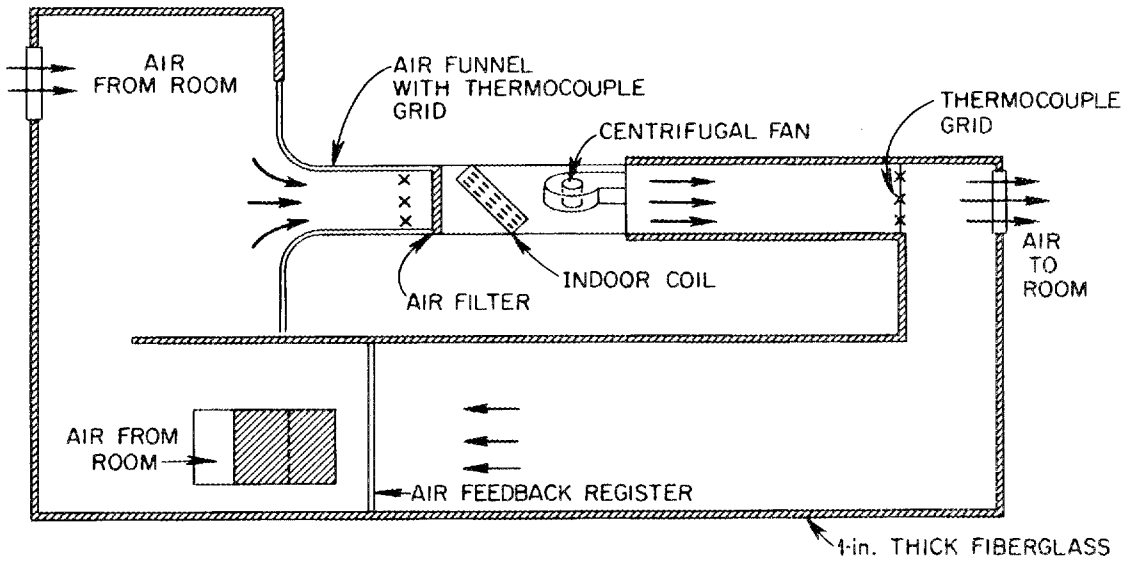


Fig. 4.1. Schematic diagram of test loop for the indoor unit.

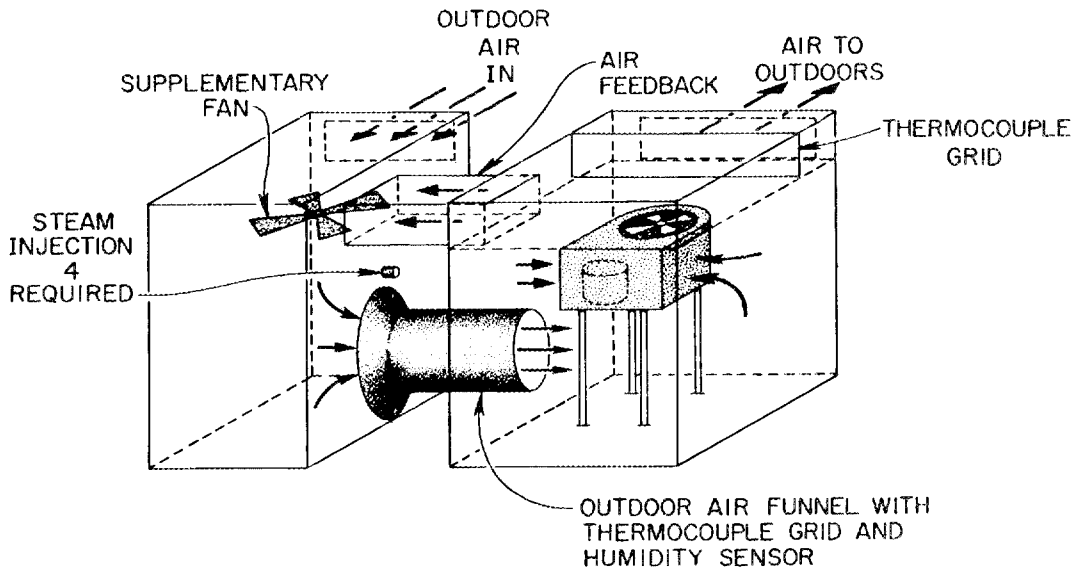


Fig. 4.2. Schematic diagram of test loop for the outdoor unit.

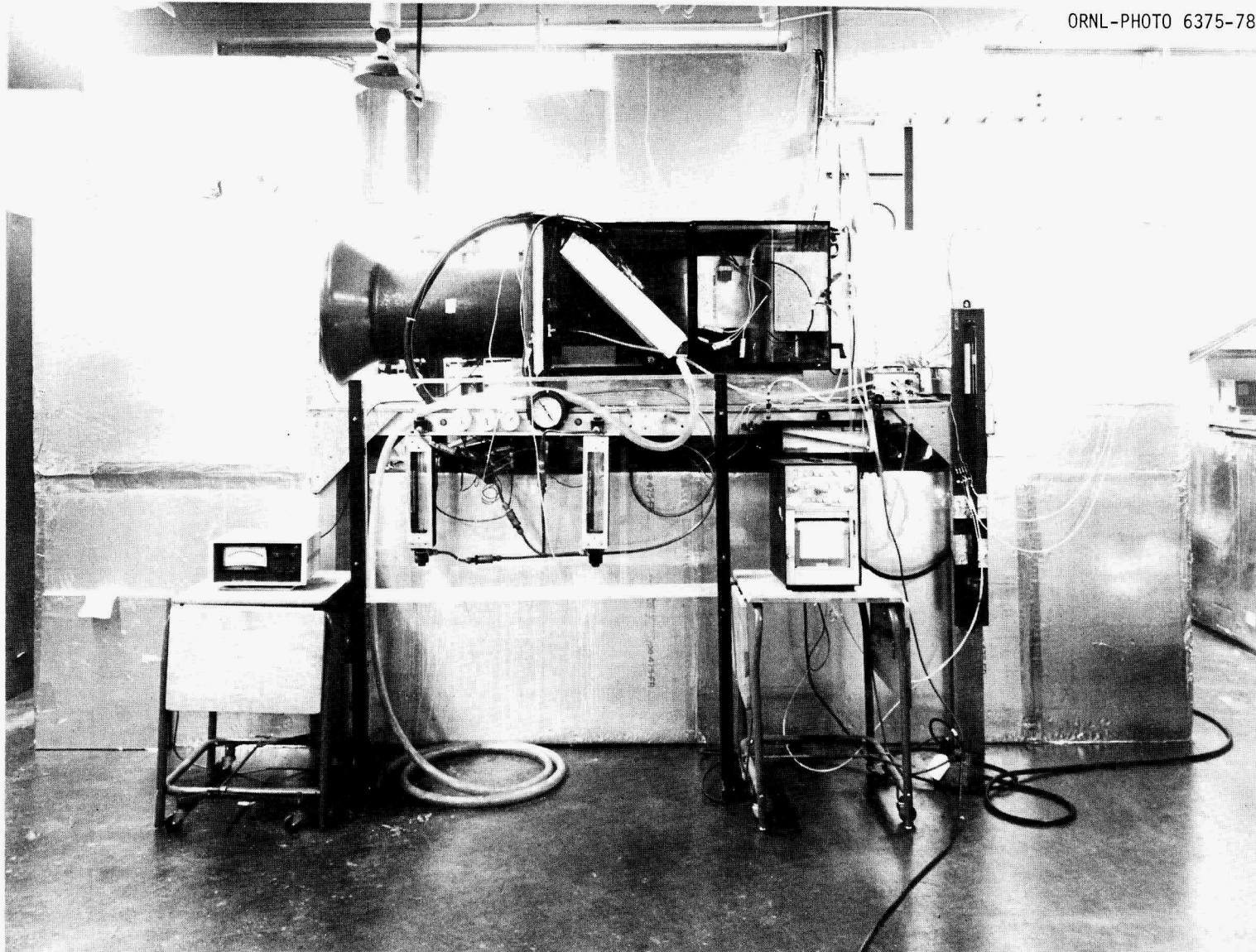


Fig. 4.3. Experimental apparatus.

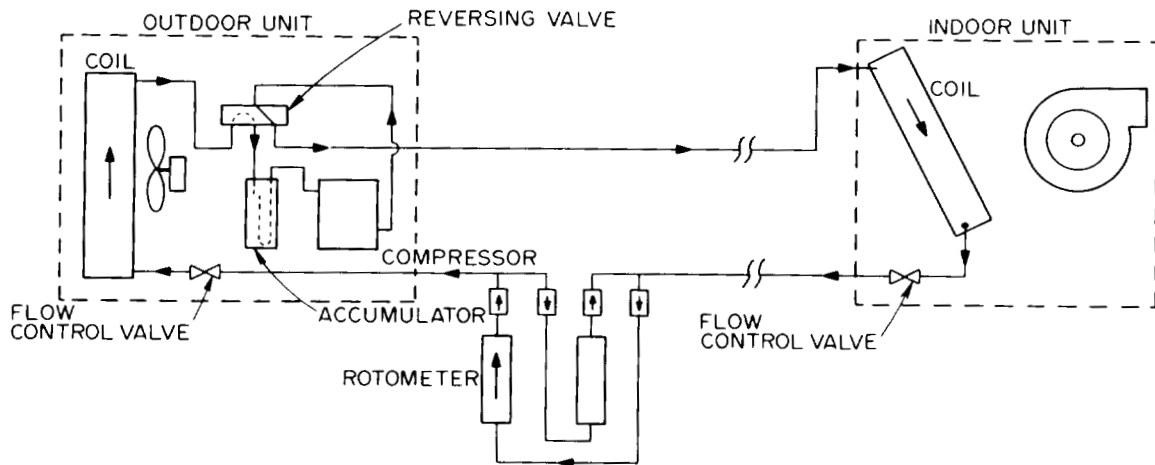


Fig. 4.4. Schematic diagram of refrigerant circuit for the heat pump in the heating mode.

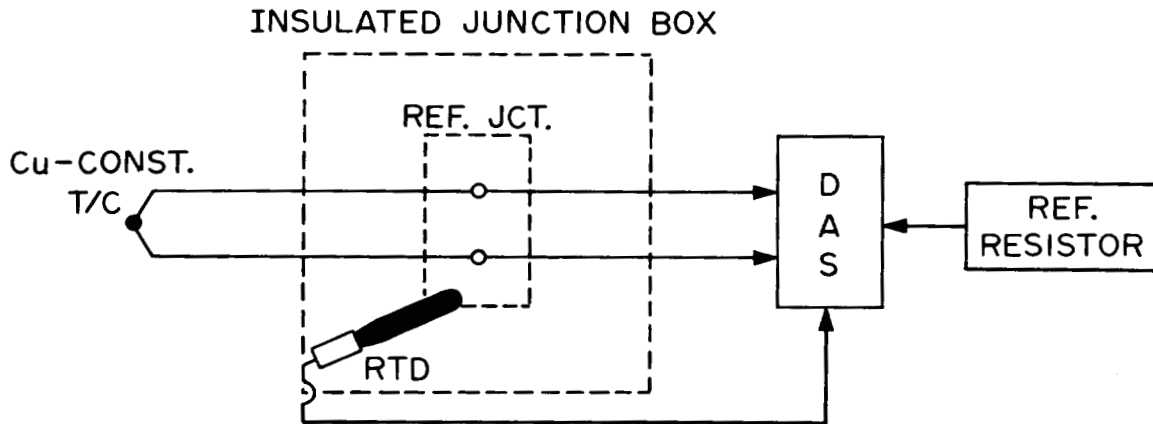


Fig. 4.5. DAS temperature measurement scheme.

$$T = T_R + (46.1 - 0.02 T_R)V - 0.414V^2, \quad (\text{chromel-alumel})$$

$$T = T_R + (48.2 - 0.05 T_R)V - 1.11V^2, \quad (\text{copper-constantan})$$

where

T = thermocouple junction temperature, °F;

T_R = reference junction temperature as measured by the RTD, °F;

V = DAS input signal, mV.

The floating reference junction provides advantages compared to a standard temperature-controlled reference box. Errors due to cycling of the control of the box temperature, typically about $\pm 1^\circ\text{F}$, are avoided, and the cost is much reduced.

4.2.2 Pressure

Steady-state refrigerant pressures were measured using bourdon-type gages and strain-gage-type dynamic pressure transducers located at the compressor-shell inlet and outlet, as well as the condenser inlet and outlet.

4.2.3 Refrigerant flow rate

Two rotameters in the refrigerant liquid line were used to determine refrigerant mass flow rate. Check valves were placed in the circuit so that one rotameter was operative in the heating mode and the other in the cooling mode. It was judged that the modest (less than 10 in. of water column) pressure drop introduced by these meters and check valves would not affect performance of the unit significantly.

4.2.4 Airflow rate

Airflow rates in the bootstrap loops were measured by velocity probe traverses using a hot-wire anemometer. The measurements were made at the air funnels installed in the testing loops for this purpose.

4.2.5 Electrical power input

Power to the compressor and each of the two fans was measured separately using thermal-watt converters, which produce d-c signals proportional to the instantaneous power consumption. The original heat pump controls were modified so that each component could be operated manually and the defrost cycle could be started and stopped manually.

4.2.6 Humidity

The humidity of the air reaching the outdoor coil was monitored by a hygrosensor placed in the air loop upstream of the outdoor unit. The hygrosensor used is one that changes its electrical resistance with the humidity of the air.

4.3 DAS and Program

The DAS in the energy conservation laboratory consists of a Digital Equipment Corp. (DEC) PDP-8E digital computer with an 8K-word core memory, a Vidar integrating digital voltmeter with an ohms converter, and a reed relay scanner. The programs used by the computer were written in a DEC FOCAL language modified locally to facilitate data acquisition. The use of an on-line computer system aids the experimenter considerably by giving almost immediate feedback of the heat pump status and performance, heat balances, and indications of drift of the process variables or component malfunction. Typically, multiple scans are taken over a prescribed period to obtain time-averaged parameters.

Simple routines for calculating the thermodynamic properties of refrigerant (R-22) and for instrument calibrations were developed and incorporated into the computer program. The computed results are found to be well within the expected accuracy ranges of the basic measurements. The R-22 property routines used are given in Appendix C; flow charts of the entire program are shown in Appendix D.

Most of the computations made in the FOCAL programs are straightforward and can be understood by reading the flow charts in Appendix D.

The calculation of compressor efficiency included in the program may be an exception. The definitions used in that calculation are for an isentropic compressor efficiency based on knowledge of the refrigerant conditions at the compressor entry and exit ports. The experimentally measured temperatures and pressures are, however, those at the entry and exit of the shell that contains the compressor and motor. Because of the thermal losses from the shell and the transfer of heat from the discharge line and the motor to the suction gas, the calculation of efficiency by this method is approximate, but is included to monitor the stability of compressor performance under varying test conditions. Compressor efficiency, η , is calculated in the program as the ratio of the change in enthalpy for ideal compression to the actual enthalpy increase:

$$\eta = (h_0^i - h_i) / (h_0 - h_i) ,$$

where h_0 is the enthalpy at compressor outlet, and h_i the enthalpy at inlet. The ideal enthalpy at outlet, h_0^i , is computed as:

$$h_0^i = h_0 - (s_0 - s_i) \left. \frac{\partial h / \partial T}{\partial s / \partial T} \right|_0 ,$$

in which s_0 and s_i are the entropy at outlet and inlet, and the derivatives with respect to temperature, T , are evaluated at outlet conditions. The enthalpies and entropies are calculated from h_g and s_g , the values for saturated vapor, using the amount of superheat, $T_i - T_s$, where T_s is the saturation temperature:

$$h_i = h_g + (\partial h / \partial T)_p (T_i - T_s) ;$$

$$s_i = s_g + (\partial s / \partial T)_p (T_i - T_s) .$$

The outlet quantities, h_0 and s_0 , are similarly calculated using the h_g and s_g at outlet conditions. The partial derivatives, $\partial T_s / \partial T$, $\partial h / \partial T$, and $\partial s / \partial T$ are calculated at the observed temperatures and pressures using the functions described in Appendix C.

5. TEST PROCEDURE

5.1 Steady-State Tests

Tests were conducted to investigate the response of performance parameters to change of the outdoor air temperature while the heat pump was operating in the steady-state heating mode. Tests were run at outdoor air temperatures of -4, -2, 4, 9, and 14°C (24, 29, 39, 48, and 57°F).

Steady-state tests were conducted by operating the unit until stable temperatures were achieved, and then taking data. For steady-state measurements it was desired that the system be operating in the heating mode with the outdoor coil operating in an essentially unfrosted condition. Visual observation of the outdoor heat exchanger indicated that nonfrosting operation was indeed achieved.

5.2 Frosting-Defrosting Tests

The frosting-defrosting tests were conducted at outdoor air temperatures of approximately -2°C (28°F) and 1°C (33°F) with the relative humidity ranging from 80 to 100%. It was judged that these temperatures and humidities represent severe frosting conditions pertinent to the evaluation of the performance degradation of the unit under frosting-defrosting operation.

The test at 100% relative humidity of the outdoor air allowed fog to reach the outdoor coil because the steam was injected into the airstream very close to the outdoor unit, thus preventing the possibility of only saturated vapor reaching the outdoor heat exchanger. The tests at about 100% relative humidity were conducted for about 50 min while the 80-85% relative humidity and 92-97% relative humidity tests were conducted for 80 to 100 min. The tests were terminated when the air-flow rates dropped to about 20% of nominal value.

5.3 Fan Tests

Tests were conducted to measure the fan motor efficiencies of both the indoor and outdoor units. The air-moving units were operated in the air loops of the testing rig, that is, in situ, but with the hermetic compressor unit turned off.

5.4 Refrigerant Charge Tests

The influence of the refrigerant charge on the performance of this heat pump system in the heating mode was evaluated by varying the charge from 63 to 127% of the value specified by the manufacturer. The experiments were conducted while maintaining an outdoor air temperature of about 10°C (50°F) dry bulb and a 21.1°C (70°F) indoor air dry bulb temperature.

The effect of variations of the refrigerant charge was first observed with the rated value of 2.86 kg (6 lb, 5 oz) of refrigerant in the system, then overcharging the unit with successively larger amounts of refrigerant up to 3.63 kg (8 lb). The undercharge tests were run subsequently, also stepwise, down to 1.81 kg (4 lb) charge. The test was concluded after observing bubbles in the refrigerant stream rotameter when the charge was dropped to 1.67 kg (3 lb, 11 oz).

6. STEADY-STATE TEST RESULTS

Heating capacity and COP, expressed as functions of the ambient temperature, are the descriptors most often presented to characterize the operation of a particular heat pump; indeed, they are essential data in applications considerations. Of greater interest in a study directed toward improving the efficiency and reliability of heat pumps, however, is the measurement of the performance of the individual components that make up the heat pump. Accordingly, a prime goal of this experiment was the collection of performance data on the major components. Characterization of fan, heat exchanger, and compressor performance are included as well as that of system heat losses. The steady-state test data are presented in Appendix A.

6.1 Heating Capacity and COP

We define the heating capacity of the heat pump as the sum of the heat rejected by the indoor coil and the power input to the indoor fan. The heating efficiency, or COP, of the heat pump is defined as the ratio of heating capacity to total power input. The latter includes the power to both indoor and outdoor fans and the power to the compressor motor. The measured heating capacity and COP as functions of outdoor air temperature are shown in Figs. 6.1 and 6.2. The graphs represent the functions as determined by two methods: one is based on the flow and temperature rise of the indoor air, the other on the flow and enthalpy change of the refrigerant plus the power input to the indoor fan. The smooth curves are second order curve fits to the data derived from experiment. Shown also, for comparison, are the values for this unit published by the Air Conditioning and Refrigeration Institute (ARI) at the established rating points of -8.3°C (17°F) and 8.3°C (47°F) as previously discussed in Sect. 2.1. The heating capacity and COP computed from airside measurements average about 8% higher than those from the refrigerant method and are more scattered because of the greater difficulty in measuring air flows and temperatures. The standard error in heating capacity is ± 0.22 kW

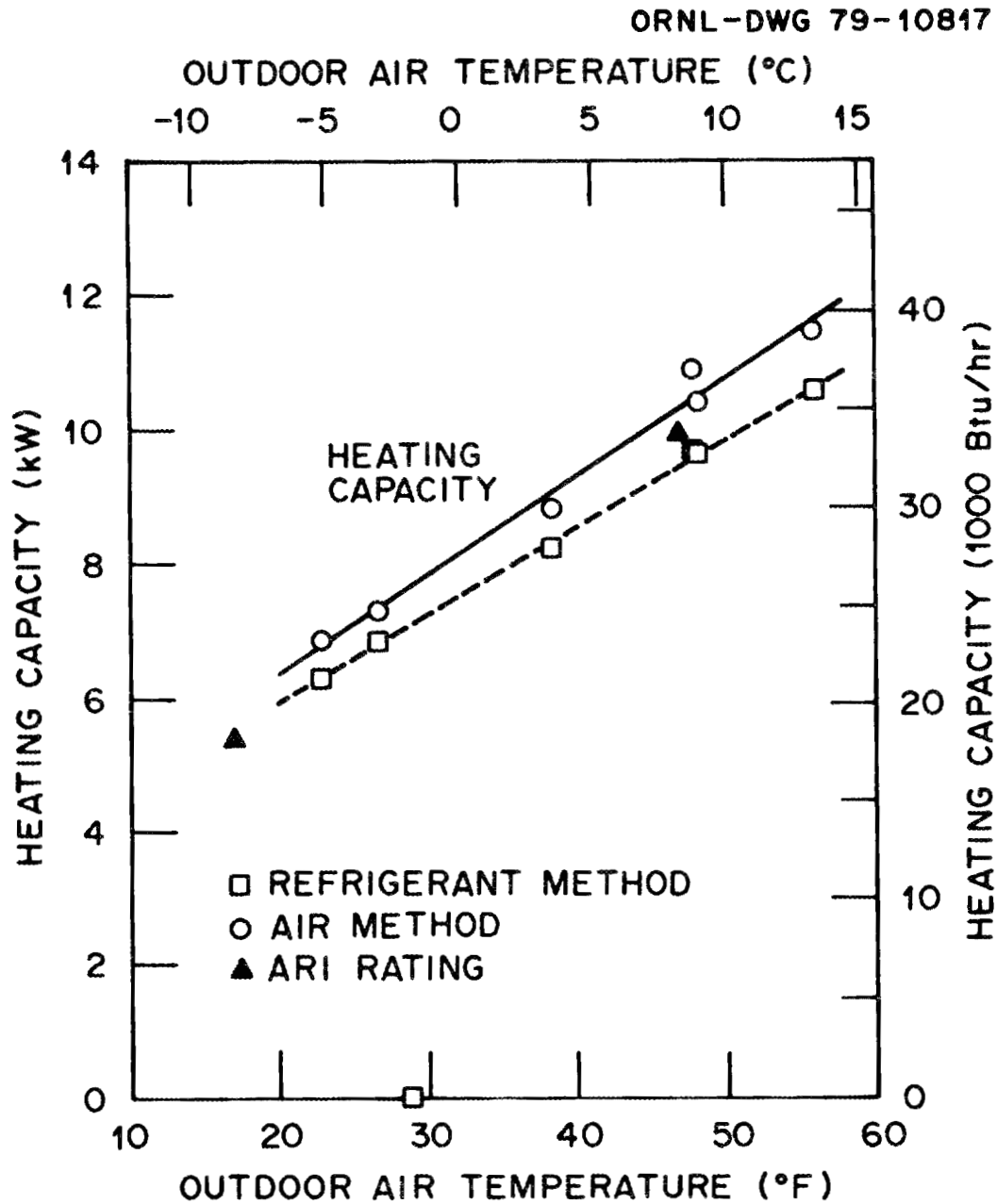


Fig. 6.1. System heating capacity as a function of outdoor air temperature.

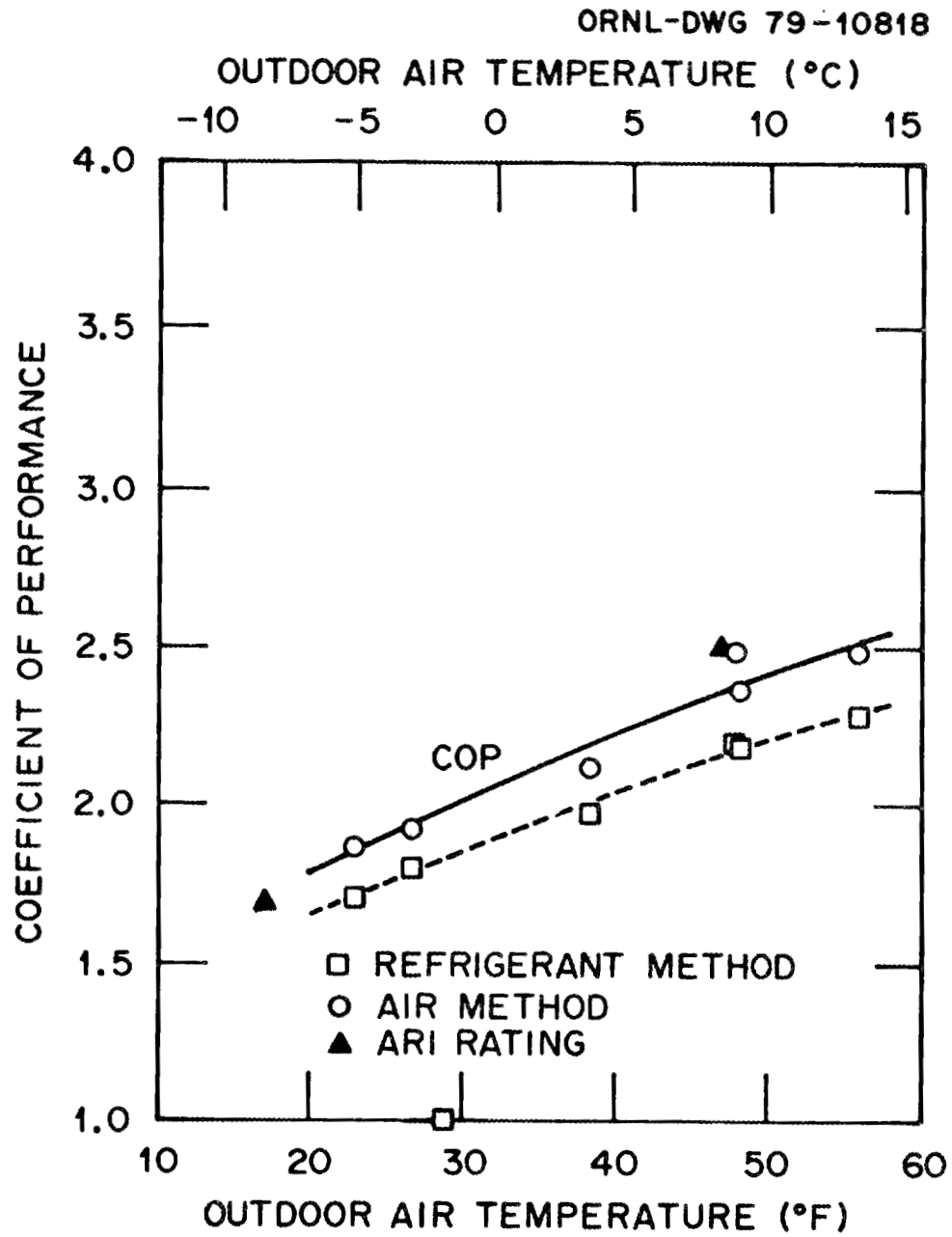


Fig. 6.2. System coefficient of performance as a function of outdoor air temperature.

for the air method and ± 0.07 kW for the refrigerant method; the corresponding measures of fit for the COP are ± 0.06 and ± 0.02 respectively.

Figure 6.3 depicts the total power input to the heat pump system as a function of outdoor air temperature. The observed power consumption at the higher rating point is 7.4% more than the ARI value; this same difference shows up in comparison of the computed COP (Fig. 6.2) with that from ARI. There is close agreement in the heating capacity at the higher rating point. No comparison, except by extrapolation, can be made at the lower rating point because limitations of the testing equipment precluded measurements at that temperature. Changes in heating capacity due to variations in the relative humidity of the outdoor air (within the non-frosting range) were not investigated.

Figures 6.1 and 6.2 show the typical characteristic of vapor-compression heat pump systems, that is, decreasing heating capacity and COP with decreasing outdoor air temperatures. The reduced heating capacity at lower ambient temperatures is due to the decrease in suction-gas density and the corresponding reduction in refrigerant mass flow rate as a consequence of the reduced outdoor coil temperatures. The decrease in the COP is mainly due to the increase in the compressor pressure ratio, which results in an increased power input to the system per unit mass flow of refrigerant.

6.2 Fan Performance

6.2.1 Indoor-unit fan

The indoor-unit fan is driven by a three-speed motor; the speeds are listed by the manufacturer as 950, 850, and 750 rpm. The actual fan speeds checked in our laboratory were essentially the same for the high and medium speed settings.

Figure 6.4 shows the results of the indoor fan evaluation at the high and medium speeds; no characteristic curves were obtained for the low speed setting. The efficiency shown is defined as the ratio of the delivered air power to the electrical power input to the fan motor. It represents the combined efficiency of the fan and motor, i.e., the

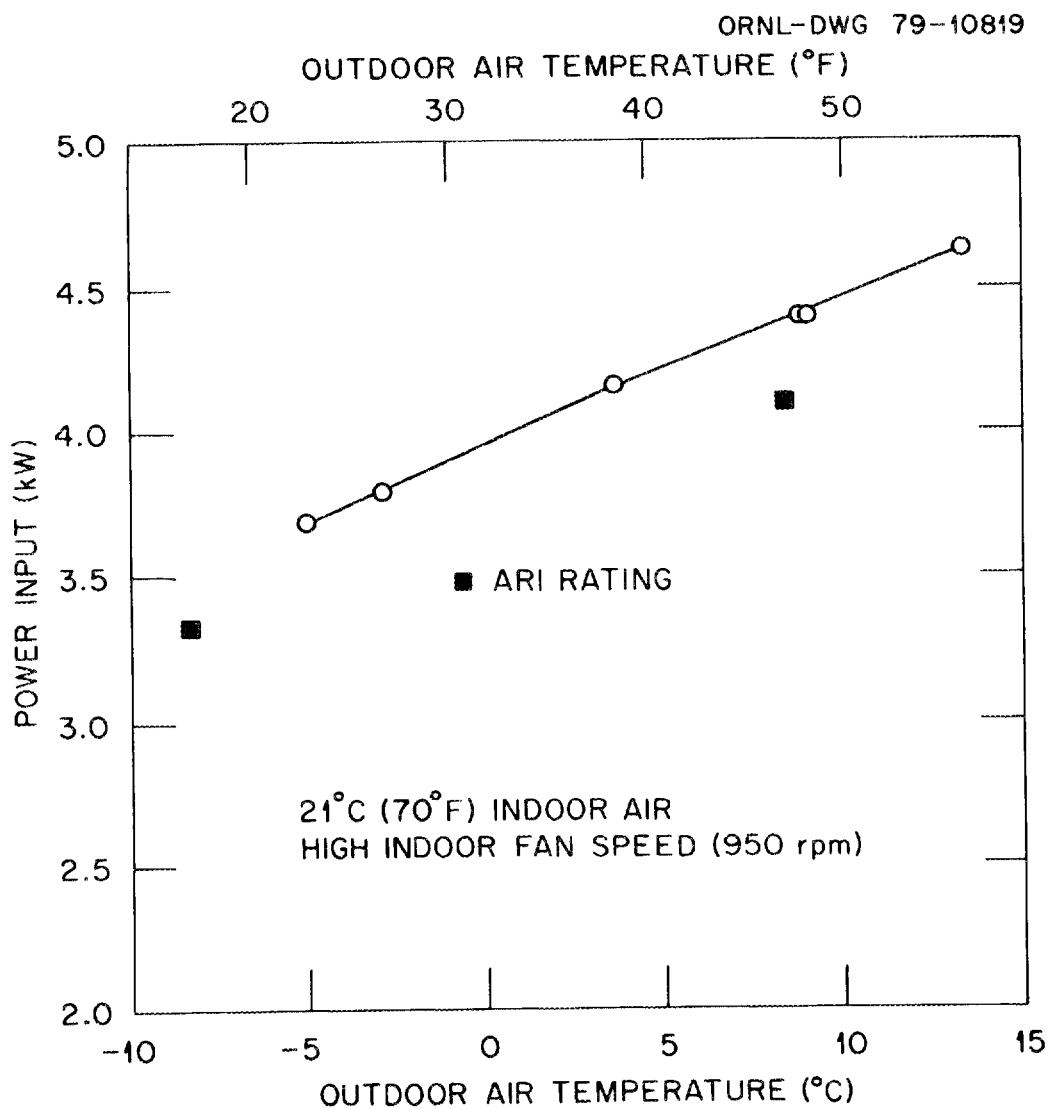


Fig. 6.3. Power input as a function of outdoor air temperature.

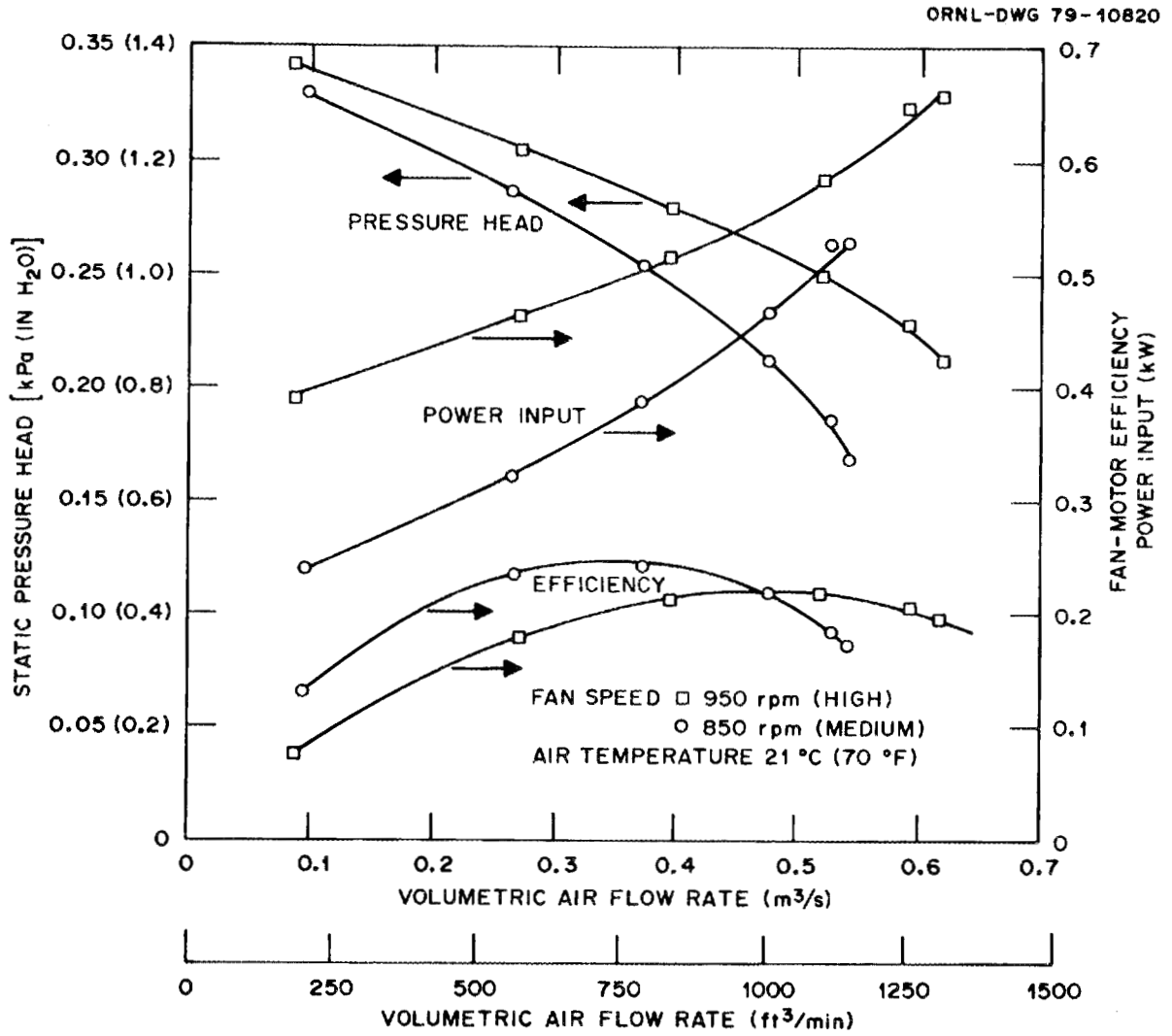


Fig. 6.4. Indoor fan characteristics.

product of the separate efficiencies. In the case of the indoor fan, this efficiency peaks at a value of about 0.25 at an airflow rate of about 0.35 m³/s (750 ft³/min) at the medium speed setting of the fan. For the high speed setting, 950 rpm, the efficiency peaks at about 0.50 m³/s (1050 ft³/min), with a value of about 0.22. The flow rates used in the system tests range from 0.51 to 0.55 m³/s (1080 to 1150 ft³/min), reasonably close to the rate for maximum efficiency at high speed of the fan and motor combination installed in the unit, and within the range of flow rates suggested by the manufacturer. The data from the tests of fan performance are shown in Appendix B.

6.2.2 Outdoor-unit fan

Figure 6.5 shows the performance characteristics of the outdoor-unit fan and motor measured without the pressure drop due to the air circulating loop. For this unit, the combined motor and fan efficiency peaks at about 1.038 m³/s (2200 ft³/min) with a value of 0.14. The rated flow of outdoor air is 1.32 m³/s (2800 ft³/min) for a unit installed according to the manufacturer's instructions at which the combined efficiency is 0.11. The outdoor fan is thus expected to operate at less than peak efficiency for an unfrosted coil. It may be anticipated, however, that frost accumulation on the outdoor coil will increase the resistance to airflow, thereby decreasing the flow rate, and shifting the operation of the fan and motor toward the peak efficiency.

6.3 Heat Exchanger and Refrigerant Metering Device Performance

As in the case of the low-first-cost heat pump previously evaluated,¹ the performance data representing the operation of the heat exchangers and the metering device are discussed together because of the interrelated operation of these components. The condensing pressure is determined by both the restriction of the metering device and the heat transfer capacity of the condenser.

Operating conditions on the evaporator side of the heat pump system are not directly controlled by the metering device; the evaporator

ORNL-DWG 79-10821

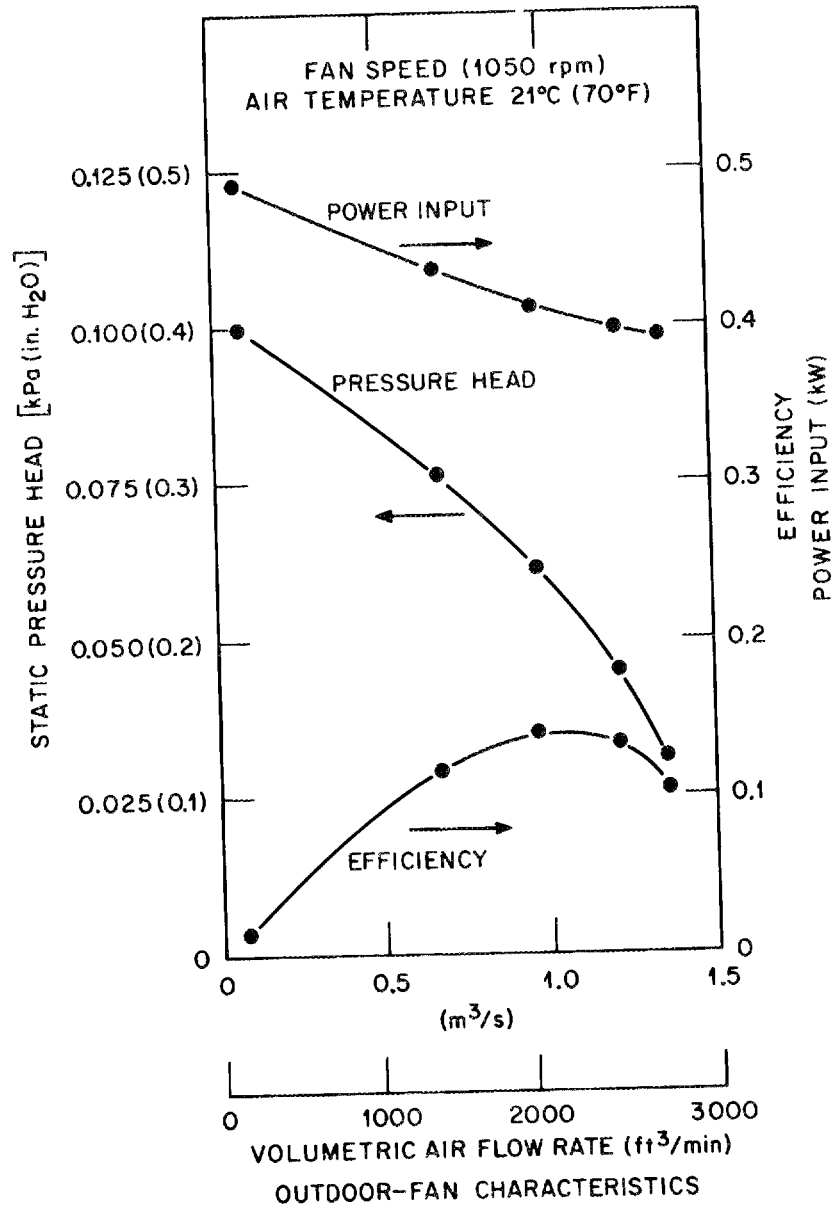


Fig. 6.5. Outdoor fan characteristics.

reaches a refrigerant temperature-pressure level which allows the flow-rate capacity of the compressor to match the flow-rate balance established on the high-pressure side of the system. The presence of a suction-line accumulator that is at least partially filled with liquid refrigerant influences the condition of the refrigerant at the evaporator exit. The experimental results show that the superheat at that point never exceeds 2.2 C° (4 F°) over the range of outdoor temperatures observed in these tests.

6.3.1 Condenser (indoor coil)

Table 6.1 shows condenser operating characteristics as a function of outdoor air temperatures ranging from -5.0 C° (23 F°) to 13.3 C° (56 F°). The refrigerant subcooling at exit from the condenser varies from 2.7 C° (4.8 F°) at the low ambient temperature to 15.7 C° (28.3 F°) at the high ambient temperature. The difference between refrigerant condensing temperature and mean air temperature (fifth column) varies from 4.9 to 22.6 C° (21.5 to 40.7 F°) for the same ambient temperature range. The sixth column shows the difference between the temperature of the refrigerant exiting the coil and the average temperature of the indoor air. This difference varies between 13.7 and 15.4 C° (24.7 and 27.7 F°).

The indoor heat exchanger provides five parallel refrigerant circuits as shown in Fig. 6.6. Measurement of return-bend temperatures reveals that some of these circuits operate with a substantial amount of liquid refrigerant in them. Figure 6.7 shows temperature profiles of one such circuit for four operating conditions. In all four cases the desuperheating is quickly accomplished. At the higher outdoor air temperatures, the two-phase region occupies less than half the circuit, with the subcooling region starting at tube number 10. For the lower ambients, the condensing region is considerably longer. The temperatures shown on the graph were measured by thermocouples attached to the return bends and covered with foamed elastomer insulation.

6.3.2 Evaporator (outdoor coil)

The operating characteristics of the evaporator (outdoor heat exchanger) are presented in Table 6.2 for the same range of outdoor air

Table 6.1. Steady-state indoor coil (condenser) performance

Outdoor air temperature ^a [°C (°F)]	Condensing temperature ^b [°C (°F)]	Exit subcooling [C° (F°)]	Heat transferred [kW (Btu/hr)]	Mean ΔT refriger.-air ^c [C° (F°)]	Minimum ΔT refriger. out-air in [C° (F°)]
-5.1 (22.9)	38.4 (101.1)	2.7 (4.9)	5.67 (19,360)	11.9 (21.5)	14.3 (25.7)
-2.9 (26.7)	39.6 (103.3)	3.9 (7.0)	6.21 (21,206)	13.0 (23.4)	14.7 (26.4)
3.6 (38.4)	45.7 (114.2)	9.9 (17.8)	7.58 (25,864)	17.4 (31.3)	14.4 (26)
9.0 (48.2)	50.0 (122.0)	14.6 (26.2)	9.03 (30,812)	20.8 (37.5)	13.7 (24.7)
13.3 (56.0)	52.2 (126.0)	15.7 (28.3)	9.94 (33,914)	22.6 (40.7)	15.4 (27.7)

^aRuns 6, 5, 4, 2, and 7 respectively, as listed in Table B.1. Nominal indoor temperature is 21°C (70°F).

^bBased on high-side pressure.

^cApproximate value taken as the difference between condensing temperature and mean air temperature.

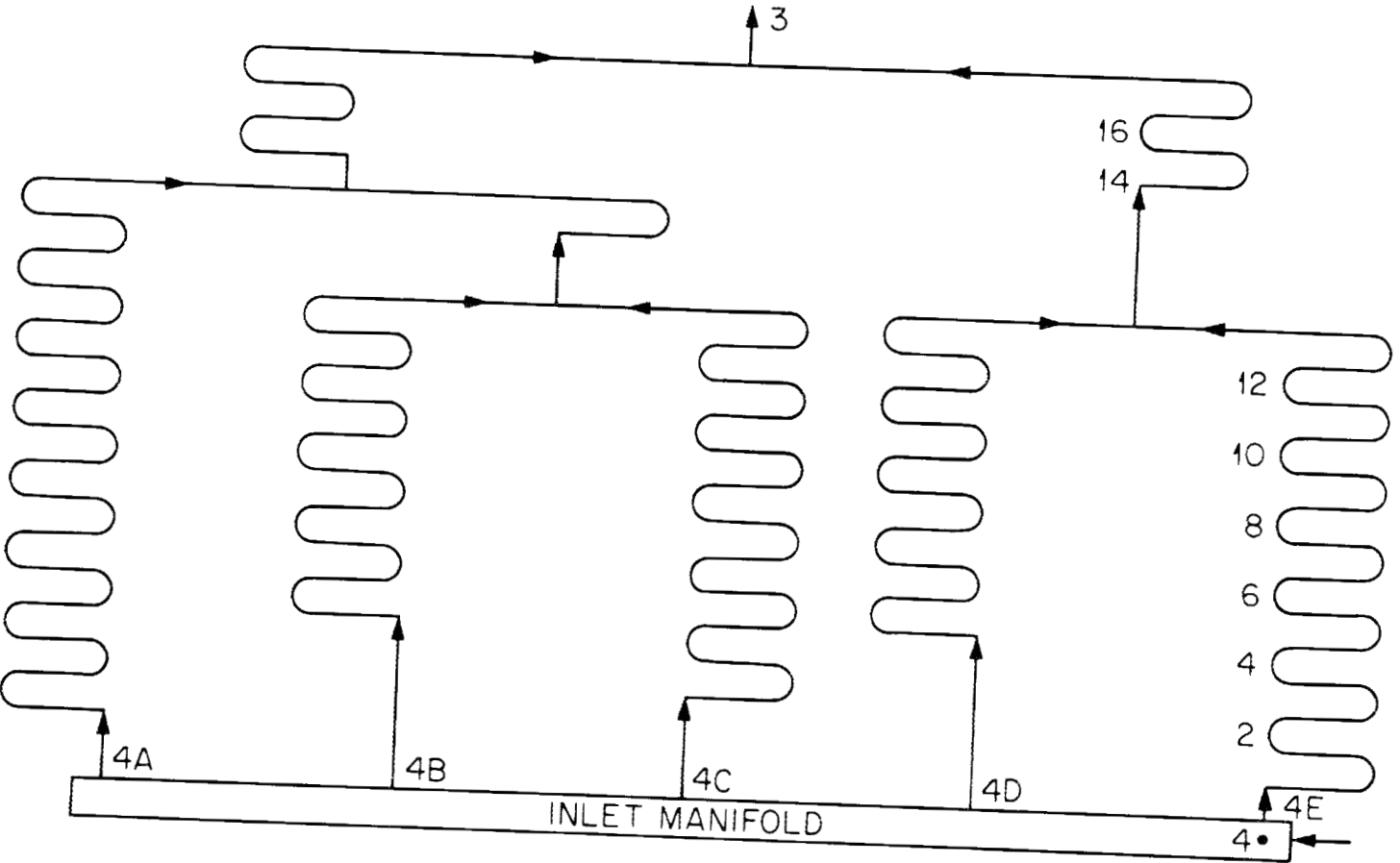


Fig. 6.6. Schematic diagram of the refrigerant circuits in the indoor coil.

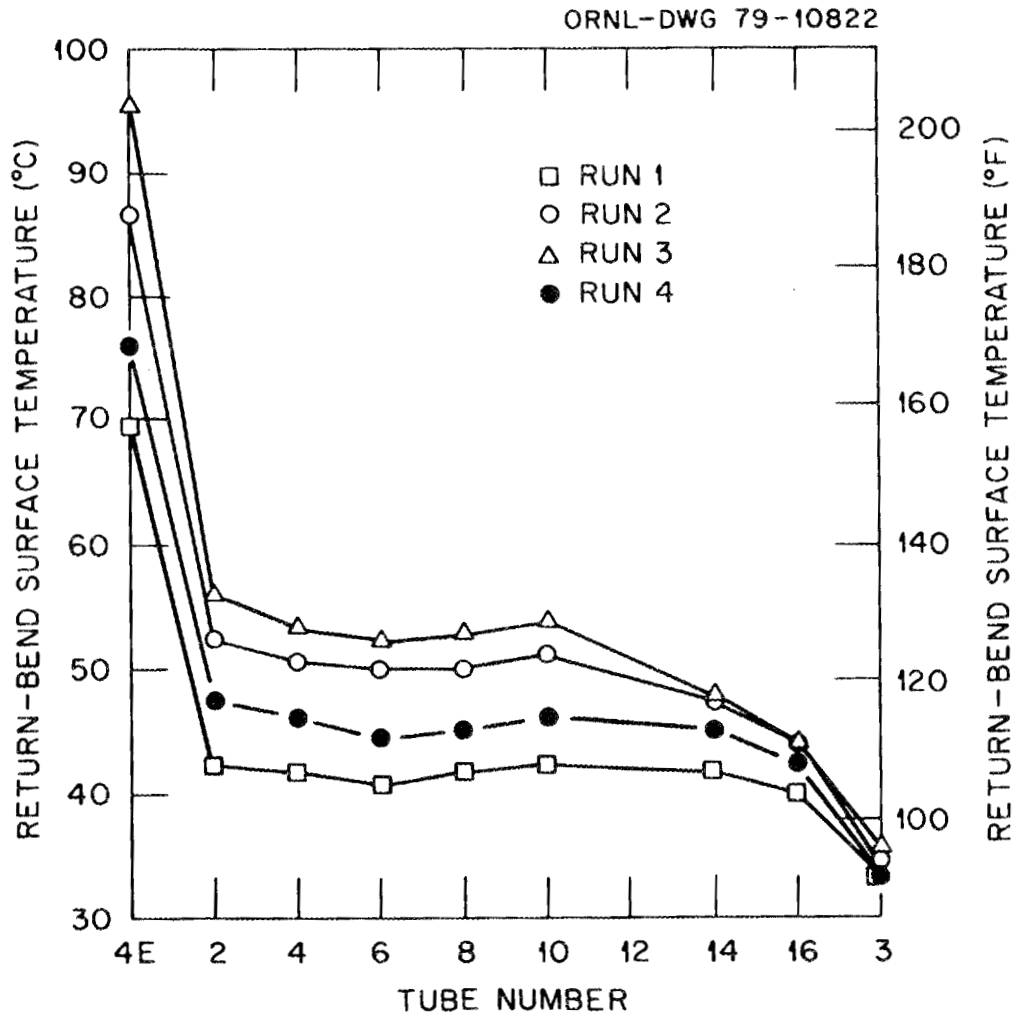


Fig. 6.7. Temperature profiles for one refrigerant circuit of the indoor coil. The outdoor air temperature was 1.0°C (33.8°F) for run 1, 13.3°C (56.0°F) for run 2, 18.6°C (65.4°F) for run 3, and 5.7°C (42.3°F) for run 4.

Table 6.2. Steady-state outdoor coil (evaporator) performance

Outdoor air temperature ^a [°C (°F)]	Evaporating temperature ^b [°C (°F)]	Exit superheat [C° (F°)]	Heat transferred [kW (Btu/hr)]	Mean ΔT air-refrig. ^c [C° (F°)]	Minimum ΔT air in-refrig. out [C° (F°)]
-5.1 (22.9)	-12.7 (9.2)	1.1 (2.0)	4.81 (16,420)	7.3 (13.1)	5.9 (10.6)
-2.9 (26.7)	-10.9 (12.4)	0.8 (1.5)	5.29 (18,049)	7.4 (13.3)	6.4 (11.6)
3.6 (38.4)	-6.3 (20.6)	0.9 (1.7)	6.37 (21,756)	8.9 (16.0)	8.1 (14.6)
9.0 (48.2)	-1.2 (29.8)	0 (0)	7.51 (25,629)	8.7 (15.6)	9.4 (17.0)
13.3 (56.0)	-0.2 (31.4)	1.9 (3.5)	8.08 (27,579)	11.3 (20.3)	10.8 (19.4)

^aRuns 6, 5, 4, 2, and 7 respectively, as listed in Table B.1. Nominal indoor air temperature is 21°C (70°F).

^bBased on observed low-side pressure.

^cApproximate value taken as the difference between mean air temperature and refrigerant evaporating temperature.

temperatures as was considered for the indoor coil. The evaporating temperatures, calculated from the observed pressure at the suction line, vary in the expected manner with changing outdoor temperature. The superheat of the refrigerant at the compressor inlet is sharply limited, probably by the presence of liquid refrigerant in the suction-line accumulator.

The approach of refrigerant temperature at the evaporator exit to that of the inlet air is in the expected range for all of the air temperatures at which tests were conducted.

6.4 System Heat Losses

Heat losses from the system ranged from 14 to 25% of the observed heating capacity. These losses occur at the compressor shell and discharge line, including the reversing valve. They are compared to the system heating capacity in Table 6.3.

Table 6.3. System heat loss rates

Outdoor air temperature [°C (°F)]	Compressor-shell heat rejection [kW (Btu/hr)]	Discharge line heat loss rate ^a [kW (Btu/hr)]	System heat capacity [kW (Btu/hr)]
-5.1 (22.9)	1.17 (3994)	0.41 (1410)	6.30 (21,503)
-2.9 (26.7)	1.15 (3942)	0.44 (1489)	6.84 (23,357)
3.6 (38.4)	1.22 (4170)	0.45 (1436)	8.21 (28,014)
9.0 (48.2)	1.11 (3793)	0.52 (1773)	9.62 (32,822)
13.3 (56.0)	0.91 (3095)	0.54 (1850)	10.57 (36,064)

^aIncludes reversing valve loss.

Heat rejection from the compressor shell is computed as the difference between the electric power input to the compressor motor and the enthalpy gain of the refrigerant between shell inlet and discharge. This loss ranges from 25 to 45% of the power input to the compressor motor, and though it possibly may be exaggerated by errors in temperature measurement due to heat conduction in the refrigerant lines near the shell,

it is obviously substantial. The loss could be reduced by insulating the compressor shell, but care must be exercised that the resulting increase in internal temperatures in the motor-compressor unit does not cause or contribute to premature failure of the electrical insulation or the lubricant system. Heat losses from the discharge line were calculated from the differences in enthalpy observed at the compressor shell discharge and the condenser inlet. These losses thus include the heat transferred to the suction gas at the reversing valve.

6.5 Compressor Operation

Compressor performance parameters for a range of ambient temperatures are shown in Table 6.4. The refrigerant mass flow rate increases with increasing outdoor air temperatures because the suction-line pressure, and therefore the density of refrigerant reaching the compressor, increases at the higher ambient temperatures. The increased mass flow rate represents an increased pumping rate of the compressor, which is reflected in the higher power consumption of the compressor motor at the higher temperatures. Conversely, the pressure ratio is seen to decrease as the outdoor air temperature increases. The decrease is rather small, however, because it is controlled by the higher temperature differences that exist at both heat exchangers at the higher ambient temperatures.

The efficiency of the motor and compressor taken together is shown in the fifth column of Table 6.4. This efficiency is calculated as the ratio of the ideal isentropic work to the observed electrical power input, with the ideal isentropic work being calculated from the observed conditions of the refrigerant at entry and the refrigerant pressure at the exit of the hermetically sealed shell containing both motor and compressor. Thus the efficiency quoted accounts for losses in the motor, irreversible thermodynamic losses due to gas throttling at the valves and muffler, suction gas heating by the motor, losses due to mechanical friction, and for internal heat transfer. It should not, of course, be compared with efficiencies based on refrigerant conditions at the suction and discharge ports of the compressor itself. The combined efficiency ranges from 0.44 to 0.49.

Table 6.4. Compressor operating characteristics

Outdoor air temperature [°C (°F)]	Power input to motor [kW (Btu/hr)]	Refrigerant mass flow rate [kg/s (lb/hr)]	Pressure ratio	Combined motor-compressor efficiency ^a	Volumetric efficiency
-4.5 (22.9)	2.61 (8,900)	0.030 (235)	4.6	0.44	0.56
-2.9 (26.7)	2.73 (9,300)	0.032 (255)	4.4	0.44	0.57
3.6 (38.4)	3.10 (10,600)	0.039 (306)	4.4	0.46	0.59
9.0 (48.2)	3.39 (11,600)	0.045 (357)	4.1	0.47	0.58
13.3 (56.0)	3.58 (12,200)	0.048 (382)	4.2	0.49	0.61

^aThis efficiency is defined as the ratio of ideal isentropic work (between actual shell inlet conditions of the refrigerant and the discharge pressure) to the electrical power input to the compressor motor.

The sixth column in Table 6.4 shows the volumetric efficiency of the compressor, based on the conditions of the refrigerant at the shell inlet. It varies from 0.56 to 0.61 and is calculated from the following expression:

$$\eta_v = \frac{\dot{m}_{\text{ref}}}{\rho_s DN} ,$$

where

η_v = volumetric efficiency,

\dot{m}_{ref} = observed refrigerant mass flow rate,

ρ_s = density of refrigerant vapor at hermetic unit shell inlet,

D = compressor displacement (swept volume),

N = compressor speed.

7. FROSTING-DEFROSTING TESTS

7.1 System Performance under Frosting Conditions

Tests of the heat pump under conditions that allow for frost formation on the outdoor coil were conducted in order to evaluate degradation of performance parameters under these conditions, and to observe the response of the system to stresses so imposed. Tests were conducted at the outdoor air temperatures and humidities shown previously in Table 2.3.

The performance parameters measured in each of the frosting tests include the heating capacity, COP, refrigerant pressures at high and low side of the system, the refrigerant mass flow rate, compressor and outdoor fan power consumption, the airflow rate through the outdoor coil, and the air pressure drop across the coil.

The airflow rates and pressure drops were, of course, measured with the outdoor unit in the testing loop and with the booster fan operating. As previously mentioned (Sect. 2.1) the flow rates and pressure drops were higher than would be expected for a unit operating in free air, but the deviation from rated airflow rates is not expected to cause more than a 5% change in any of the performance parameters, with the possible exception of the power consumed by the outdoor fan motor. Comparisons with similar tests where no booster fan was needed indicate that the variation of the outdoor fan motor power is not atypical.

7.1.1 Test at 0.6°C (33°F) and 100% relative humidity

The test at 100% relative humidity subjected the heat pump to one of the more severe frosting conditions that it may encounter. The steam injector was placed in the airflow pattern upstream of the outdoor coil. At 100% relative humidity, the arrangement allowed fog to reach the coil. Under these conditions, frost formation was rapid and heavy enough to require that the tests be terminated after 50 min because the airflow rate had dropped to less than 20% of its nominal value, accompanied by rapid decreases in the refrigerant pressures and flow rate, a condition that may not provide for proper cooling of the compressor motor.

Figures 7.1 through 7.4 show the variation of the measured parameters as functions of time after the outdoor coil surface reaches 0°C (32°F). At the conclusion of the tests, the heating capacity and COP had fallen to 82% and 88% of their starting values (Fig. 7.1), a remarkably small decrease in view of the drop in airflow rate to 16% of its original value (Fig. 7.2). Refrigerant pressures and flow rate decreased by amounts similar to those observed for the heating capacity and COP. The decreased refrigerant flow rate allows for a corresponding drop in power input to the compressor motor, while the rapidly increasing air pressure drop across the coil requires an increase in the power consumption rate of the outdoor fan.

7.1.2 Tests at 0.6°C (33°F) and 92 to 97% relative humidity

The severity of the frosting test at 100% relative humidity can be appreciated by comparison of the results of those tests with the tests at the same ambient dry bulb temperature but slightly lower relative humidity. The tests at 92 to 97% relative humidity revealed the same degradation of performance, but at an appreciably slower rate; comparisons of Figs. 7.5 through 7.8 with their counterparts, Figs. 7.1 through 7.4, show that the unit could run almost twice as long at the lesser humidity before the performance parameters had dropped to the levels observed at the conclusion of the more severe tests.

7.1.3 Tests at -2.2°C (28°F) and 80 to 85% relative humidity

Further reduction of the relative humidity, even though it was accompanied by a small drop in the dry bulb temperature, produced test results that are strikingly different from the results of the tests described above. After about 90 min of frosting operation all of the measured performance parameters, except the air pressure drop across the outdoor coil, were within 10% of their starting values. While the air-side pressure drop had risen noticeably, the airflow rate had decreased only 3%. As may be seen in Figs. 7.9 through 7.12, none of the parameters had begun changing rapidly near the end of the tests as they had in the tests at higher humidities.

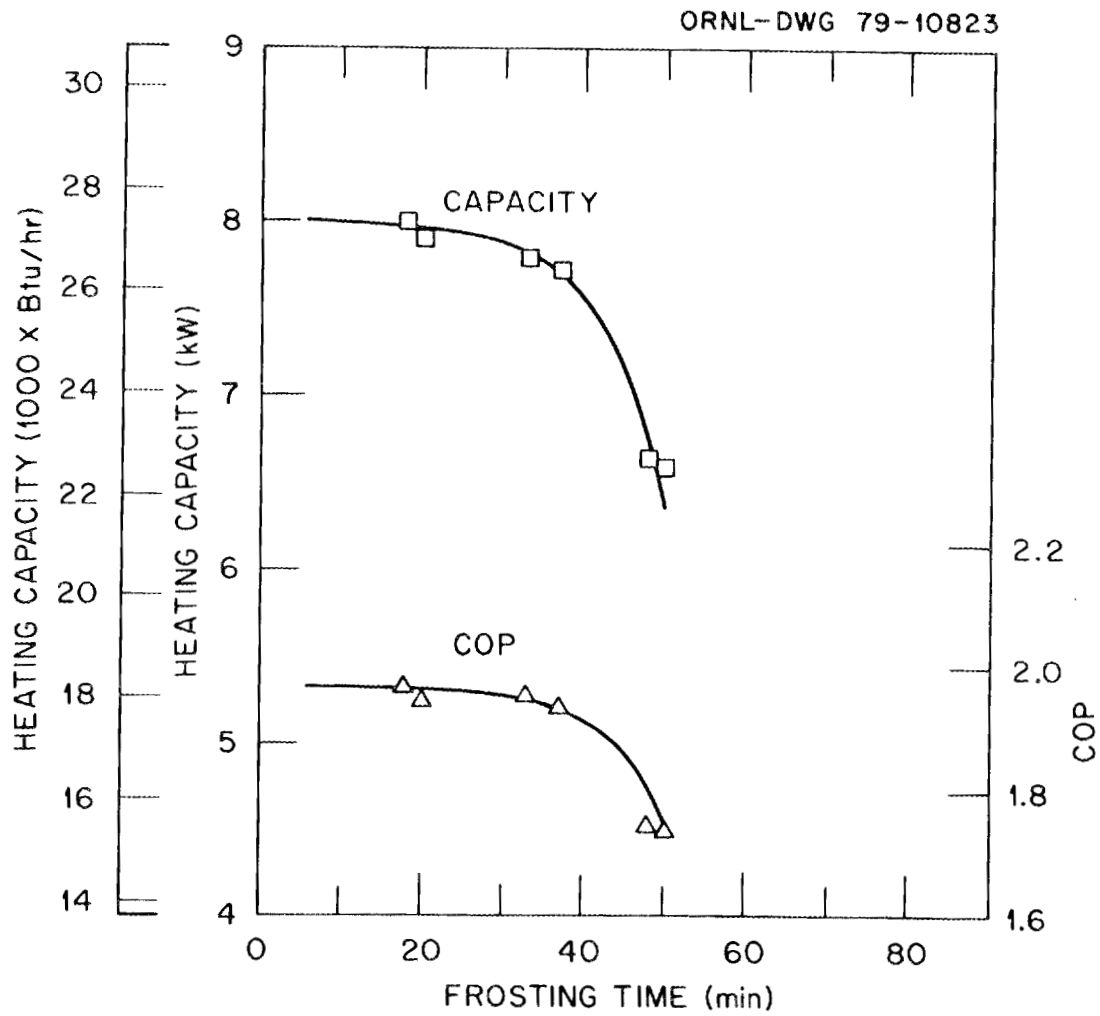


Fig. 7.1. Heating capacity and COP during a 50 min frosting period with outdoor air at 0.6°C and 100% relative humidity.

ORNL-DWG 79-10824

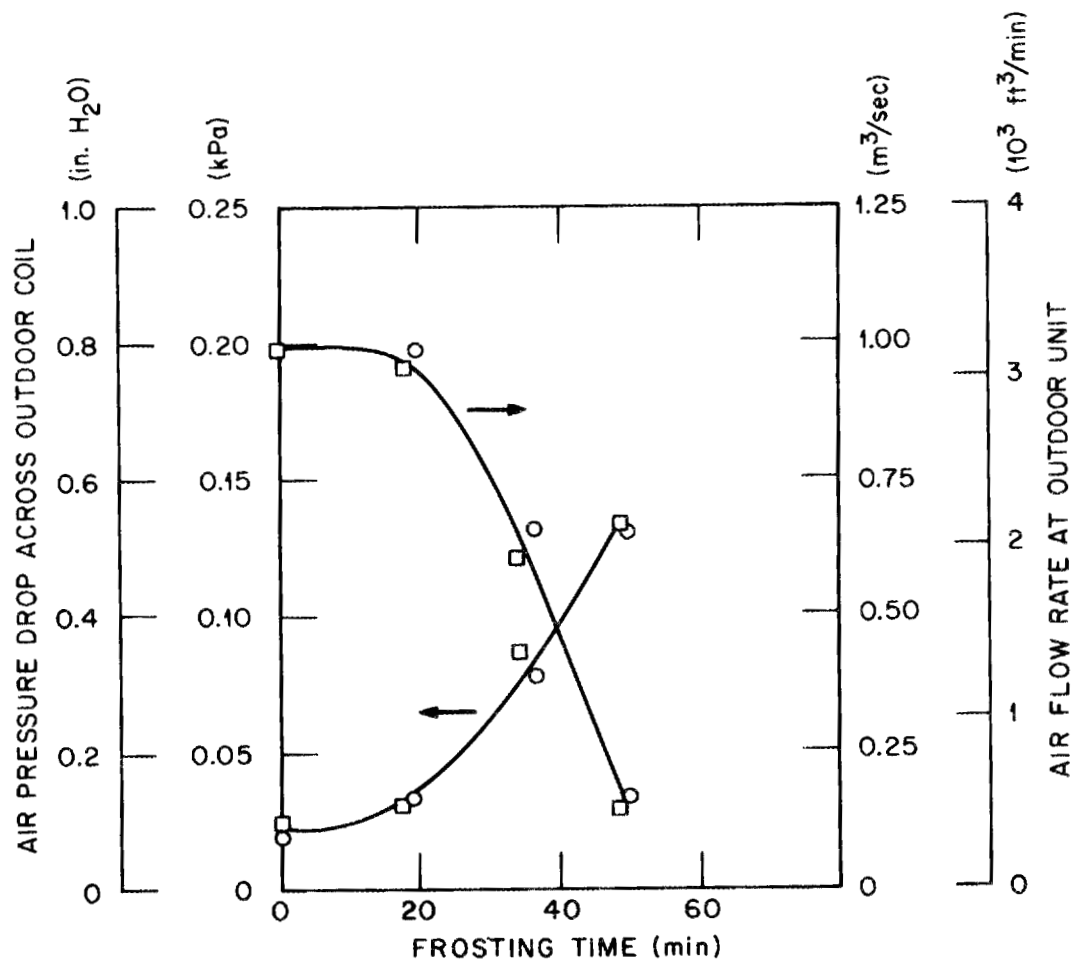


Fig. 7.2. Outdoor-coil air pressure drop and airflow rate during 50 min frosting period with outdoor air at 0.6°C and 100% relative humidity.

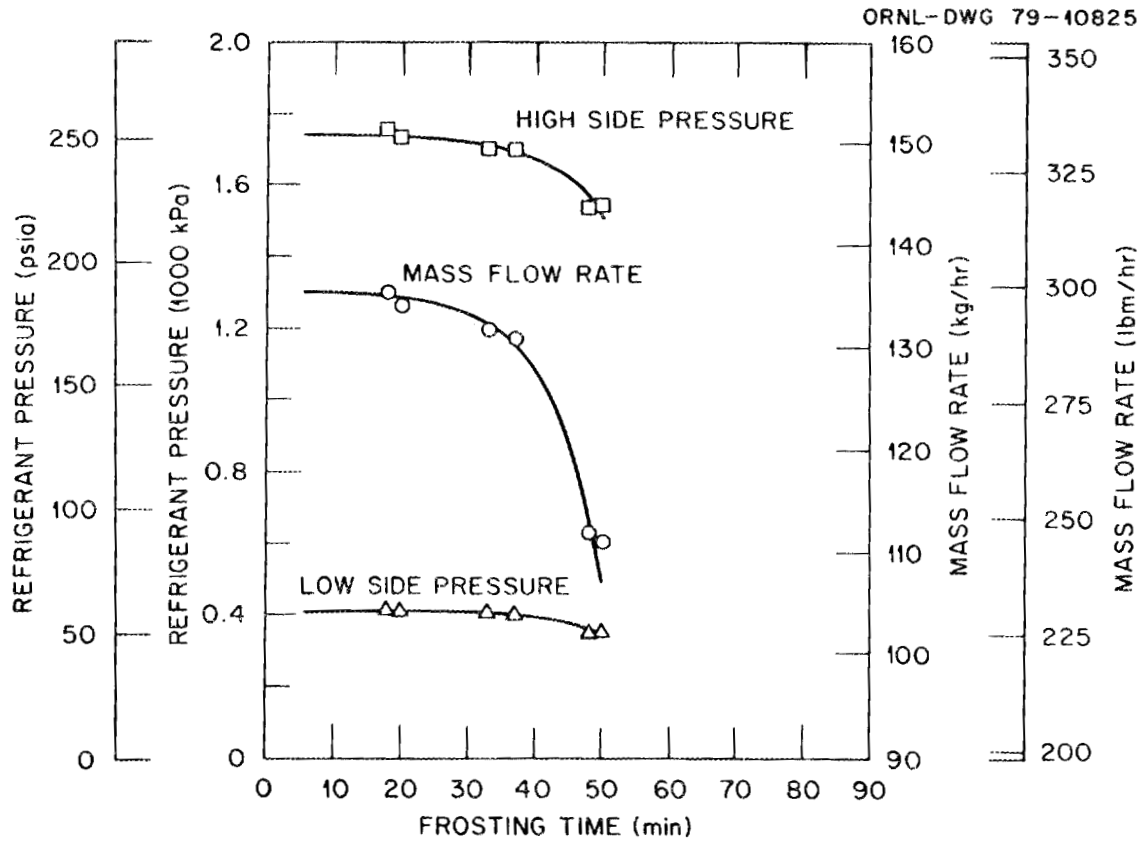


Fig. 7.3. Refrigerant pressures and flow-rates during a 50 min frosting period with outdoor air at 0.6°C and 100% relative humidity.

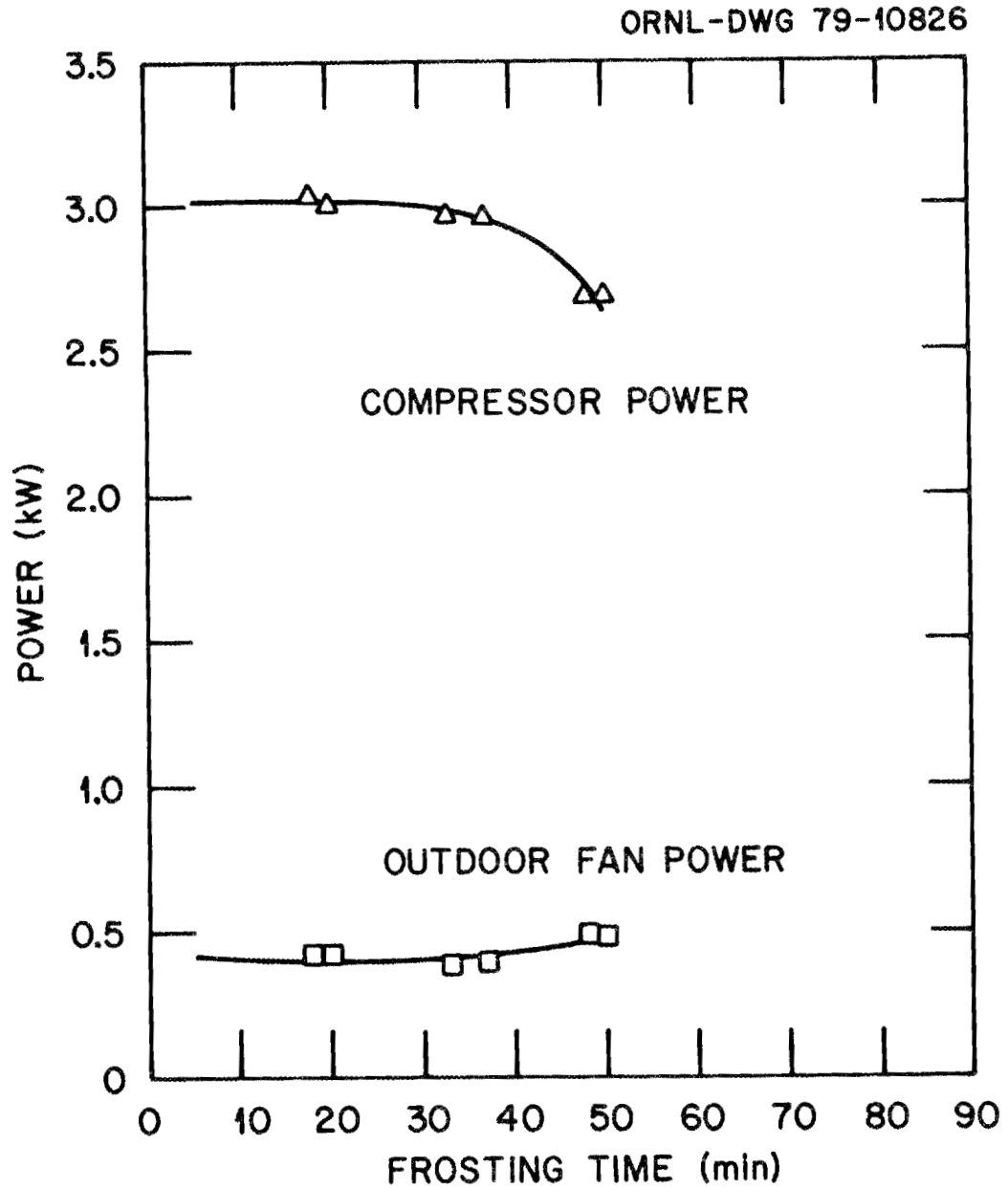


Fig. 7.4. Compressor and outdoor fan power consumption during a 50 min frosting period with outdoor air at 0.6°C and 100% relative humidity.

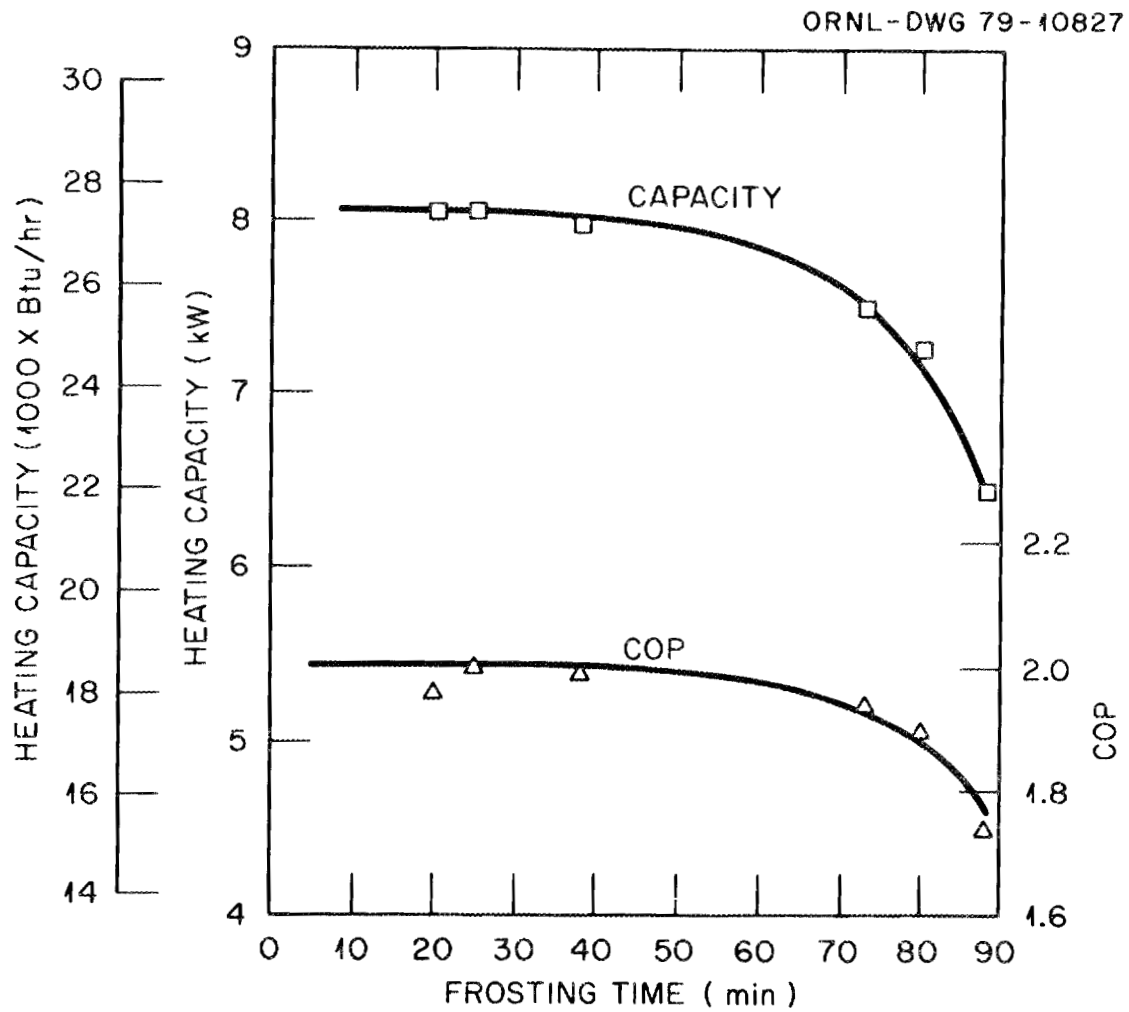


Fig. 7.5. Heating capacity and COP during a 90 min frosting period with outdoor air at 0.6°C and 92-97% relative humidity.

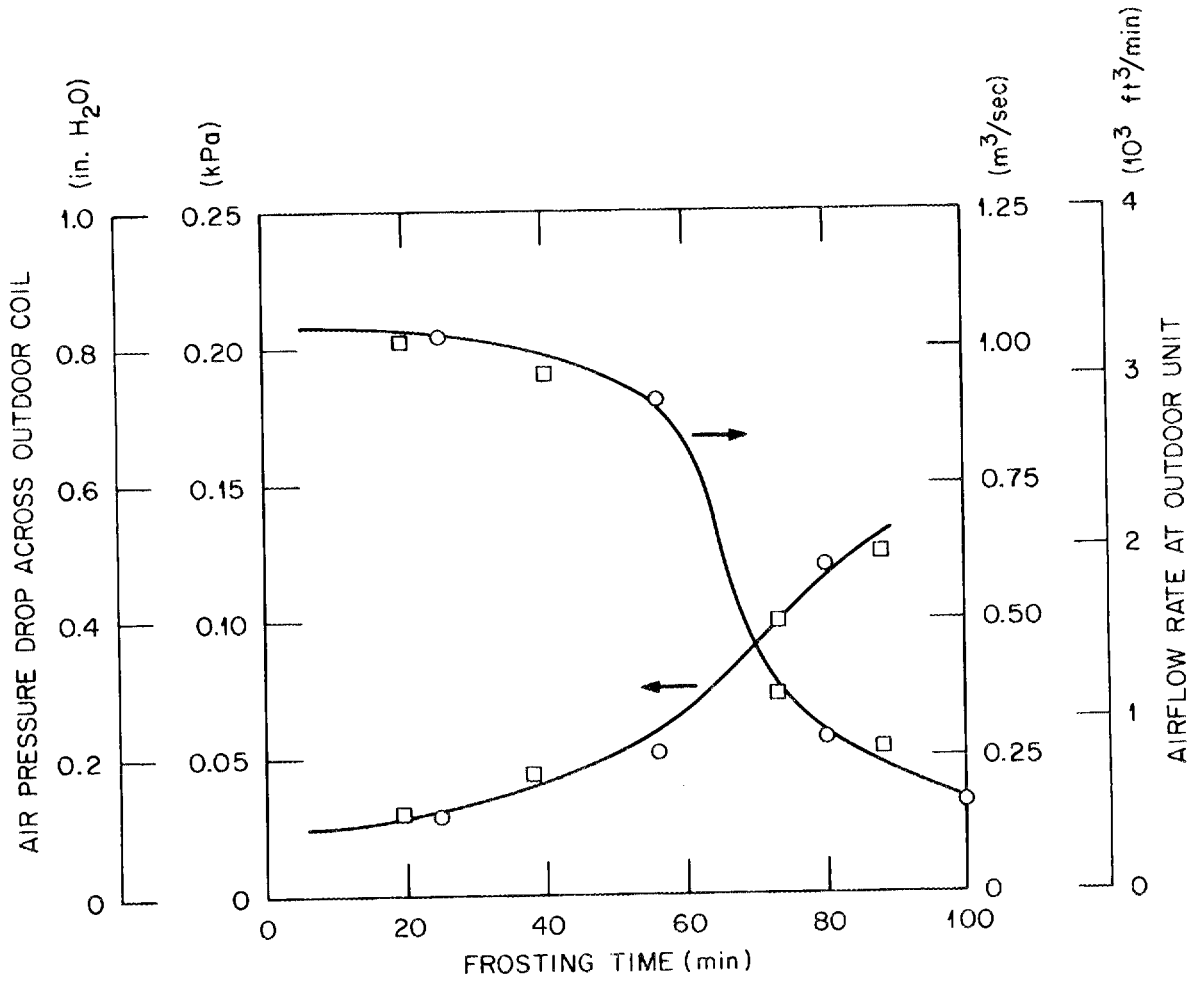


Fig. 7.6. Outdoor-coil air pressure drop and airflow rate during a 90 min frosting period with outdoor air at 0.6°C and 92-97% relative humidity.

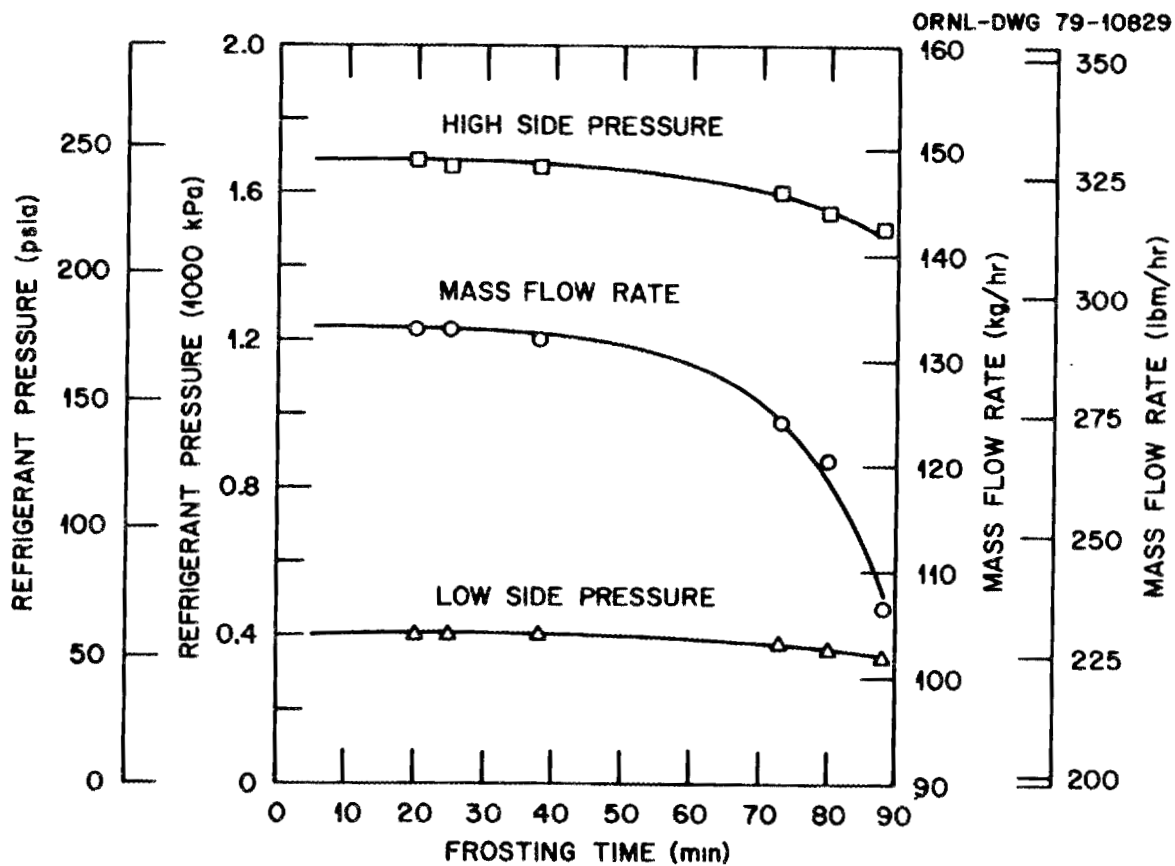


Fig. 7.7. Refrigerant pressures and flow rates during a 90 min frosting period with outdoor air at 0.6°C and 92-97% relative humidity.

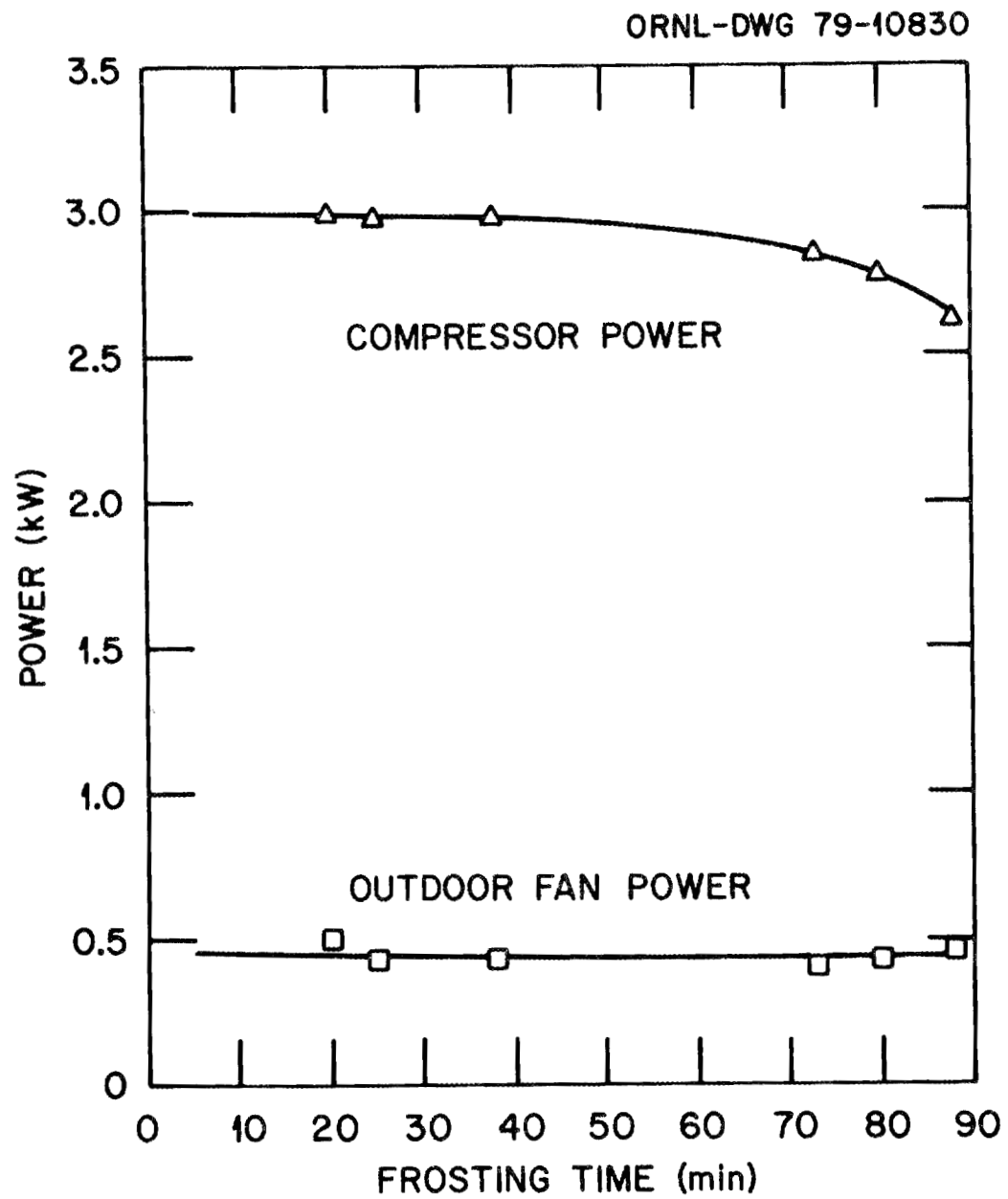


Fig. 7.8. Compressor and outdoor fan power consumption during a 90 min frosting period with outdoor air at 0.6°C and 92-97% relative humidity.

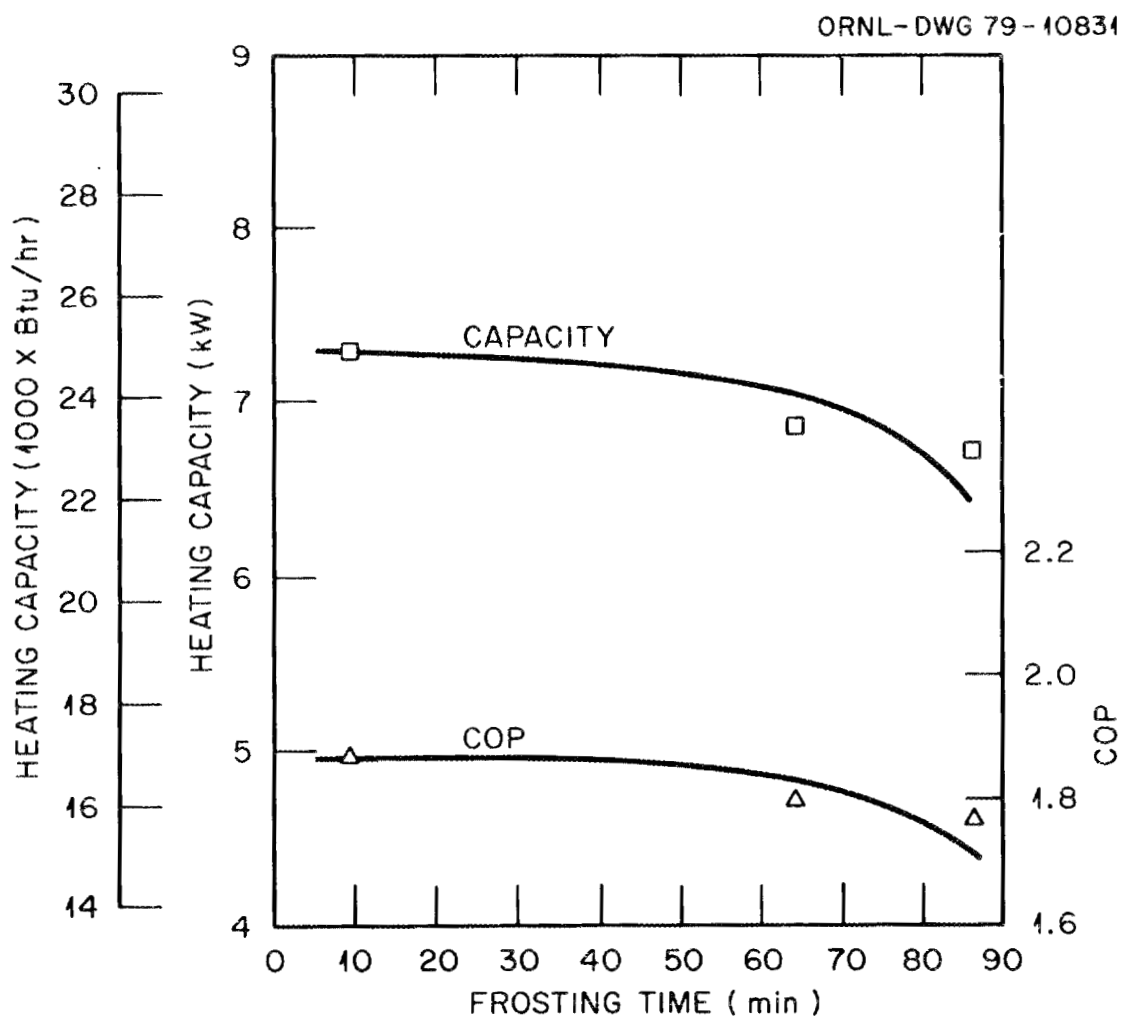


Fig. 7.9. Heating capacity and COP during a 90 min frosting period with outdoor air at -2.2°C and 80-85% relative humidity.

ORNL-DWG 79-10832

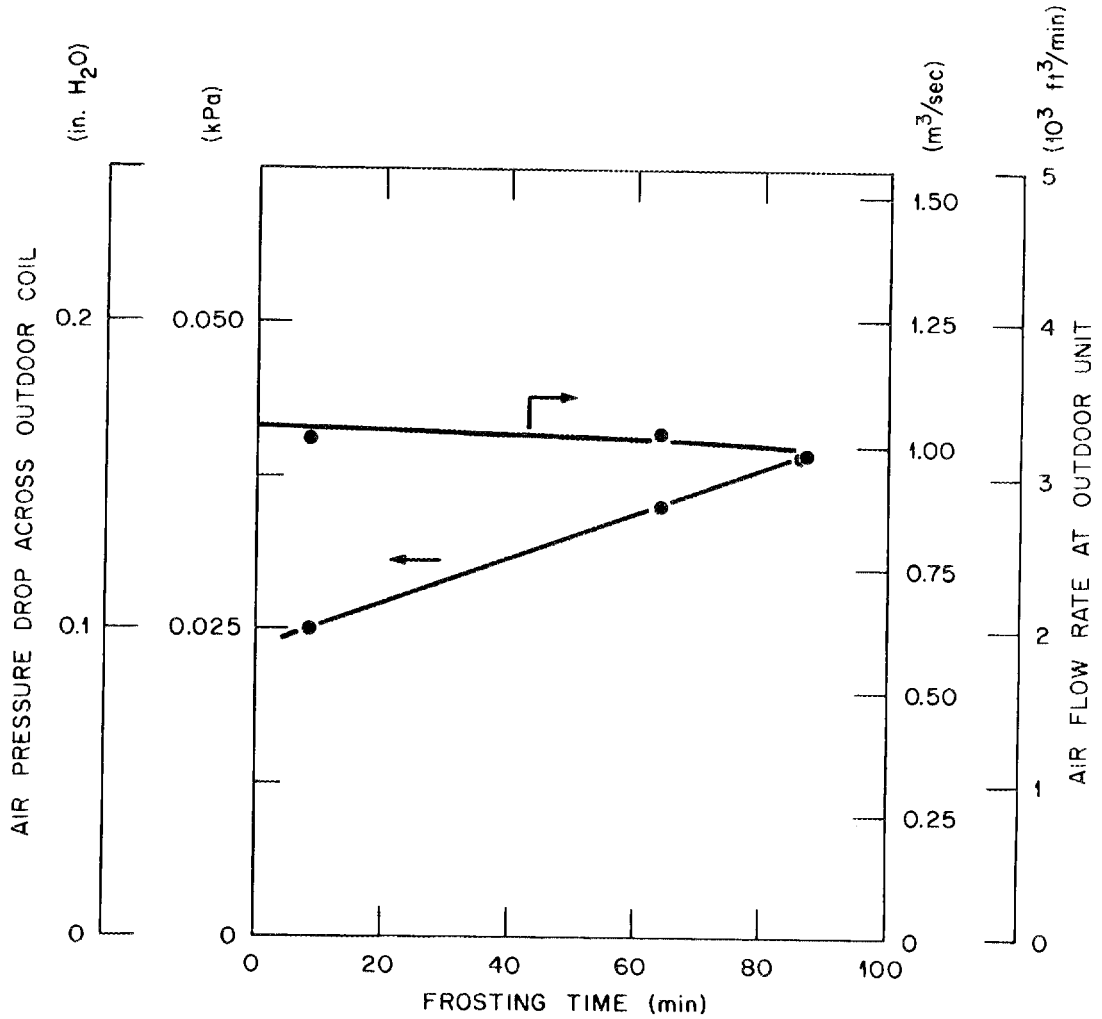


Fig. 7.10. Outdoor-coil air pressure drop and airflow rate during a 90 min frosting period with outdoor air at -2.2°C and 80-85% relative humidity.

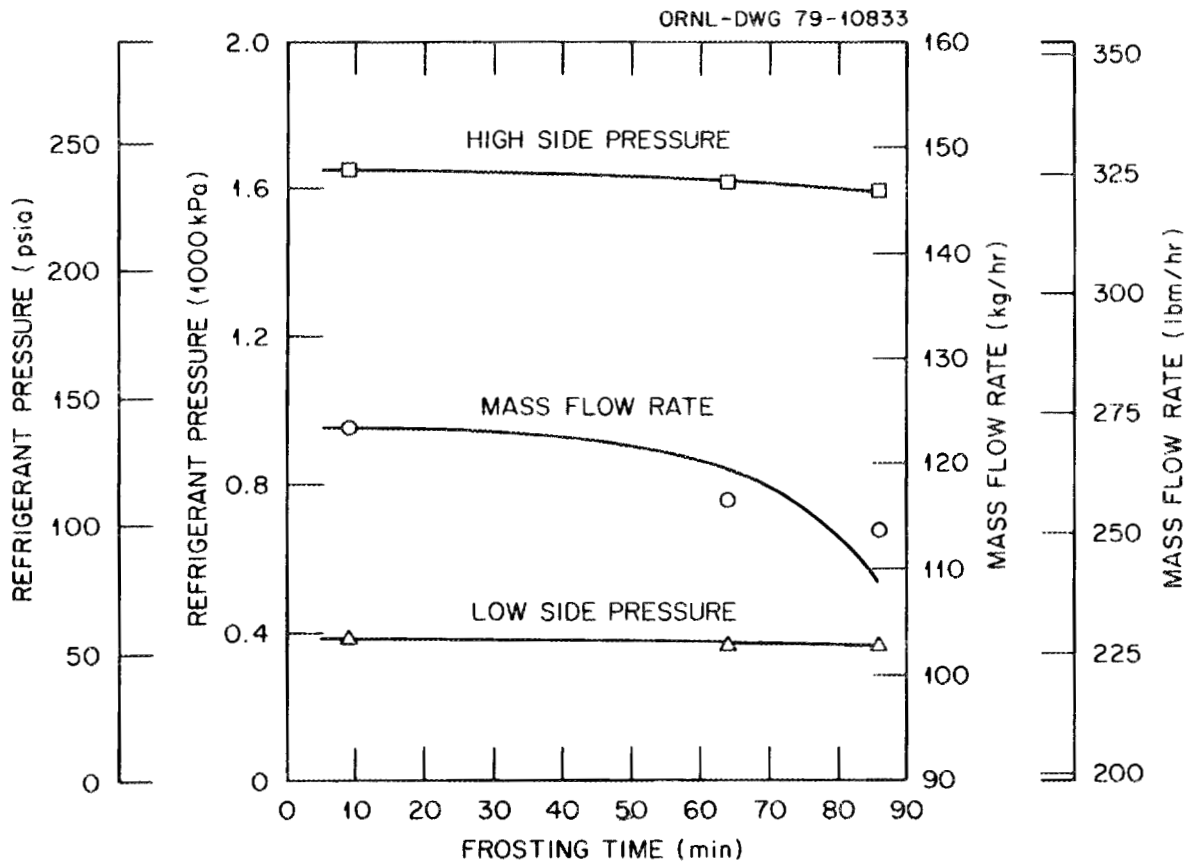


Fig. 7.11. Refrigerant pressures and flow rates during a 90 min frosting period with outdoor air at -2.2°C and 80-85% relative humidity.

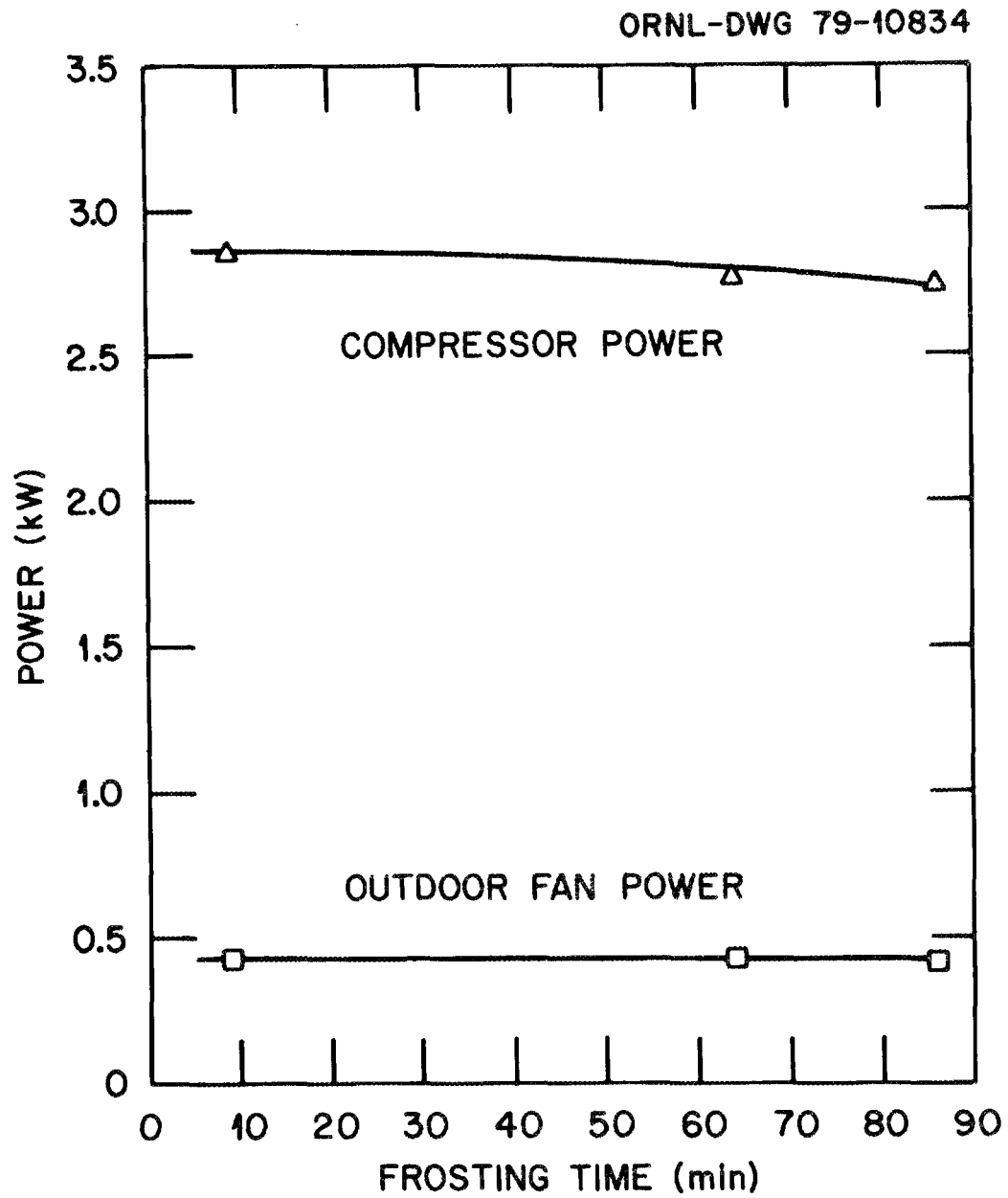


Fig. 7.12. Compressor and outdoor fan power consumption during a 90 min frosting period with outdoor air at -2.2°C and 80-85% relative humidity.

7.1.4 Defrost water collection

After the operation of the heat pump under frosting-defrosting conditions, an indication of the amount of frost accumulated on the heat exchanger surfaces was obtained by measuring the amount of water discharged by the system drain. This is an approximate method because it does not account for the water that remains on the heat exchanger surfaces and in the sheet metal tray that forms the bottom of the outdoor unit. Table 7.1 shows the data for the defrost water measured. It is apparent that some of the water formed during the first defrosting period remains on the coil or in the tray, as indicated by the greater amounts of water collected after subsequent defrosting periods.

Table 7.1. Frost accumulation as evaluated by defrost water drain collection

Outdoor air temperature [°C (°F)]	Relative humidity (%)	Approximate frosting period (min)	Water collected (ml)
0.6 (33)	100	50	1100 first defrost 1300 second defrost
0.6 (33)	92-97	90	2800 first defrost 3200 second defrost
-2.2 (28)	80-85	90	1750

7.2 Compressor Performance during the Defrosting Period

During the defrosting period, the high- and low-side refrigerant pressures and the power input to the compressor motor were recorded as functions of time after the initiation of the defrosting operation. The outdoor fan is turned off during this period, and the power consumed by the indoor fan motor is expected to remain at a constant value. The transducer used to record the low-side pressure was placed in the suction line, between the accumulator and the inlet to the compressor, and thus between the reversing valve and the compressor; the signal it sends to the strip chart recorder always represents the lowest pressure in the system regardless of the position of the reversing valve. The transducer

used to record high-side pressure is in the liquid line that connects the two heat exchangers and thus records the pressure just upstream of the flow control device for either mode of operation.

Figure 7.13 shows the recorded pressure and compressor motor input power at the end of the 50-min frosting period and the subsequent defrosting period for the tests with 0.6°C (33°F) outdoor air temperature and 100% relative humidity. Figure 7.14 shows the corresponding interval for the 90-min tests at 0.6°C (33°F) and 92 to 97% relative humidity; Figure 7.15 is for the tests at -2.2°C (28°F), 80 to 85% relative humidity.

As might be expected, the defrosting interval was longer for the more severe frosting conditions, lasting about 3.6 min following the frosting interval at 100% relative humidity, and decreasing to 2.75 min following the frosting tests at 80 to 85% relative humidity. The excursions of the recorded variables are seen to be similar for all three of the defrosting intervals.

Before the start of the defrosting operation, the indoor coil, which has been acting as the condenser, is filled in part by liquid refrigerant, partly by two-phase refrigerant. (There is very little superheating of the refrigerant in the suction line due to presence of liquid refrigerant in the suction-line accumulator.) At the start of the defrosting period, the reversing valve connects the discharge line of the compressor to the outdoor coil and the suction line (which contains the accumulator) to the end of the indoor coil that contains superheated vapor. The rapid rise in the low-side pressure during the first few seconds of the defrosting period results from the rapid transfer of superheated and two-phase refrigerant from the indoor coil (which is initially at high-side pressure) via an unrestricted path to the suction port of the compressor. This rapid movement of refrigerant is reflected also in the sudden drop in high-side pressure observed in Fig. 7.14.

After the initial rapid fluctuations, both high- and low-side pressures decrease as the indoor coil is emptied of liquid refrigerant and the refrigerant condenses in the still cold and heavily frosted outdoor coil. The high-side pressure begins to rise after 30 to 45 sec of defrosting operation as the heated refrigerant begins to warm the outdoor coil. The

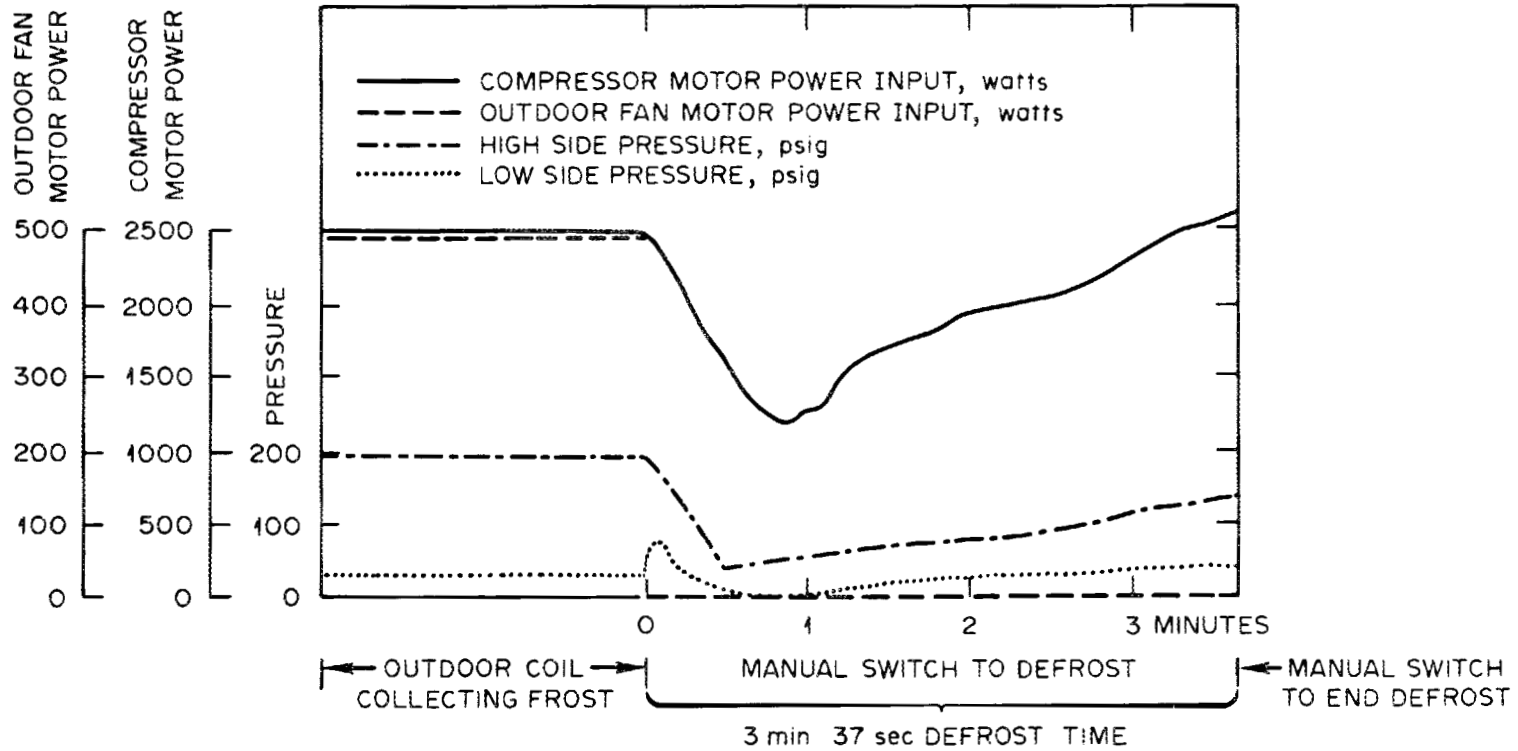


Fig. 7.13. Power consumption and system pressures during a defrosting period following a 50 min frosting interval with the outdoor air at 0.6°C and 100% relative humidity.

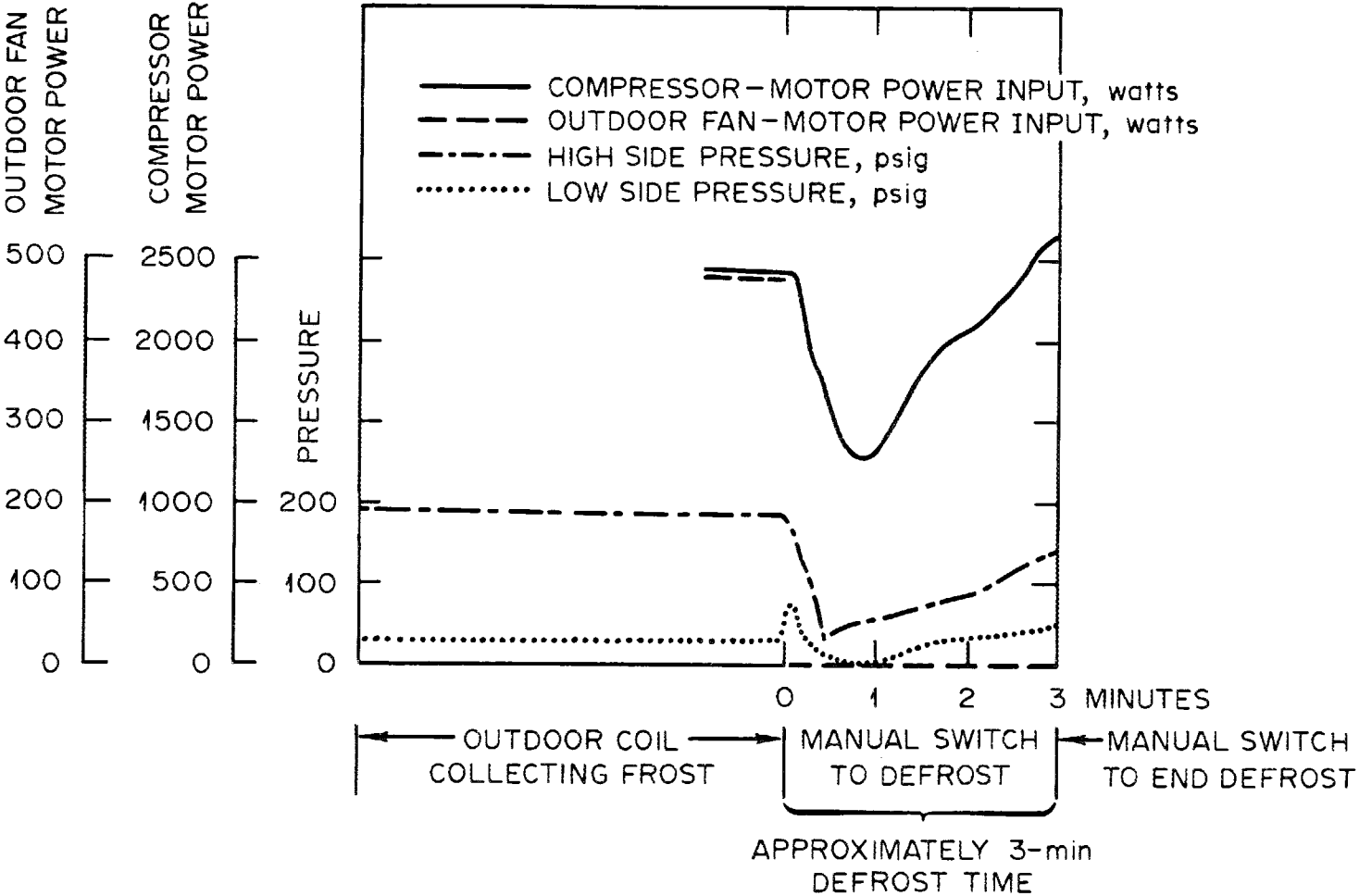


Fig. 7.14. Power consumption and system pressures during a defrosting period following a 90 min frosting interval with the outdoor air at 0.6°C and 92-97% relative humidity.

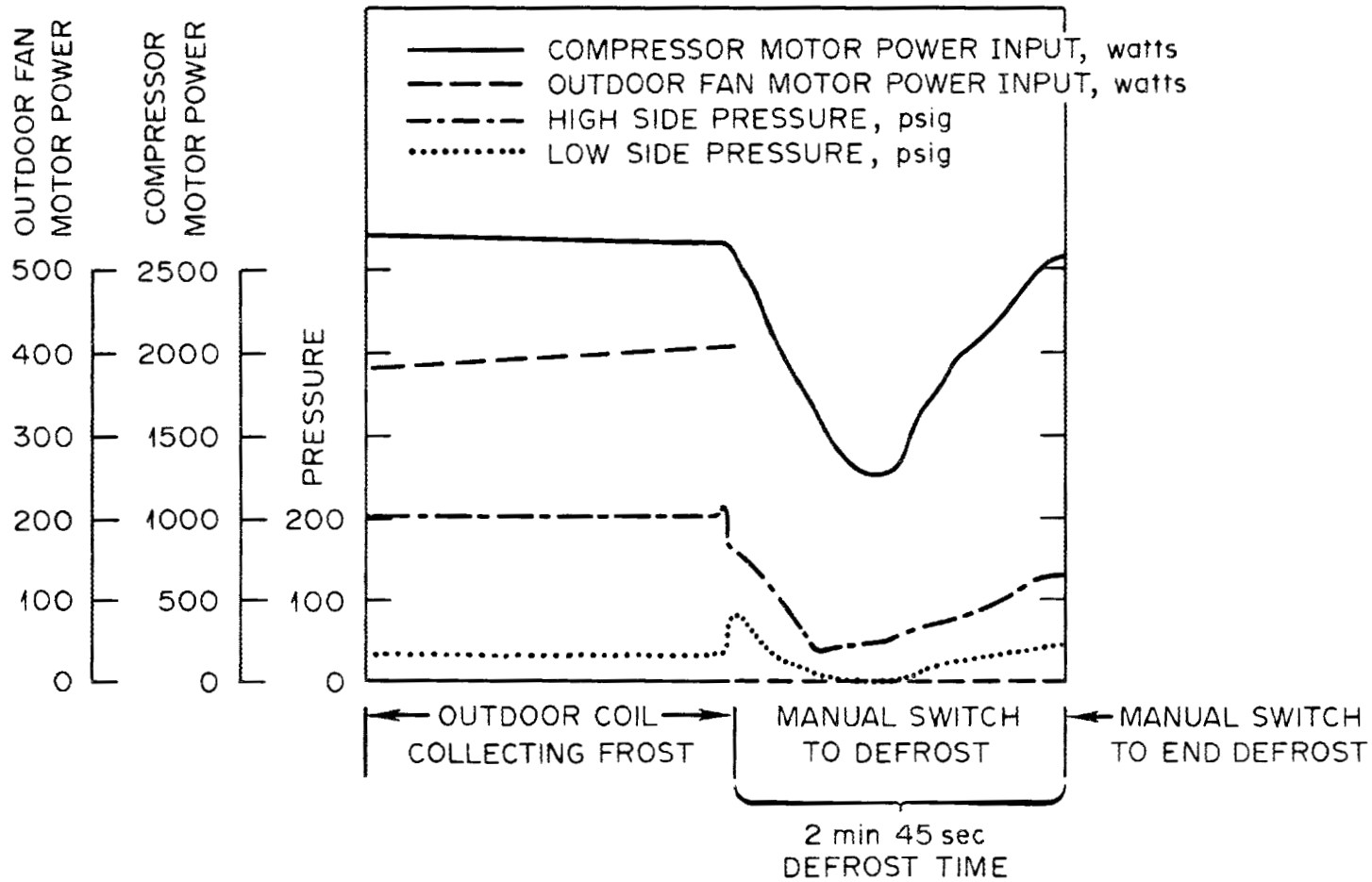


Fig. 7.15. Power consumption and system pressures during a defrosting period following a 90 min frosting interval with the outdoor air at -2.2°C , and 80-85% relative humidity.

rise in the low-side pressure does not start until the high-side pressure has recovered enough to start passing refrigerant through the flow control device in the line between the outdoor and indoor coils. At this point in the defrosting operation, normal operation of the vapor compression cycle resumes, except that the outdoor fan is still turned off. Consequently, the pressures begin to rise, and would reach an overload condition were the defrosting operation not halted. A temperature sensor on the outdoor coil signals the end of the defrost period when the coil reaches about 18°C (65°F), which occurs well before dangerous operating conditions are reached. Compressor power follows the low-side pressure during the defrosting interval.

At the conclusion of the defrosting operation, the reversing valve switches the compressor discharge to the inlet of the indoor coil, and the outlet of the outdoor coil to the suction line. The resulting perturbations last about one minute.

8. REFRIGERANT CHARGE VARIATION TESTS

All of the tests reported in the preceding sections of this report were conducted with the heat pump charged with the amount of refrigerant specified by the manufacturer. In operation, the charge may be reduced by leaks in the system. Attempts to compensate for lost refrigerant after the repair of leaks may result in excess charge. The low-first-cost heat pump previously tested,¹ which lacks a suction-line accumulator, was found to be highly sensitive to charge, whereas the efficiency of the heat pump selected for these tests remains essentially constant when the actual charge is within about 20% of the rated charge of 2.86 kg (6 lb, 5 oz).

Tests were conducted with the heat pump operating in the heating mode at an outdoor air temperature of 10°C (50°F) and indoor air temperature of 21°C (70°F). The amount of refrigerant in the circuit was varied from 1.81 kg (4 lb) to 3.63 kg (8 lb).

As was previously noted in the steady-state tests, the suction-line superheat remained very low at all outdoor air temperatures. This effect was attributed to the presence of liquid refrigerant in the suction-line accumulator when the system is properly charged with refrigerant. As shown in Fig. 8.1, the suction-line superheat remains at or near 0°C (0°F) until the charge is reduced to about 2.72 kg (6 lb). Further reduction of the refrigerant charge results in substantial increase of the superheat. The suction-line superheat remains at approximately zero when the unit is overcharged since there is an ample supply of liquid refrigerant in the accumulator. Refrigerant pressures are seen (Fig. 8.2) to remain nearly constant in the overcharge range, and to drop as the superheat increases in the undercharge range.

As a result of the lowered suction line pressure and increased superheat in the undercharged condition, refrigerant mass flow rates decrease rapidly (Fig. 8.3) when the charge is reduced below the value of 2.72 kg (6 lb), at which point the superheat begins to rise. A consequence of the reduced mass flow rate is the reduction of the heating capacity, which is the product of the mass flow rate and the change

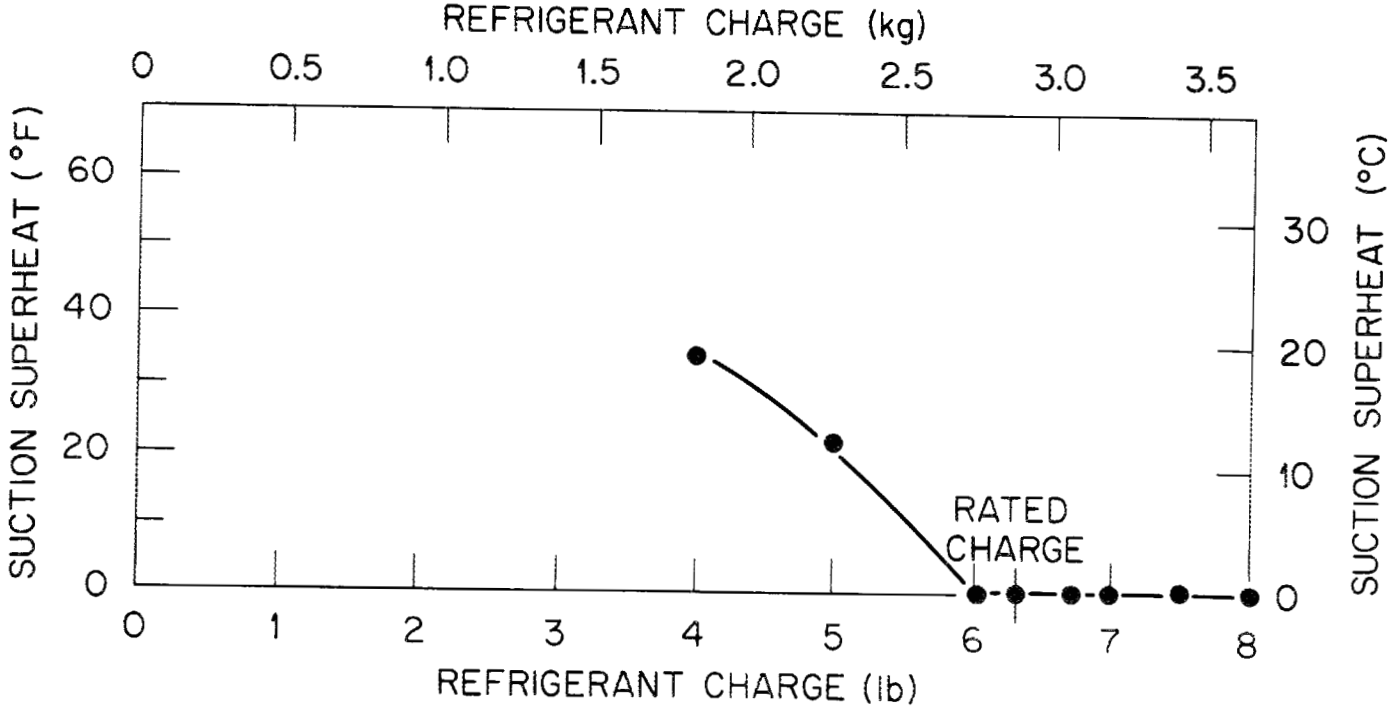


Fig. 8.1. Suction gas superheat as a function of refrigerant charge.

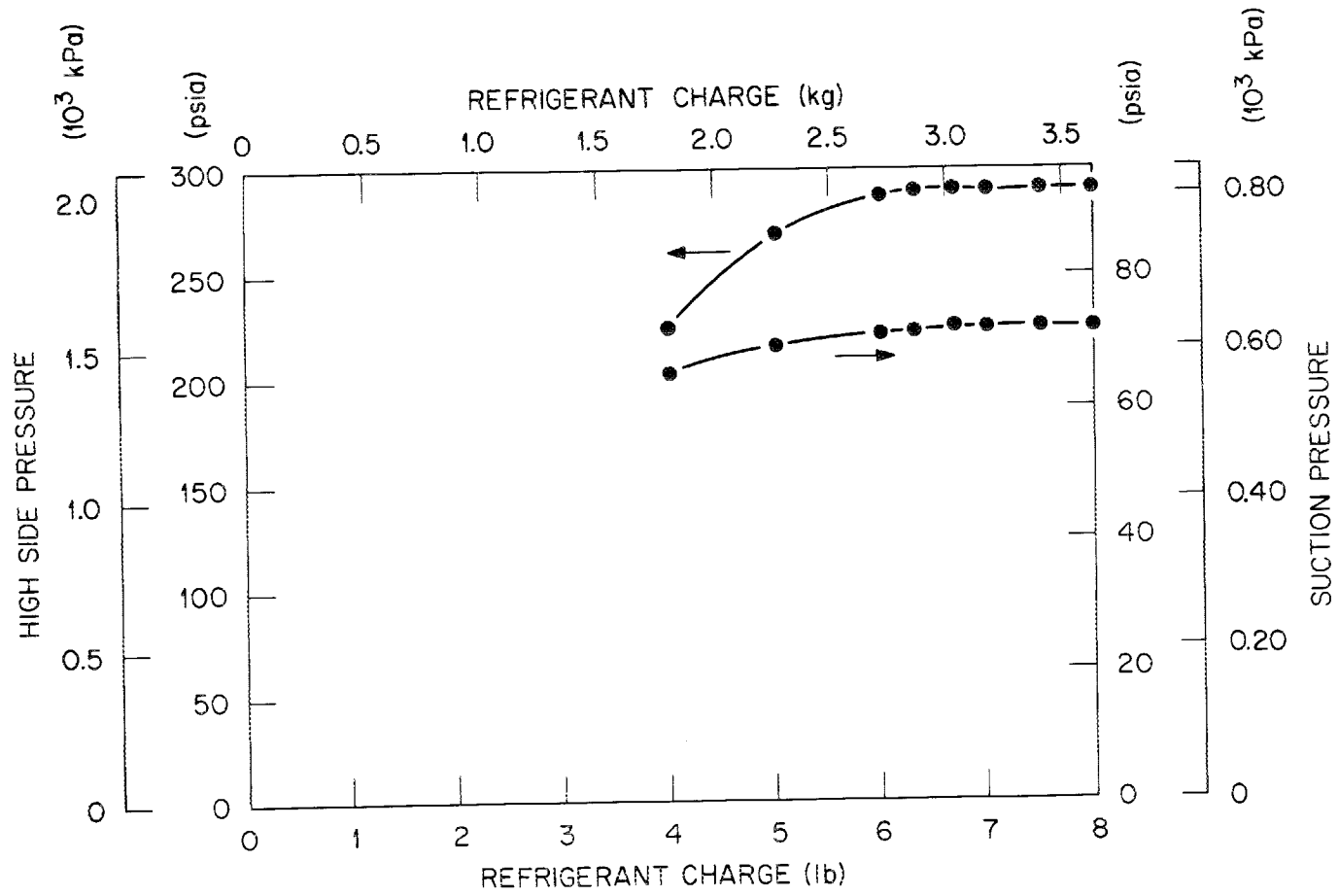


Fig. 8.2. System pressures as a function of refrigerant charge.

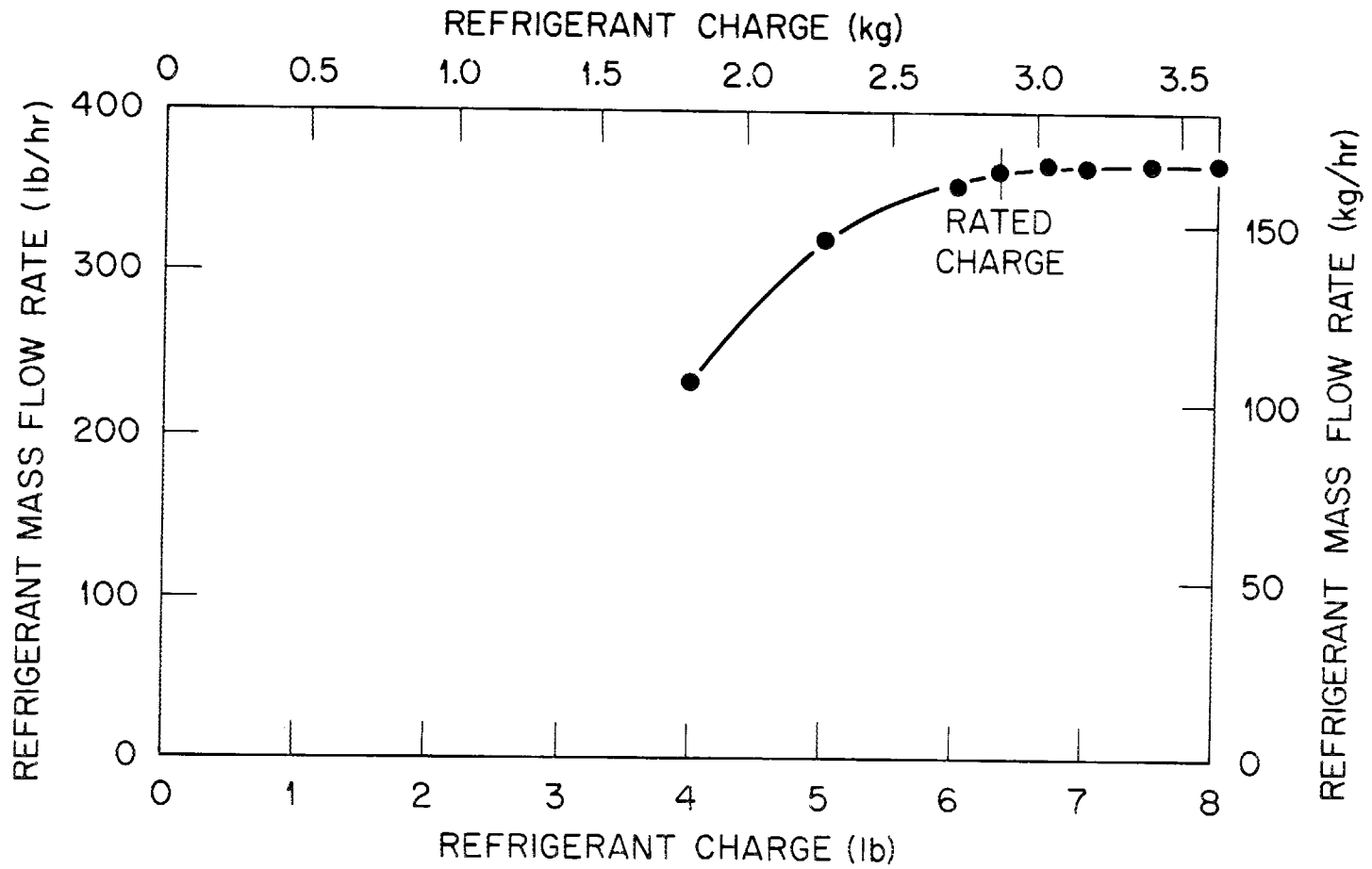


Fig. 8.3. Mass flow rate of refrigerant as a function of refrigerant charge.

in enthalpy. The variation of heating capacity with charge is shown in Fig. 8.4. As would be expected, the mass flow rate and heating capacity remain at the values found for a properly charged system when the system is overcharged. The curve for the COP as a function of charge, shown in Fig. 8.5, is essentially flat in the overcharge range and drops off in the undercharge range, but less steeply than do those for heating capacity and refrigerant mass flow rate. The COP of the previously tested low-first-cost unit¹ as a function of charge is shown in the same graph for comparison.

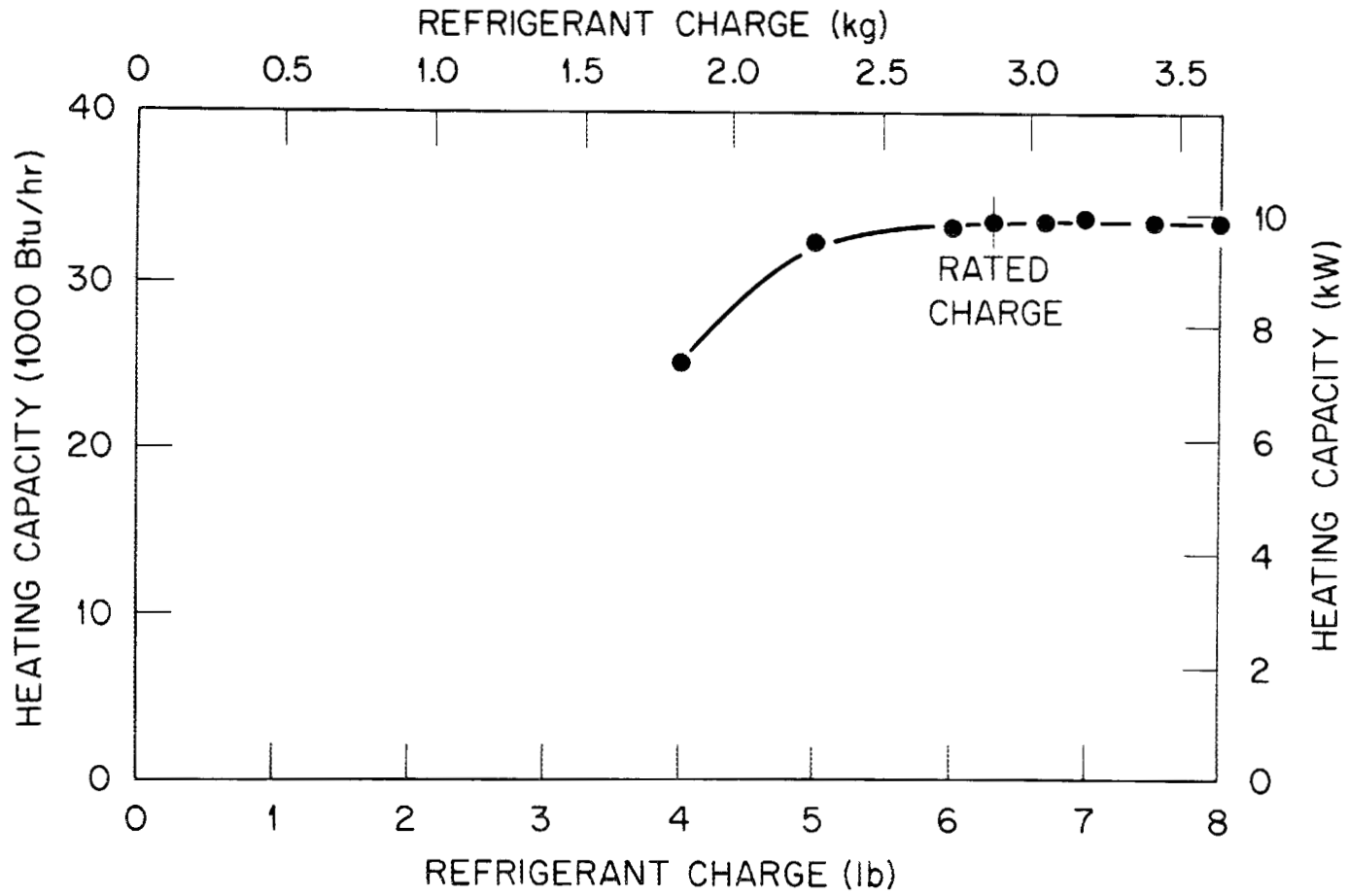


Fig. 8.4. Heating capacity as a function of refrigerant charge.

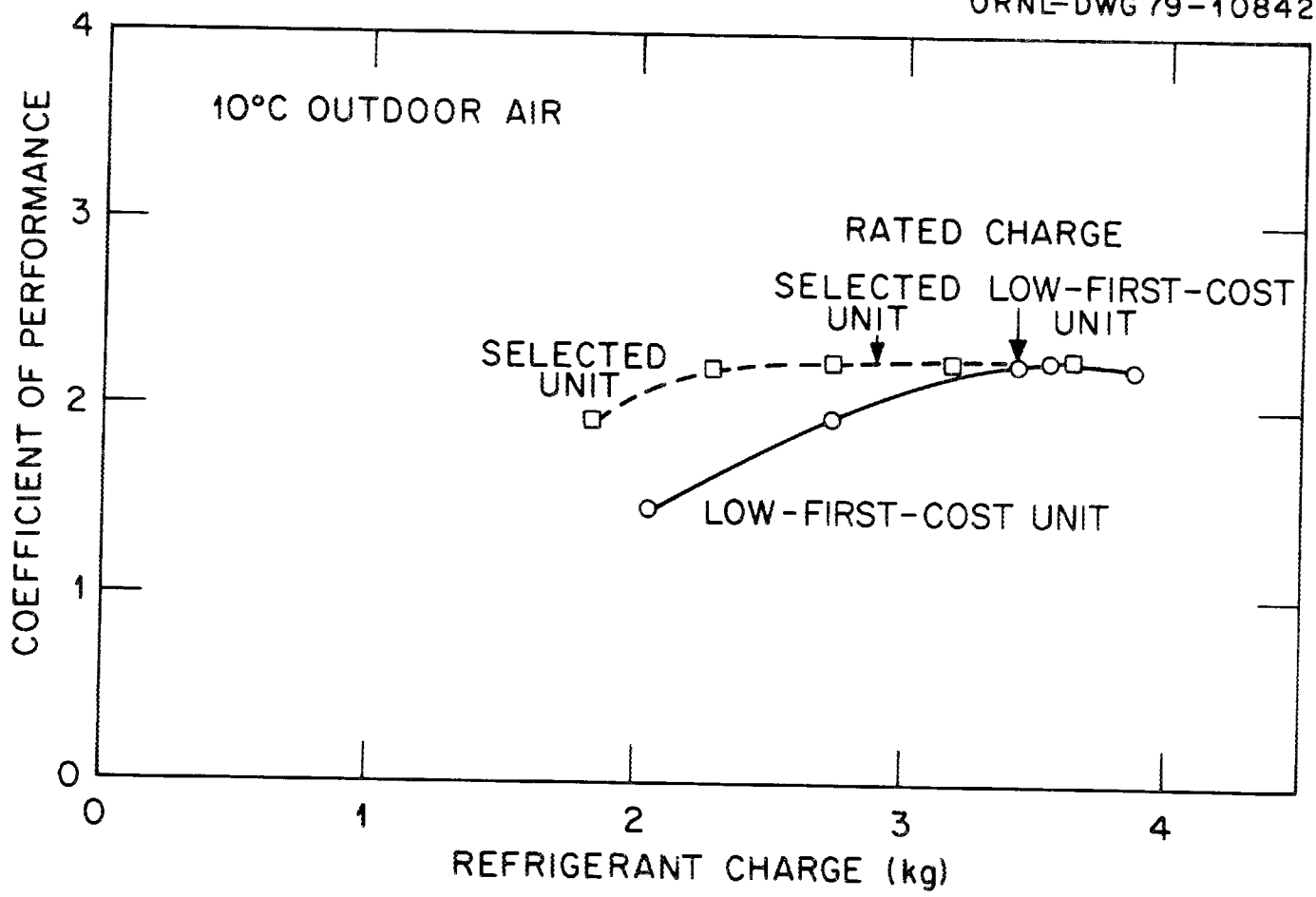


Fig. 8.5. Coefficient of performance as a function of refrigerant charge. The COP of the low-first-cost unit, which lacks a suction line accumulator, is shown for comparison.

ACKNOWLEDGMENTS

Thanks are due to D. E. Holt, who was responsible for the assembly and operation of the laboratory apparatus; to J. E. Summers and N. E. Morgan, for their help in solving instrument application problems; and to J. T. Farmer and T. Duncan who helped maintain the refrigerant loop in working condition.

The authors are grateful for the assistance and advice of R. D. Ellison and F. A. Creswick in reviewing and editing the report.

The help of W. L. Jackson in preparing the computer program for the evaluation of the testing data and preparation of the computer plot routines is gratefully acknowledged.

REFERENCES

1. A. A. Domingorena, *Performance Evaluation of a Low-First-Cost, Three-Ton, Air-to-Air Heat Pump in the Heating Mode*, ORNL/CON-18 (October 1978).
2. R. D. Ellison and F. A. Creswick, *A Computer Simulation of Steady-State Performance of Air-to-Air Heat Pumps*, ORNL/CON-16 (March 1978).
3. Thermocouple Conversion Tables, NBS Circular 561.

APPENDICES

Appendix A. Experimental Data

Table A.1 shows the data collected and the results of some of the calculations needed for evaluating the performance of the heat pump system operating under the steady-state (non-frosting) conditions in the heating mode. Table A.2 gives the same information for the frosting runs. Data from the refrigerant charge variation tests are presented in Table A.3. Air-side measurements were not required for these tests.

Table A.1. Test data from steady-state runs.

RUN NO.	DATE	AIR TEMPERATURES, F				REFRIGERANT TEMPERATURES, F						PRESSURES, PSIA		AIR FLOW RATE, CFM		AIRFLOW RATE, INDOOR COIL, LBM/HR	REFRIG. FLOW RATE, LBM/HR	POWER INPUT, W		POWER INPUT, KW		HEATING CAPACITY, KW		COP			
		OUTDOOR COIL		INDOOR COIL		EVAP. IN	EVAP. OUT	COMP. IN	COMP. OUT	COND. IN	COND. OUT	FLOW CONTRL IN	ATMOS. PRESS., IN. HG	COMP. SUCT.	FLOW CONTRL IN			OUT-DOOR COIL	IN-DOOR COIL	OUTDOOR FAN	INDOOR FAN	COMPRESSOR	TOTAL	REFRIG. METHOD	AIR METHOD	REFRIG. METHOD	AIR METHOD
		IN	OUT	IN	OUT																						
2	1/24/78	48.2	41.6	70.3	98.7	38.7	32.3	29.5	193.4	170.3	95.8	90.3	29.15	69.4	281.7	3034	1138	4916	356.8	425	589	3.39	4.40	9.62	10.41	2.18	2.36
3	1/24/78	47.9	41.3	69.8	98.1	38.5	31.9	29.3	193.5	170.3	95.0	89.0	29.08	69.2	279.7	3034	1199	5180	357.2	424	589	3.38	4.40	9.66	10.89	2.20	2.48
4	1/30/78	38.4	33.6	70.5	95.3	30.9	25.0	22.3	182.3	158.5	96.4	90.2	29.33	58.4	254.7	3170	1080	4698	305.8	432	630	3.10	4.16	8.21	8.82	1.97	2.12
5	1/30/78	26.7	23.7	69.9	89.9	21.5	16.1	13.9	173.1	144.6	96.3	88.3	29.28	49.8	220.3	3198	1090	4735	255.3	440	630	2.73	3.80	6.84	7.29	1.80	1.92
6	1/31/78	22.9	20.7	70.5	88.8	18.4	13.3	11.2	170.0	140.5	96.2	89.7	29.32	46.7	213.9	3244	1125	4860	234.6	442	628	2.61	3.68	6.30	6.87	1.71	1.87
7	2/ 2/78	56.0	46.5	70.0	100.6	43.8	37.5	34.9	209.3	186.7	97.7	91.8	29.35	71.4	296.5	3029	1156	5036	381.8	421	630	3.58	4.63	10.57	11.47	2.28	2.48

Table A.2. Test data for frosting/defrosting tests.

REFRIG. CHARGE (LBM)	AIR TEMPERATURES		REFRIGERANT TEMPERATURES, F							PRESSURES, PSIA		REFRIG. FLOW RATE, LBM/HR	POWER INPUT, W		POWER INPUT, KW		HEATING CAPACITY REFRIG. METHOD, KW	COP REFRIG. METHOD
	OUTDOOR COIL IN, F	INDOOR COIL IN, F	EVAP. IN	EVAP. OUT	COMP. IN	COMP. OUT	COND. IN	COND. OUT	FLOW CONTRL IN	COMP. SUCT.	FLOW CONTRL IN		OUTDOOR FAN	INDOOR FAN	COMPRESSOR	TOTAL		
8.00	50.0	69.9	39.3	33.3	31.8	185.3	169.5	93.7	89.8	72.0	291.0	368.0	420	590	3.43	4.44	9.92	2.23
7.50	50.3	69.7	39.2	33.3	31.8	189.8	172.6	93.7	89.6	71.9	291.0	367.2	416	590	3.43	4.44	9.98	2.25
7.00	49.4	69.8	38.9	32.9	31.4	188.2	171.8	93.3	89.4	72.0	289.0	365.0	418	590	3.42	4.43	9.92	2.24
6.69	50.9	70.0	39.7	33.6	32.2	189.4	172.6	94.0	89.8	72.2	290.0	369.0	416	590	3.45	4.45	10.02	2.25
6.31	50.3	70.2	39.4	33.2	31.8	189.7	172.6	93.9	90.0	71.7	290.0	365.0	418	590	3.43	4.44	9.92	2.24
6.00	49.9	70.8	38.8	32.8	31.2	195.5	177.5	94.6	90.4	71.6	288.0	357.0	419	590	3.41	4.42	9.81	2.22
5.00	49.9	69.7	37.6	46.2	51.1	224.6	203.8	94.6	90.3	69.0	268.0	321.0	420	590	3.25	4.26	9.46	2.22
4.00	50.0	70.4	27.8	52.6	60.8	239.7	206.0	95.8	90.8	65.5	225.0	234.0	417	590	3.73	4.73	7.14	1.51

Table A.3. Test data for charge variation tests.

REL. HUM., %	DATE	PROSTING TIME, MIN	AIR TEMPERATURES, F				REFRIGERANT TEMPERATURES, F								PRESSURES, PSIA		AIR FLOW RATE, CFM		POWER INPUT, W		POWER INPUT, KW		HEATING CAPACITY, KW		COP			
			OUTDOOR COIL		INDOOR COIL		EVAP. IN	EVAP. OUT	COMP. IN	COMP. OUT	COND. IN	COND. OUT	FLOW CONTRL IN	ATMOS. PRESS., IN. HG	COMP. SUCT.	FLOW CONTRL IN	OUT-DOOR COIL	IN-DOOR COIL	AIRFLOW RATE, INDOOR COIL, LBM/HR	REFRIG. FLOW RATE, LBM/HR	OUTDOOR FAN	INDOOR FAN	COMPRESSOR	TOTAL	REFRIG. METHOD	AIR METHOD	REFRIG. METHOD	AIR METHOD
			IN	OUT	IN	OUT																						
100	3/12/78	18	33.5	31.5	70.8	94.9	28.8	22.7	21.8	181.9	158.5	96.8	90.7	29.29	60.7	254.7	3059	1090	4709	298.6	420	610	3.34	4.07	8.00	8.58	1.97	2.11
100	3/12/78	20	33.1	30.9	70.7	94.4	28.2	22.5	21.1	179.6	156.5	95.6	90.4	29.29	59.7	252.0	3174	1090	4709	295.6	419	610	3.01	4.04	7.90	8.44	1.95	2.09
100	3/12/78	33	35.4	30.7	70.8	94.1	28.0	21.8	20.4	179.7	156.9	96.8	90.3	29.29	58.5	247.2	1946	1090	4709	290.5	396	610	2.97	3.97	7.79	8.31	1.96	2.09
100	3/12/78	36	33.7	30.3	70.4	93.8	27.7	22.0	20.3	178.5	154.8	96.4	89.8	29.25	58.5	246.2	2114	1090	4709	288.6	398	610	2.96	3.97	7.72	8.34	1.94	2.10
100	3/12/78	48	40.7	25.1	70.4	90.4	22.2	15.3	14.7	174.1	147.1	96.5	90.0	29.29	51.2	223.2	470	1090	4709	246.8	490	610	2.69	3.79	6.64	7.22	1.75	1.91
100	3/12/78	50	39.5	25.5	70.2	90.2	22.2	16.1	14.8	173.8	146.8	96.5	89.6	29.29	51.6	223.7	566	1090	4709	244.8	485	610	2.69	3.79	6.59	7.22	1.74	1.90
92-97	3/12/78	20	33.2	30.5	70.5	95.2	27.7	22.0	20.8	182.3	160.0	92.9	86.9	29.29	58.7	244.7	3216	1090	4735	293.4	497	610	2.99	4.09	8.04	8.82	1.96	2.16
92-97	3/12/78	25	33.3	30.9	69.6	94.5	27.7	22.1	20.7	180.7	158.5	91.8	85.9	29.29	58.7	242.7	3260	1090	4741	293.6	425	610	2.98	4.02	8.05	8.90	2.00	2.21
92-97	3/12/78	38	33.5	30.7	70.8	95.0	27.6	21.8	20.7	180.4	158.4	92.7	86.8	29.33	58.0	242.0	3058	1090	4741	291.4	427	610	2.98	4.01	7.97	8.67	1.99	2.16
92-97	3/12/78	73	38.0	30.8	70.6	93.4	25.3	20.0	18.0	177.0	154.6	92.6	86.8	29.33	54.2	232.0	1147	1090	4741	274.0	404	610	2.85	3.86	7.50	8.20	1.94	2.12
92-97	3/12/78	80	36.7	28.2	70.3	92.4	24.0	18.5	16.7	174.2	151.1	92.5	86.5	29.29	52.5	224.0	901	1090	4735	265.9	426	610	2.78	3.82	7.27	7.96	1.90	2.08
92-97	3/12/78	88	42.3	31.1	70.2	90.4	21.3	16.4	14.0	172.6	147.3	93.3	87.2	29.33	49.7	217.7	855	1090	4741	235.1	451	610	2.63	3.69	6.44	7.34	1.74	1.99
80-85	3/12/78	9	29.8	27.4	71.2	92.7	24.8	18.7	19.1	174.5	151.7	96.1	90.0	28.90	56.5	239.7	3237	1090	4643	272.2	429	610	2.86	3.90	7.29	7.64	1.87	1.96
80-85	3/12/78	64	27.9	25.4	71.5	92.0	22.3	16.4	15.4	174.7	148.6	97.0	90.0	28.90	53.7	234.7	3300	1090	4643	256.9	425	610	2.78	3.81	6.86	7.31	1.80	1.92
80-85	3/12/78	86	27.7	24.9	71.1	91.5	21.6	16.9	15.0	174.2	147.6	97.0	90.1	28.90	53.5	231.7	3116	1090	4656	250.8	421	610	2.75	3.78	6.71	7.30	1.77	1.93

Appendix B. Fan-Motor Efficiency Evaluation

Table B.1 shows the data used to determine the pressure head and power consumption of the indoor-unit fan as functions of the airflow rates.

Table B.1. Indoor fan test data

	Volume rate of air (cfm)	Static-developed head (in. H ₂ O)	Fan-motor input power (kW)
850 rpm	203	1.32	0.239
	560	1.15	0.320
	787	1.02	0.388
	1017	0.85	0.466
	1116	0.745	0.527
	1144	0.675	0.526
950 rpm	181	1.37	0.390
	576	1.22	0.461
	836	1.12	0.515
	1099	0.99	0.586
	1252	0.915	0.650
	1308	0.85	0.658

The information contained in Table B.1 was used to evaluate the overall efficiency of the fan-motor unit, as shown in Table B.2.

Table B.2. Overall efficiency of the indoor fan-motor unit as a function of airflow rate

Volumetric flow rate [m ³ /s (cfm)]		Static-developed head [kPa (in. H ₂ O)]		Air power (kW)	Power input (kW)	Overall efficiency
MED. SPEED 850 rpm						
0.890	203	0.329	1.32	0.0314	0.239	0.131
0.264	560	0.286	1.15	0.0754	0.32	0.236
0.371	787	0.254	1.02	0.094	0.388	0.242
0.480	1017	0.212	0.85	0.1012	0.466	0.217
0.527	1116	0.186	0.745	0.0973	0.527	0.184
0.540	1144	0.168	0.675	0.0904	0.526	0.172
HIGH SPEED 950 rpm						
0.085	181	0.341	1.37	0.029	0.39	0.074
0.272	576	0.304	1.22	0.0823	0.461	0.179
0.395	836	0.279	1.12	0.1096	0.515	0.213
0.519	1099	0.247	0.99	0.1274	0.586	0.217
0.591	1252	0.228	0.915	0.1342	0.65	0.206
0.617	1308	0.212	0.85	0.1302	0.658	0.198

The four experimental runs used to obtain the curves for the head vs capacity and input-power vs capacity for the outdoor fan are displayed in Table B.3.

Table B.3. Outdoor fan test data

Volume rate of air (cfm)	Static-developed head (in. H ₂ O)	Fan-motor input power (kW)
151	0.40	0.491
1419	0.305	0.435
2037	0.245	0.413
2548	0.18	0.400
2837	0.125	0.396

The overall fan efficiency as a function of the volumetric airflow rate is displayed in Table B.4.

Table B.4. Overall efficiency of the outdoor fan-motor unit as a function of airflow rate

Volumetric flow rate [m ³ /s (cfm)]		Static- developed head [kPa (in. H ₂ O)]		Air power (kW)	Power input (kW)	Overall efficiency
0.071	151	0.100	0.40	0.00707	0.491	0.014
0.670	1419	0.076	0.305	0.0507	0.435	0.117
0.961	2037	0.061	0.245	0.0584	0.413	0.14
1.203	2548	0.045	0.18	0.0537	0.400	0.134
1.339	2837	0.031	0.125	0.0415	0.396	0.105

Appendix C. Algorithms for Calculating Thermodynamic Properties of Refrigerant 22

The equations listed below were derived from the 1964 E. I. duPont refrigerant 22 tables and apply over the operating range of the heat pump (10°F-150°F). They were coded and included with the computer programs described in Appendix E. The accuracy of the approximations as noted are judged to be consistent with the measurement accuracies.

1. Saturation temperature (T_{sat}) in °F. Maximum error ± 0.3 .

$$T_{\text{sat}} = D[16.79 + D(1.48 + 0.467D)] - 103.6 ,$$

where

$$D = \ln(P_{\text{sat}}),$$

$$P_{\text{sat}} = \text{saturation pressure, psia.}$$

2. Enthalpy of saturated vapor (h_g) in Btu/lb. Maximum error ± 0.1 .

$$h_g = 104.5 + T_{\text{sat}}[0.0937 - T_{\text{sat}}(0.279 + 0.015T_{\text{sat}}) \times 10^{-4}].$$

3. Enthalpy of saturated liquid (h_f) in Btu/lb. Maximum error ± 0.05 .

$$h_f = 10.355 + T_{\text{sat}}[0.2732 + T_{\text{sat}}(0.54 + 0.01059T_{\text{sat}}) \times 10^{-4}].$$

4. Specific heat of liquid at constant pressure (c_p) in Btu/lb·F°. Maximum error ± 0.002 .

$$c_p = 0.265 + T_{\text{sat}}[0.5868 \times 10^{-3} - T_{\text{sat}}(0.4337 - 0.003353T_{\text{sat}}) \times 10^{-5}].$$

5. Density of the liquid (ρ) in lb/ft³. Maximum error ± 0.15 .

$$\rho = 83.56 - T_{\text{sat}}(0.09229 + 0.31864T_{\text{sat}} \times 10^{-3}).$$

6. Entropy of saturated vapor (s_g) in Btu/lb·F°. Maximum error $\pm 0.4 \times 10^{-3}$.

$$s_g = 0.2372 - P_{\text{sat}} [0.28387 - P_{\text{sat}} (0.1069 \times 10^{-2} - 0.161 P_{\text{sat}} \times 10^{-5})] \times 10^{-3} .$$

7. Partial derivative of enthalpy with respect to temperature, i.e., change in superheated vapor enthalpy per F° superheat, in (Btu/lb)/F°. Maximum error ± 0.006 .

$$\partial h / \partial T \Big|_p = 0.15 + 0.32 P_{\text{sat}} \times 10^{-3} .$$

8. Partial derivative of entropy with respect to temperature, i.e., change in superheated vapor entropy per F° superheat, in (Btu/lb·°F)/F°. Maximum error $\pm 0.2 \times 10^{-4}$.

$$\partial s / \partial T \Big|_p = (0.32 + 3.0 P_{\text{sat}} \times 10^{-4}) \times 10^{-3} .$$

Appendix D. Computer Program for the
Data Acquisition System

The data acquisition system used in the experiments described in this report consisted principally of an analog-to-digital converter, a scanner, and a Digital Equipment Corp. PDP-8E minicomputer. The programs stored in the minicomputer were written in a modified version of the FOCAL language; they are presented here in flow-chart form so that they may be readily adapted to other computer systems. Complete copies of the program are available on request.

Note that at the introduction to each flow chart, the teletype (TTY) entries required to run that particular program are noted, e.g., to run the heat balance and COP program one would enter "GØ 3.1".

Supplementary data storage locations for use in FOCAL programs are identified as FSTR locations. Data System inputs are typically averaged and stored in arrays as A(I). Those listed in the flow charts are identified as follows:

<u>A()</u>	<u>Description</u>
100	Refrigerant temperature at compressor shell outlet
103	Refrigerant temperature at indoor coil distribution manifold
106	Indoor coil (condenser) discharge refrigerant temperature
107	Outdoor coil (evaporator) inlet refrigerant temperature
110	Outdoor coil refrigerant temperature (midpoint of coil)
111	Outdoor coil outlet refrigerant temperature
114	Refrigerant temperature at inlet to compressor shell
116	Outdoor coil inlet air temperature
117	Outdoor coil outlet air temperature
161	Indoor coil inlet air temperature
162	Indoor coil outlet air temperature
166	Compressor power
167	Outdoor fan power
168	Compressor suction pressure
169	Compressor discharge pressure

The equations used to calculate COP and heating capacity (indoor coil power) are:

COP (based on refrigerant side measurements):

$$\text{COP(R)} = Q(\text{R}) / (3.413 \text{ CD}) ,$$

COP (based on air side measurements):

$$\text{COP(A)} = Q(\text{A}) / (3.413 \text{ CD}) ,$$

where

$Q(\text{R})$ = indoor coil power, refrigerant side

$$= \dot{M}_R (h_4 - h_7) + Q_{\text{indoor fan}}$$

$Q(\text{A})$ = indoor coil power, air side

$$= \dot{M}_A C_{p(\text{A})} (T_{\text{out}} - T_{\text{in}})_{\text{air}}$$

CD = input power (watts)

$$= Q_{\text{indoor fan}} + Q_{\text{compressor}} + Q_{\text{outdoor fan}}$$

\dot{M}_R, \dot{M}_A = refrigerant and indoor fan flows, lb/hr

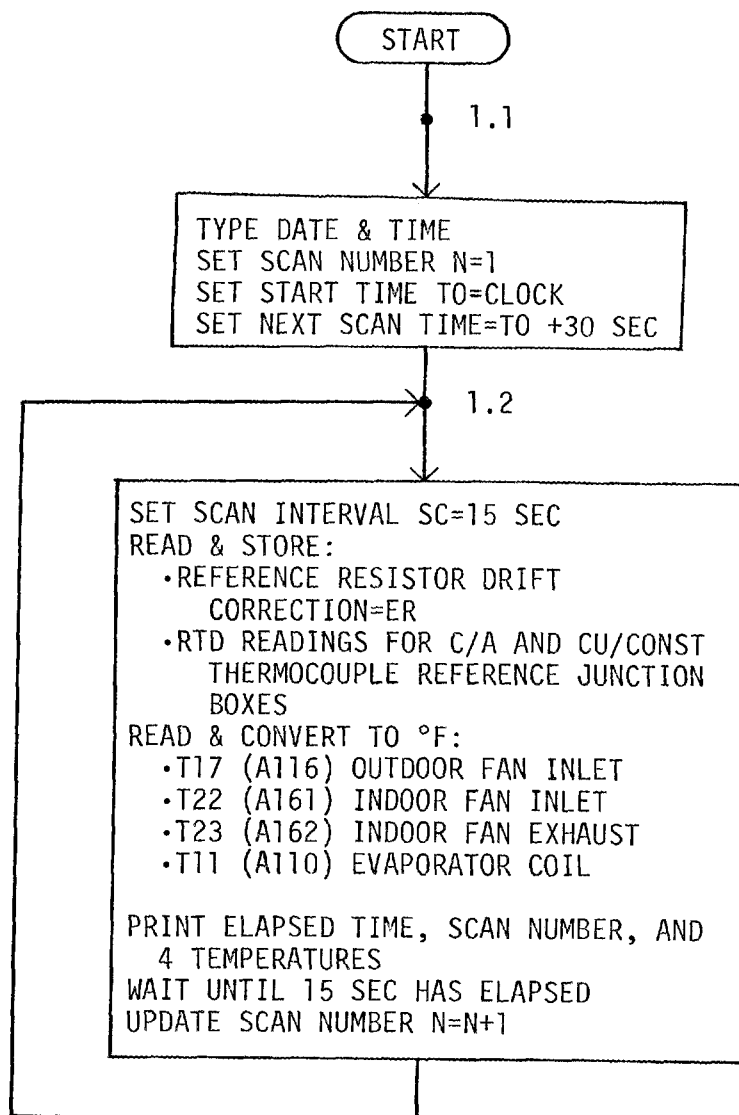
h_4, h_7 = refrigerant enthalpies at indoor coil inlet, outlet, Btu/lb

$C_{p(\text{A})}$ = specific heat of air, = 0.24 Btu/lb°F

Preliminary Scan Program (record 4 points at 15-second intervals to determine when process is at desired operating conditions)

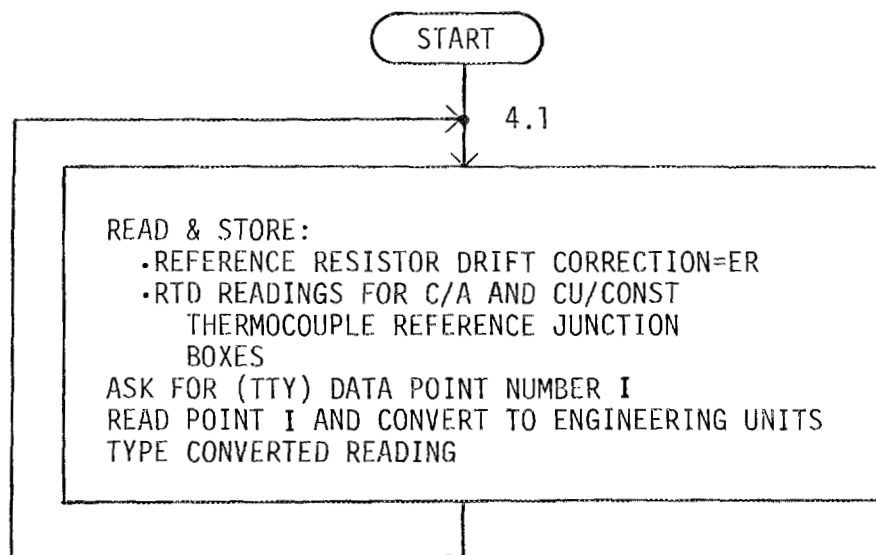
To Start: GØ

To Continue: GØ 1.2



Auxiliary Program to Read Arbitrary DAS Inputs

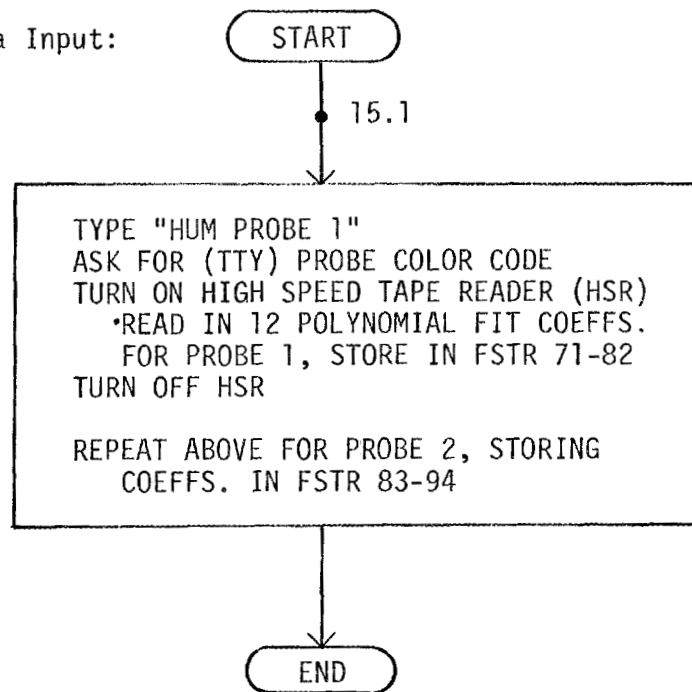
To Start: DØ 4



Auxiliary Program to Input Humidity Sensor Probes' Calibration Data and to Measure and Convert Probe Outputs

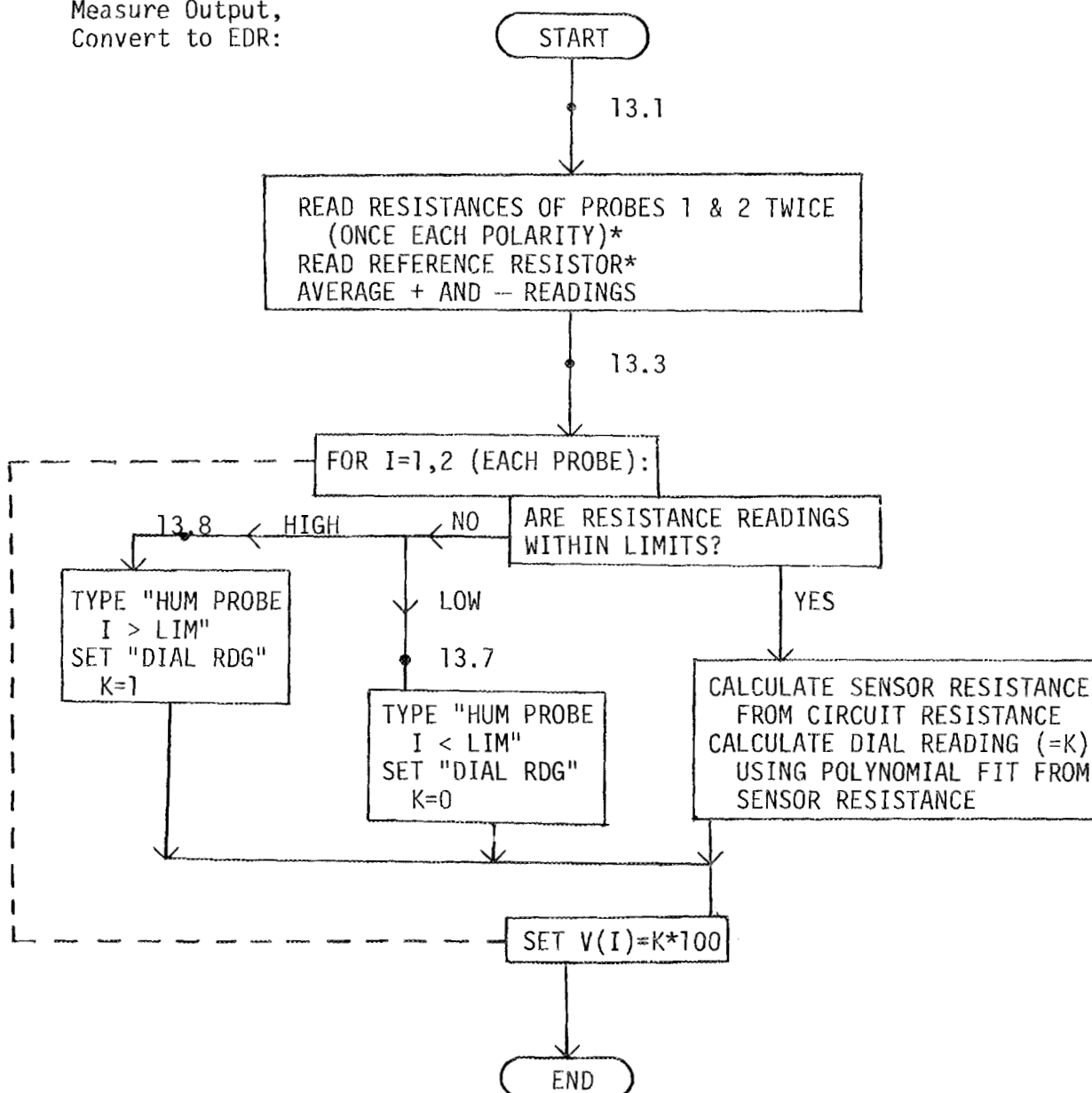
To Start: DØ 15 (calibration data input)
DØ 13 [measure output, convert to equivalent dial reading (EDR)]
DØ 3.5-3.55 (convert EDR to per cent relative humidity)

Calibration Data Input:



Auxiliary Program to Input Humidity Sensor Probes' Calibration Data and to Measure and Convert Probe Outputs (continued)

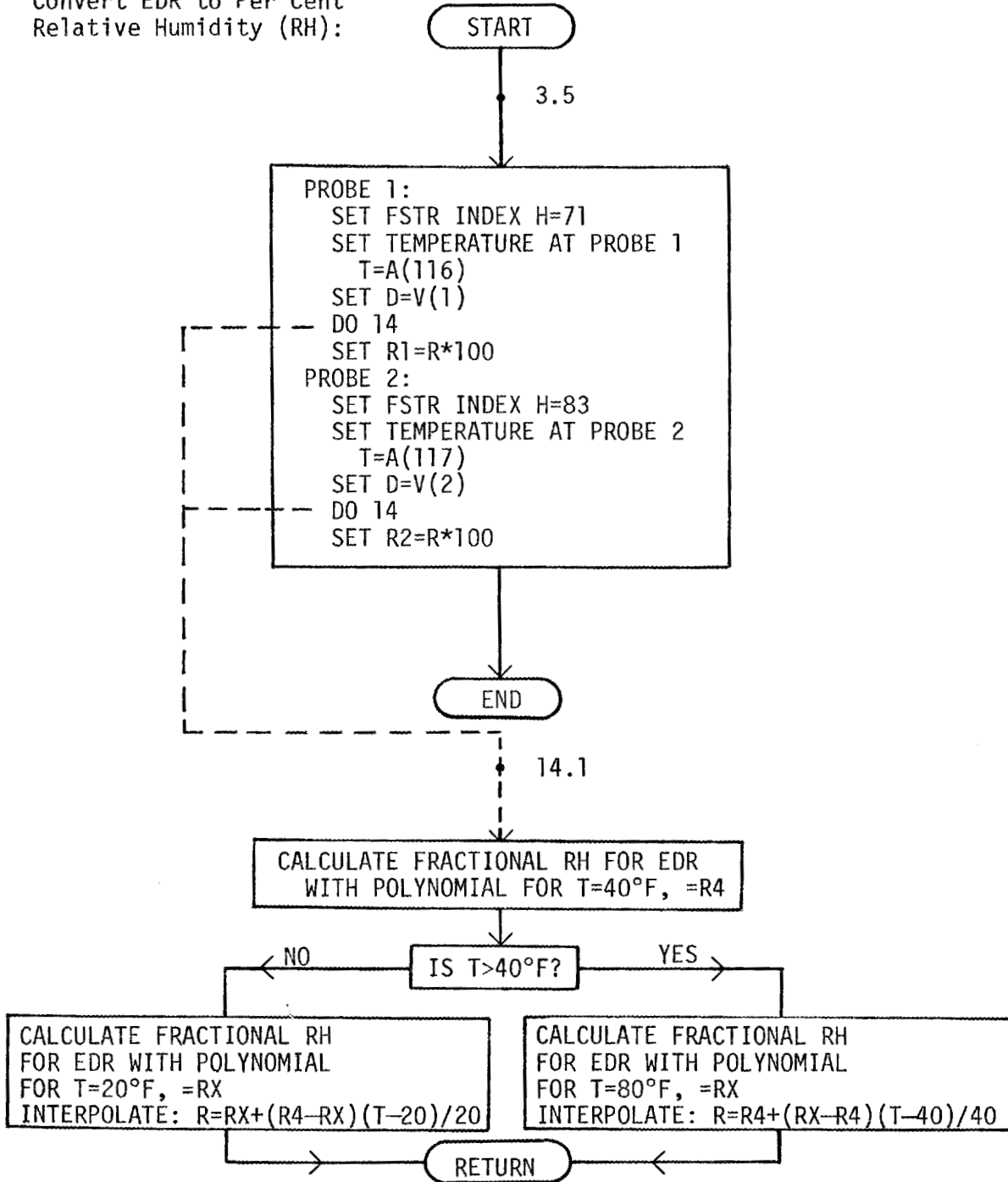
Measure Output,
Convert to EDR:



*Dunmore-type lithium-chloride hygrosensors are polarity sensitive and normally require a-c excitation. Prolonged d-c causes migration and calibration shifts.

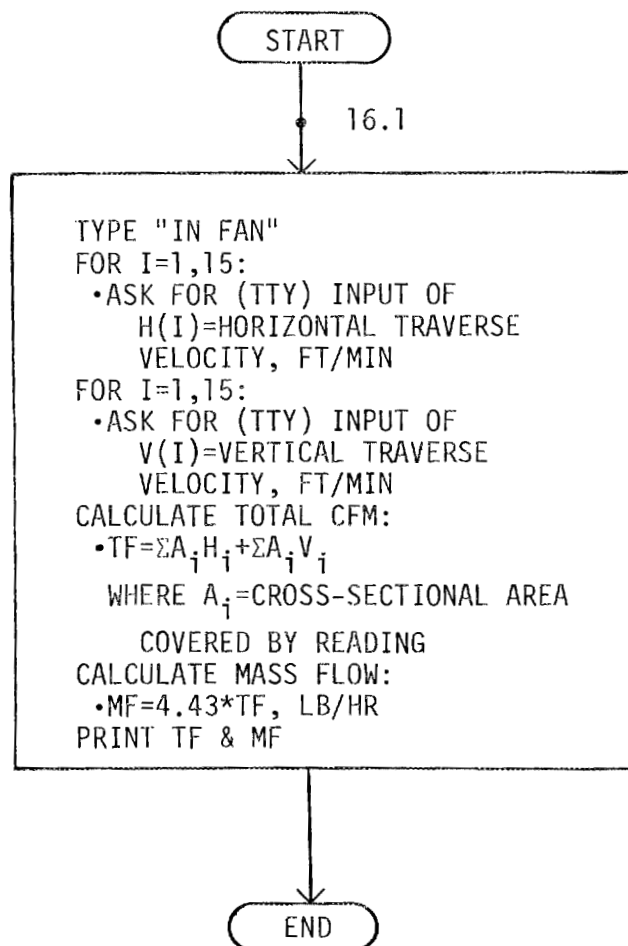
Auxiliary Program to Input Humidity Sensor Probes' Calibration Data and to Measure and Convert Probe Outputs (continued)

Convert EDR to Per Cent Relative Humidity (RH):



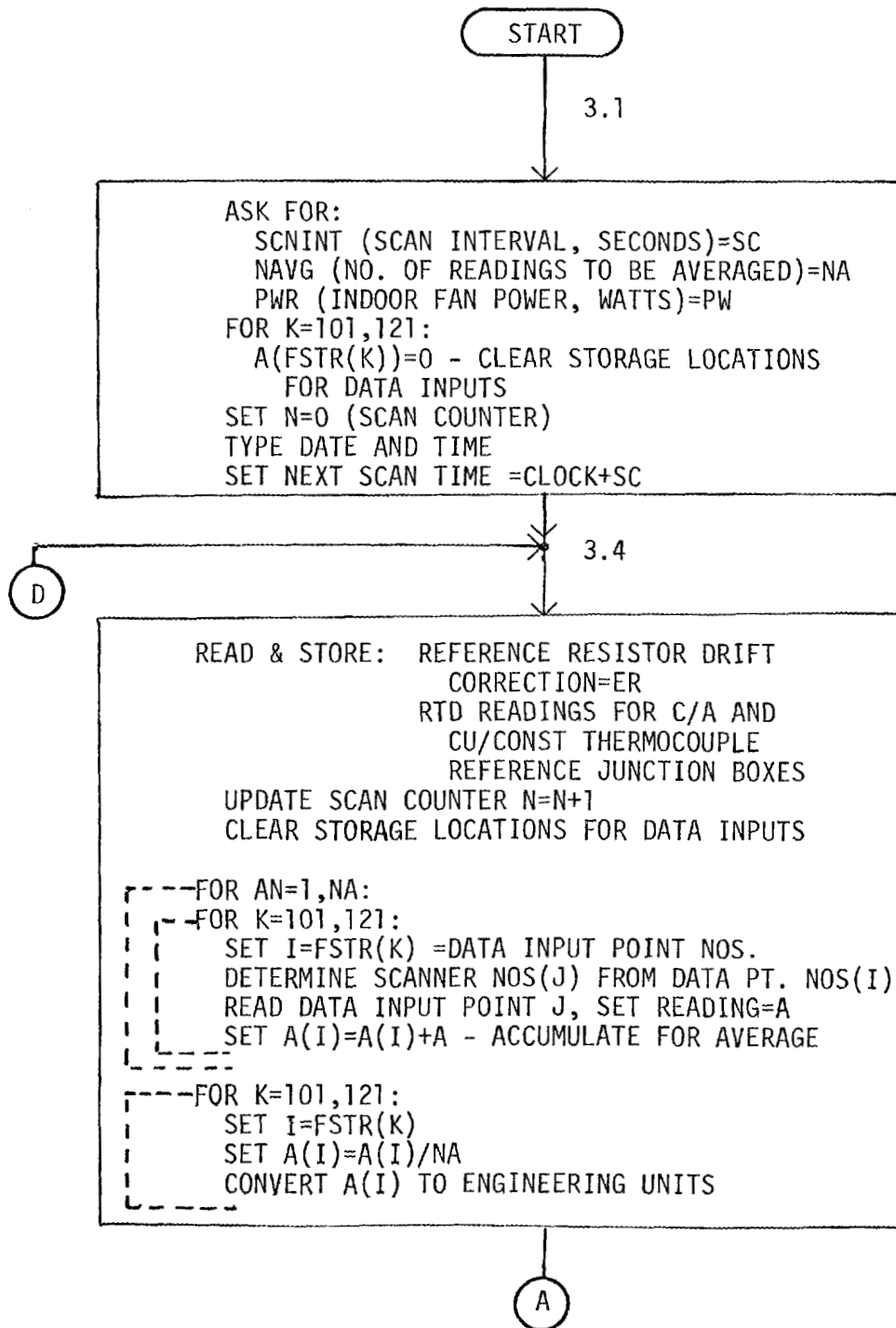
Auxiliary Program to Read Indoor Fan Flow (Manual Readings via Hot-Wire Anemometer)

To Start: DØ 16

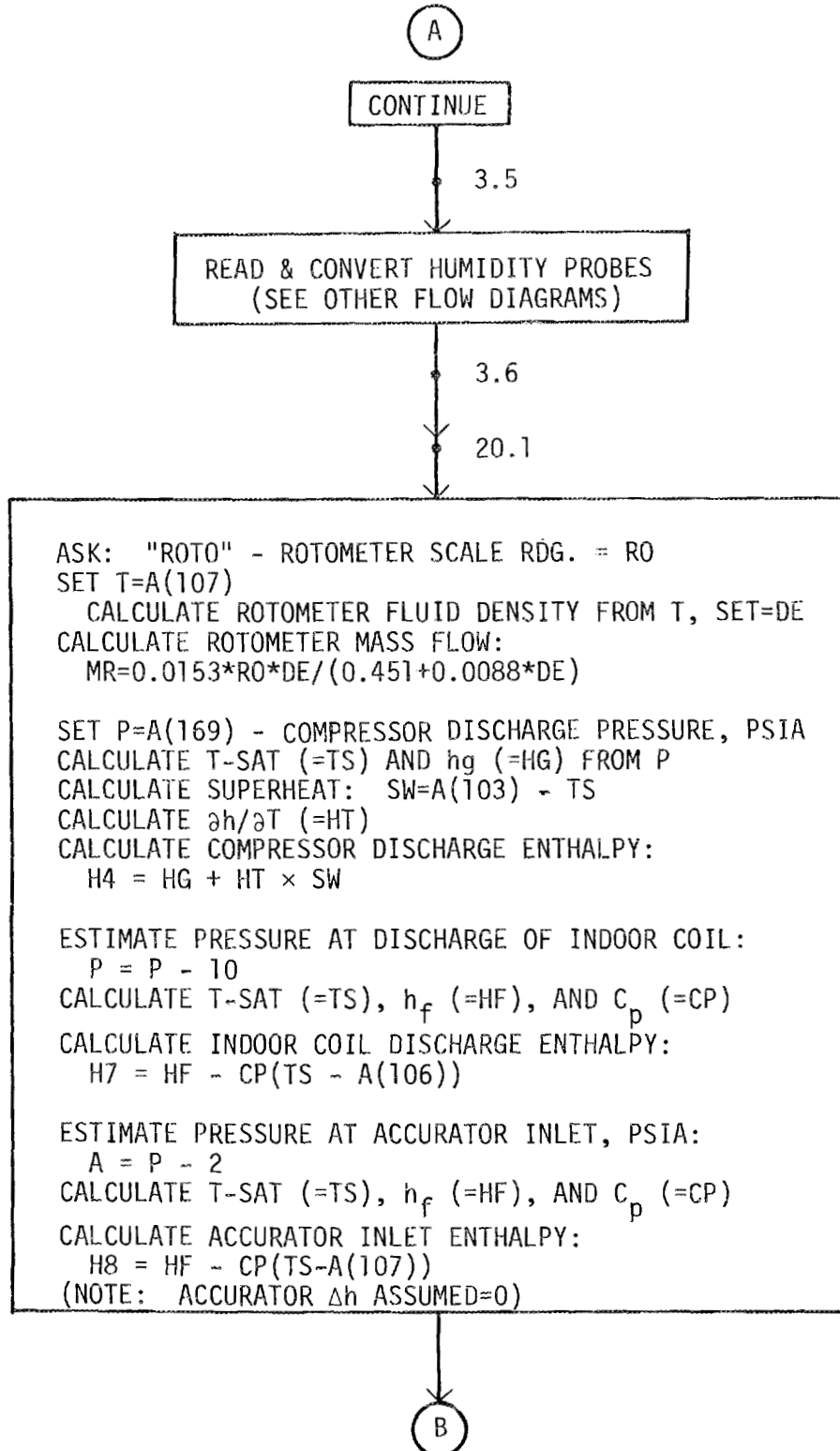


Heat Balance and COP Program - Heating Mode

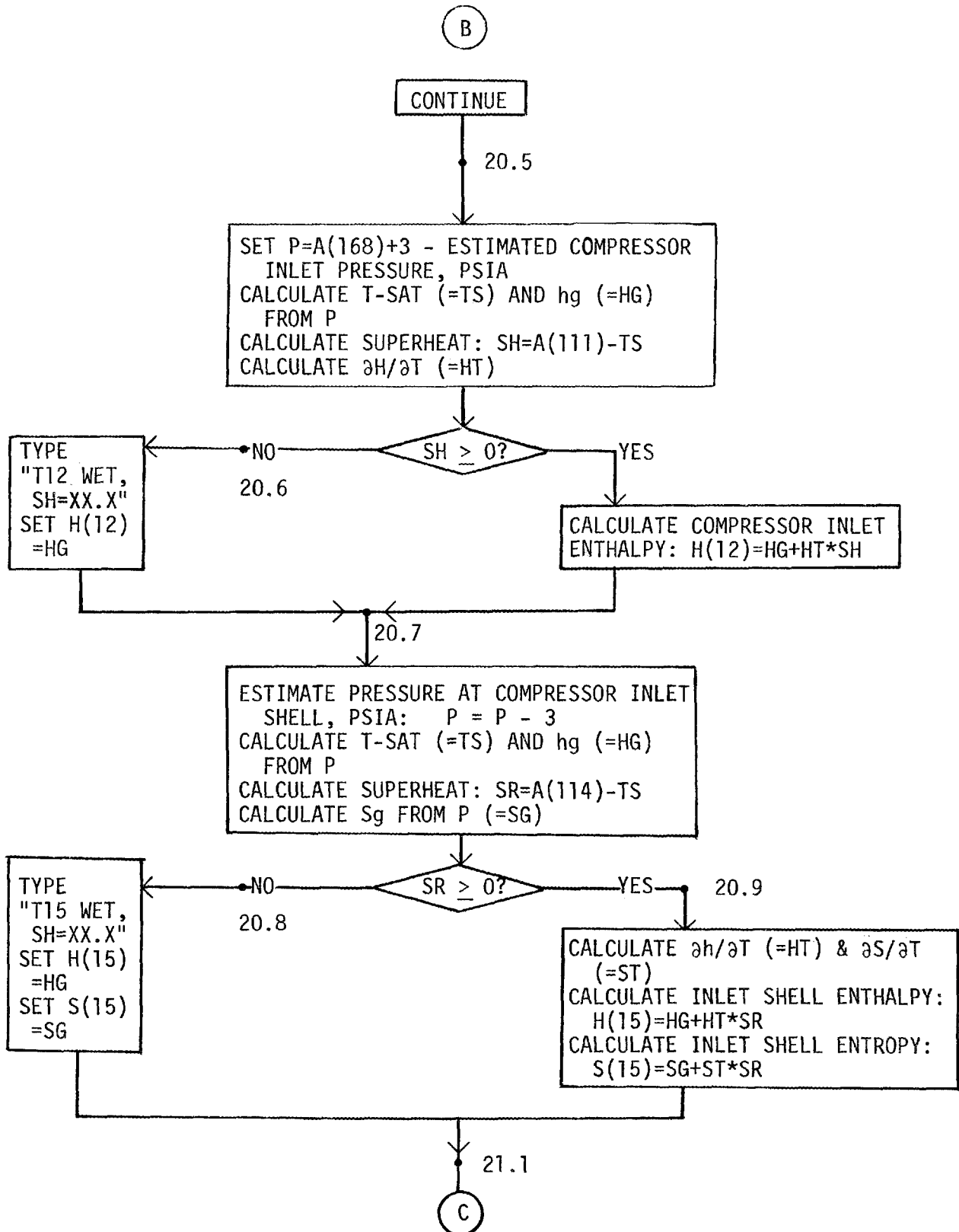
To Start: GO 3.1



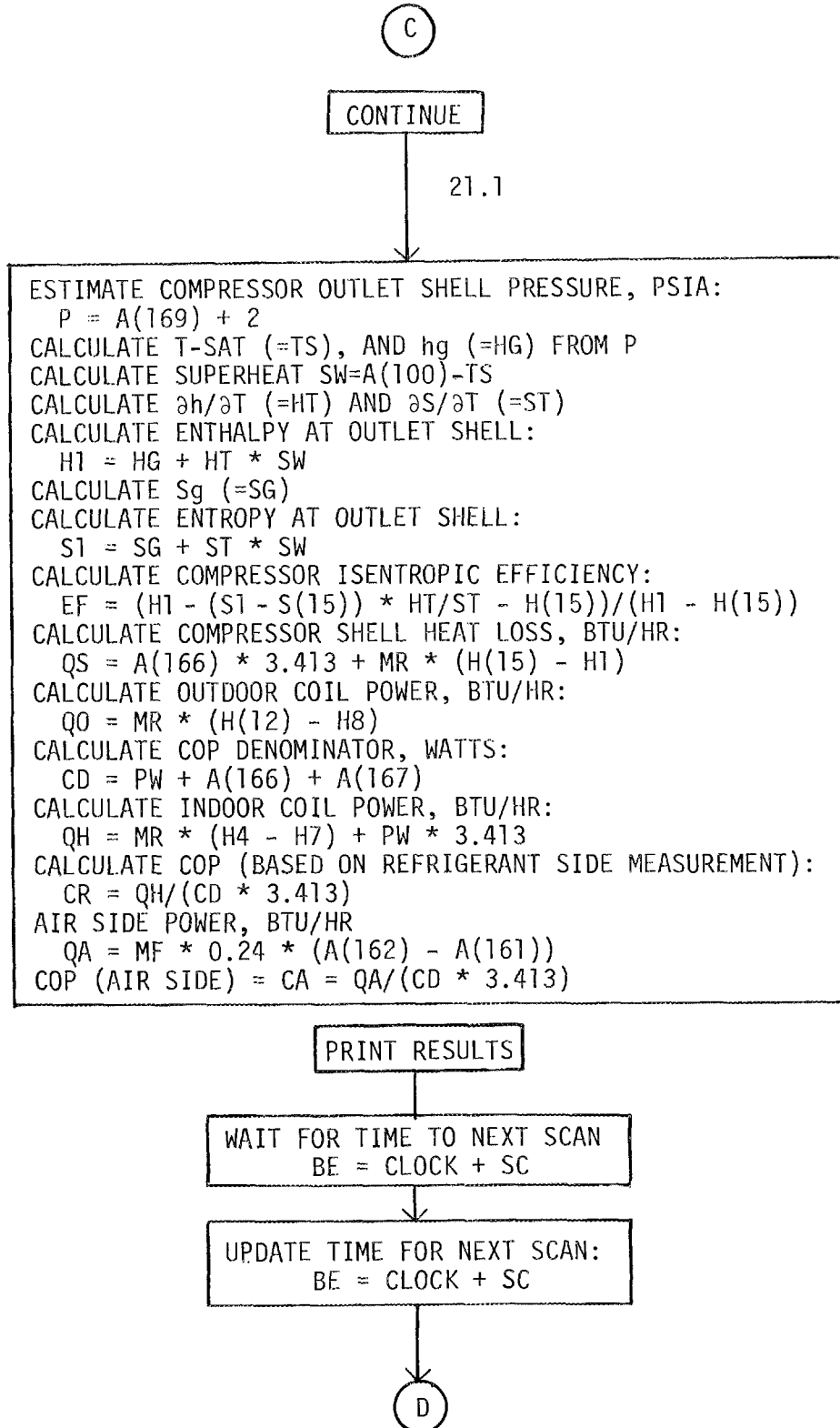
Heat Balance and COP Program - Heating Mode (continued)



Heat Balance and COP Program - Heating Mode (continued)



Heat Balance and COP Program - Heating Mode (continued)



INTERNAL DISTRIBUTION

- | | |
|----------------------|--------------------------------------|
| 1. L. A. Abbatiello | 33-52. P. M. Love |
| 2. S. I. Auerbach | 53. C. R. Martin |
| 3. S. J. Ball | 54. J. W. Michel |
| 4. R. W. Barnes | 55. W. A. Miller |
| 5. V. D. Baxter | 56. R. E. Minturn |
| 6. D. J. Bjornstad | 57-61. W. R. Mixon |
| 7. J. R. Buchanan | 62. N. E. Morgan |
| 8. R. S. Carlsmith | 63. J. C. Moyers |
| 9. W. S. Chern | 64. E. A. Nephew |
| 10. C. V. Chester | 65. D. L. O'Neal |
| 11. K. R. Corum | 66. A. M. Perry |
| 12. F. A. Creswick | 67. H. Postma |
| 13. R. M. Davis | 68. C. K. Rice |
| 14. J. G. Delene | 69. M. W. Rosenthal |
| 15. R. D. Ellison | 70. T. H. Row |
| 16. P. D. Fairchild | 71. E. G. Struxness |
| 17. J. T. Farmer | 72. J. E. Summers |
| 18. S. K. Fischer | 73. D. B. Trauger |
| 19. W. Fulkerson | 74. J. L. Trimble |
| 20. V. O. Haynes | 75. D. J. Walukas |
| 21. N. E. Hinkle | 76. T. J. Wilbanks |
| 22. E. A. Hirst | 77. J. V. Wilson |
| 23. D. E. Holt | 78. H. E. Zittel |
| 24. C. C. Hopkins | 79. A. Zucker |
| 25. M. M. Hutchinson | 80. Biology Division Library |
| 26. W. L. Jackson | 81-82. Central Research Library |
| 27. P. L. Johnson | 83. Document Reference Section |
| 28. S. I. Kaplan | 84-85. Energy Information Library |
| 29. D. Kaserman | 86. Laboratory Records - RC |
| 30. W. P. Levins | 87-89. Laboratory Records Department |
| 31. R. S. Livingston | 90. ORNL Patent Office |
| 32. H. M. Long | |

EXTERNAL DISTRIBUTION

91. Mr. Roy Abbott, Advance Technology Operations, General Electric Company, AP6, Appliance Park, Louisville KY 40225
92. Mr. Richard S. Alben, General Electric, GE R&D Center, Building K-1, Room 5B37, Post Office Box 8, Schenectady NY 12301
93. Dr. Lawrence Ambs, Associate Professor, Department of Mechanical Engineering, University of Massachusetts, Amherst MA 01003
94. Dr. James C. Brisee, Director, North Carolina Energy Institute, Department of Commerce, Post Office Box 12235, Research Triangle Park NC 27709
95. Mr. Joe Canal, General Electric Company, Troup Highway, Tyler TX 75711

96. Mr. John J. Cuttica, Chief, Technology and Consumer Products Branch, MS 2221C, Department of Energy, 20 Massachusetts Avenue NW, Washington DC 20545
- 97-101. Mr. Albert A. Domingorena, Carrier Corporation, Building TR-4, Carrier Parkway, Post Office Box 4808, Syracuse NY 13221
102. Mr. G. W. Gatecliff, Research Laboratory, Tecumseh Products Company, Ann Arbor MI 48105
103. Dr. L. R. Glicksman, Department of Mechanical Engineering, Massachusetts Institute of Technology, Cambridge MA 02139
104. Mr. S. D. Goldstein, Manager, Advanced Development Lab, Climate Control Division, The Singer Company, 1300 Federal Boulevard, Carteret NJ 07008
104. Mr. Gerald C. Groff, Research Division, Carrier Corporation, Syracuse NY 13201
104. Dr. C. C. Hiller, Sandia Laboratories, Livermore CA 94550
105. Mr. F. Honnold, Consumer Products Division, Carrier Corporation, Syracuse NY 13201
106. Mr. T. Jacoby, Tecumseh Products Company, Tecumseh MI 49286
107. Mr. H. Jaster, General Electric Corporation Research and Development, General Electric Company, Schenectady NY 12301
108. Mr. F. Kalivoda, Copeland Corporation, Sydney OH 45365
109. Mr. Rube Kelto, Tecumseh Products Company, Tecumseh MI 49286
110. Mr. R. W. King, Copeland Corporation, Sydney OH 45365
111. Mr. Robert Mauro, Electric Power Research Institute, Palo Alto CA 94304
112. Mr. John Millhone, Director, Office of Buildings and Community Systems, Department of Energy, 20 Massachusetts Avenue NW, Washington DC 20545
113. Mr. Neno Nenov, Linde Division, Union Carbide Corporation, Tonawanda NY 14150
114. Mr. Michael Perlsweig, Department of Energy, Division of Conservation Research and Technology, 20 Massachusetts Avenue NW, Washington DC 20545
115. Dr. Kurt W. Riegel, Director, Consumer Products Division, MS 2221C, Department of Energy, 20 Massachusetts Avenue NW, Washington DC 20545
116. Mr. John D. Ryan, Program Manager, Technology and Consumer Products Branch, MS 2221C, Department of Energy, 20 Massachusetts Avenue NW, Washington DC 20545
117. Mr. D. E. Sherpereel, Research and Engineering Center, Whirlpool Corporation, Benton Harbor MI 49022
118. Dr. M. H. Somerville, Engineering Experiment Station, University of North Dakota, Grand Forks ND 58202
119. Mr. W. F. Stoecker, University of Illinois, Urbana IL 61801
120. Mr. M. Wilden, University of New Mexico, Albuquerque NM 87115
121. Institute of Energy Analysis, ORAU-Library
122. Research and Technical Support Division, DOE-ORO
123. Assistant Manager, Energy Research and Development, DOE-ORO
- 124-150. Technical Information Center, DOE, Post Office Box 62, Oak
- 151-701. External Energy Conservation Distribution Mailing List and Conservation Technology Office (Building 9102-1, Room 2)